

Infiltration of Stormwater from Highway Operations to Reduce Coastal Pollution

FINAL REPORT

**Chittaranjan Ray
Michelle H. Teng**

December 2012

**PREPARED IN COOPERATION WITH THE
State of Hawaii Department of Transportation
and
Federal Highway Administration**

**DEPARTMENT OF CIVIL AND ENVIRONMENTAL ENGINEERING
UNIVERSITY OF HAWAI'I AT MĀNOA
Honolulu, Hawai'i 96822**

Infiltration of Stormwater from Highway Operations to Reduce Coastal Pollution

FINAL REPORT

by

Chittaranjan Ray, P.E.
Principal Investigator

Michelle H. Teng, P.E.
Co-Investigator

December 2012

University of Hawaii at Manoa
Department of Civil and Environmental Engineering
2540 Dole Street, Holmes Hall 383
Honolulu, HI 96822

State of Hawaii Department of Transportation and Federal Highways Administration

ACKNOWLEDGEMENTS AND DISCLAIMER

The authors are grateful for the funding and support provided by the Hawaii Department of Transportation (HDOT) and the Federal Highway Administration (FHWA).

The authors greatly appreciate the valuable contributions provided by:

Robert Shin (HDOT)
Curtis Matsuda (HDOT)
Todd Nishioka (HDOT)

The authors wish to acknowledge the contributions of Ghasem Alavi, Matteo D'Alessio, Jaromir Dusek, Arvind Mohanram, Philip Moravcik, Seo Jin Ki, Joseph Lichwa, Laxman Sharma, Michal Snehota, Martina Sobotkova, Bunnie Yoneyama, Katrin Zander, and Elke Zeller.

THE CONTENTS OF THIS REPORT REFLECT THE VIEW OF THE AUTHORS, WHO ARE RESPONSIBLE FOR THE FACTS AND ACCURACY OF THE DATA PRESENTED HEREIN. THE CONTENTS DO NOT NECESSARILY REFLECT THE OFFICIAL VIEWS OR POLICIES OF THE STATE OF HAWAII, DEPARTMENT OF TRANSPORTATION, OR THE FEDERAL HIGHWAY ADMINISTRATION. THIS REPORT DOES NOT CONSTITUTE A STANDARD, SPECIFICATION, OR REGULATION.

CONTENTS

1. Introduction	1
2. Purpose and Scope	1
3. Site Locations and Soil Characteristics	2
3.1. Oahu Highway Locations and Descriptions	2
3.2. Identification of Sites for Study	2
3.3. In Situ Measurement of Hydraulic Conductivity, Bulk Density, and Infiltration Rate	4
3.4. Measurement of Soil Water Retention in the Laboratory	5
3.5. Evaluation of Salinity and pH in Soils Along Oahu Highways	5
3.6. Heavy Metal Concentration in Soils Along Oahu Highways	7
3.6.1. Batch Sorption Tests for Heavy Metals	7
3.6.2. Measurements of Desorption Coefficient of Soil	8
4. Highway Runoff Water Quality on Oahu — Measurement and Analysis	10
4.1. Stormwater Runoff Sampling	10
4.2. Analysis of Existing Water Quality Data of Highway Runoff on Oahu and in California	12
4.3. Heavy Metal Concentration in Sediments in Runoff from H3 Drain Outlets	12
4.4. Zeta Potential of H3 Runoff	13
4.5. Particle Size Distribution of H3 Runoff	14
5. Development of Site Suitability Map for Sitting Infiltration Trenches	14
6. Column Studies to Evaluate Clogging Potential	17
6.1. Introduction	17
6.2. Experimental Procedure	18
6.2.1. Intermittent Flow Experiment	18
6.2.2. One-Step Outflow Experiment	18
6.2.3. Long-Term Infiltration-Outflow Experiment	18
6.3. Soil Sampling	19
6.3.1. For the Intermittent Flow and One-Step Outflow Experiments	19
6.3.2. For the Long-Term Infiltration-Outflow Experiment	19
6.4. Collection of Highway Storm Runoff	20
6.5. Experimental Setup Design	21

6.5.1.	Intermittent Flow and One-Step Outflow Experiments	21
6.5.2.	Long-Term Infiltration-Outflow Experiment	23
6.6.	Results and Discussion	25
6.6.1.	Intermittent Flow Experiments	25
6.6.2.	Results of One-Step Outflow Experiment	28
6.6.3.	Long-Term Infiltraton-Outflow Experiment	30
7.	Modeling of Water Movement from a Potential Trench Site Along Oahu’s Highway	33
7.1.	Simulation of Infiltration for Different Soils	33
7.2.	Modeling of Trench Operation	37
7.2.1.	Case Study I	39
7.2.2.	Case Study II	40
7.2.3.	Case Study III	41
7.2.4.	Case Study IV	42
7.2.5.	Case Study V	43
8.	Drainage Time and Size of the Infiltration Trench	43
9.	Summary of Findings	45
9.1.	Capabilities of Selected Natural Soils to Infiltrate Stormwater and Adsorb Pollutants from Runoff Water	45
9.2.	Stormwater Runoff from the Highway	45
9.3.	Site Suitability Index Using GIS	45
9.4.	Laboratory Experiments	46
9.5.	Modeling	46
10.	References	47
11.	Appendix	53

Figures

1.	Oahu highway and state roadway system	2
2.	Summary of the various analyses and tests	3
3.	Selection of sampling sites for potential of infiltration trenches	3
4.	Heavy metal concentration in soils from 15 sites along Oahu highways	7
5.	Median metal concentrations in the soils along Oahu's highways	13
6.	Two-level screening approach to identify candidate locations for implementing infiltration trenches	15
7.	Best locations for implementing infiltration trenches on the island of Oahu	16
8.	Locations of column sampling	19
9.	Collecting soil cores for column laboratory studies	20
10.	Collected soil core sample from Poamoho	20
11.	Collection of stormwater at H3	21
12.	Schematic of the experimental setup for four columns	22
13.	Laboratory setup of four columns connected to data-logger for intermittent and one-step outflow experiment	23
14.	Schematic view of experimental setting	24
15.	Experimental setup to measure reduction of hydraulic conductivity in soil column	24
16.	Average hydraulic conductivity values during drying cycles in four columns	26
17.	Clogging layer during (a) wet cycle, and (b) after nine days of drying	26
18.	Outflow rates for the 1st, 2nd, and 3rd runs of wet/dry cycles of the North Shore, Kunia, Pali, and Sandy Beach	29
19.	Results of clogging column experiments and soil clogging experiments	31
20.	Accumulation of sediment in gravel layer	32
21.	Image of development of a clogging layer in soil column	32
22.	Cracked clogging layer after five days of column during dry cycle	32
23.	Dimensions of flow domain	34
24.	Cumulative flux through the trench for the simulated soils	36
25.	Cumulative flux through the sidewall and bottom of the trench for Kawaihapai soil	37
26.	Pressure head distributions in the simulated domain for two soils after infiltration of 2 L volume of stormwater	37
27.	2D flow domain	39
28.	Water table and pressure heads in the infiltration trench during case study I	39
29.	Fluxes and pressure heads in 20, 40, 80, and 100 cm below the infiltration trench bottom during case study I	40
30.	Water table pressure heads in the infiltration trench during case study II	40

31.	Fluxes and pressure heads at 20, 40, 80, and 100 cm below the infiltration trench bottom during case study II	41
32.	Water table and pressure heads in the infiltration trench during case study III	41
33.	Fluxes and pressure heads in the infiltration trench during case study III	42
34.	Water table and pressure heads in the infiltration trench during case study IV	42
35.	Fluxes and pressure heads in the infiltration trench during case study IV	43
36.	Pressure heads in the simulated domain at selected times	44
37.	Fluxes and pressure heads in the infiltration trench during case study V	44

Tables

1.	Comparison of soil data measured for this study with data from literature	4
2.	Measured bulk density, saturated water content, estimated saturated hydraulic conductivity, residual water content, and van Genuchten parameters for soils along Oahu highways	6
3.	Measured pH and electrical conductivity for soils along highways on Oahu	6
4.	Distribution coefficients of heavy metals on to sample soils, charcoal, and various bio-chars	8
5.	Desorption coefficients for soils along Oahu's highways based on SPLP	10
6.	Concentration of different constituents in runoff from H3 and Honolulu tap water for comparison	11
7.	Concentration of heavy metals in sediments in runoff from H3	11
8.	Estimated and measured maximum dissolved metal concentration in highway runoff on Oahu and California	12
9.	Zeta potential in runoff from H3 during different storm events	14
10.	Characteristics of highway runoff water used in clogging experiment	21
11.	Summary of K values during intermittent flow	25
12.	Duration of experiments	28
13.	Characteristics of highway runoff water used in clogging experiment	31
14.	Soil hydraulic characteristics of fourteen different soil types used in simulations	35
15.	Simulated times required for infiltration of 2L of stormwater	36
16.	Review of modeled cases with different conditions	38
17.	Review of modeled cases with different conditions and given time to reach steady state flow or no flow	45

Appendix

A.	Google map locations of sites to investigate soil properties for infiltration capacity	55
B.	Measured and estimated hydraulic conductivity and retention curves	60
C.	Sampling H3 runoff	68
D.	Comparative concentration of heavy metals in runoff from H3 during May 2008 and California during 2000–2003	69
E.	Summary statistics of highway runoff quality on Oahu, Hawaii and California	70
F.	Comparison of cations and anions of storm runoff with tap water	71
G.	Concentrations of heavy metals in runoff from H3	73
H.	Cumulative particle size distribution for particles ranging from 1 to 1000 nm in fourteen samples collected during eight storm events in H3 runoff	74
I.	Cumulative particle size distribution for particles ranging from 1 to 1000 μm in H3 runoff during seven storm events	74
J.	Detailed description of a suitability index map development	75
K.	Review of literature	97
L.	Chemical analysis of pH, conductivity, turbidity and dissolved organic carbon, total organic carbon, TSS, and TDS during intermittent flow experiment of Kunia column	101
M.	Chemical analysis of (a) anions and (b) cations during intermittent flow experiment of Kunia column	102
N.	Chemical analysis of heavy metals during intermittent flow experiment of Kunia column	103
O.	Chemical analysis of pH, conductivity, turbidity and dissolved organic carbon, total organic carbon, TSS, and TDS during intermittent flow experiment of North Shore column	104
P.	Chemical analysis of (a) anions, and (b) cations during intermittent flow experiment of North Shore columns	105
Q.	Chemical analysis of heavy metals during intermittent flow experiment of North Shore column	106
R.	Chemical analysis of pH, conductivity, turbidity and dissolved organic carbon, total organic carbon, TSS, and TDS during intermittent flow experiment of Sandy Beach column	107
S.	Chemical analysis of (a) anions, and (b) cations during intermittent flow experiment of Sandy Beach column	108
T.	Chemical analysis of heavy metals during intermittent flow experiment of Sandy Beach column	109
U.	Chemical analysis of pH, conductivity, turbidity and dissolved organic carbon, total organic carbon, TSS, and TDS during intermittent flow experiment of Pali column	110

V.	Chemical analysis of (a) anions, and (b) cations during intermittent flow experiment of Pali column	111
W.	Chemical analysis of heavy metals during intermittent flow experiment of Pali column	112
X.	Outflow rate and cumulative outflow calculated from balance data for (a) North Shore, (b) Kunia, (c) Sandy Beach, and (d) Pali columns	113
Y.	Pressure heads in four depths for (a) North Shore, (b) Kunia, (c) Sandy Beach, and (d) Pali columns	114
Z.	Chemical analysis of pH, conductivity, turbidity and dissolved organic carbon, total organic carbon, TSS, and TDS during wet/dry cycling experiment of North Shore column	115
AA.	Chemical analysis of pH, conductivity, turbidity and dissolved organic carbon, total organic carbon, TSS, and TDS during wet/dry cycling experiment of Kunia column	116
BB.	Chemical analysis of pH, conductivity, turbidity and dissolved organic carbon, total organic carbon, TSS, and TDS during wet/dry cycling experiment of Pali column	117
CC.	Chemical analysis of pH, conductivity, turbidity and dissolved organic carbon, total organic carbon, TSS, and TDS during wet/dry cycling experiment of Sandy Beach column	118
DD.	Chemical analysis of (a) anion, and (b) cations during one step outflow experiment of North Shore column	119
EE.	Chemical analysis of (a) anion, and (b) cations during one step outflow experiment of Kunia column	120
FF.	Chemical analysis of (a) anion, and (b) cations during one step outflow experiment of Pali column	121
GG.	Chemical analysis of (a) anion, and (b) cations during one step outflow experiment of Sandy Beach column	122
HH.	Summary of chemical analysis done on North Shore and Kunia sample	123
II.	Summary of chemical analysis done of Pali and Sandy Beach sample	124
JJ.	Electrical conductivity, turbidity, total suspended solids, and total dissolved solids during the first long-term column experiment on Sandy Beach	125
KK.	Influent and effluent of (a) electrical conductivity, (b) turbidity, (c) total suspended solids, and (d) total dissolved solids during the second long-term column experiment on Sandy Beach	126
LL.	Concentration of anions and cations in the influent and effluent of second long-term infiltration-outflow experiment on Sandy Beach	127

1. Introduction

The coastal waters of Hawaii are extremely important for recreation as well as for the health of the marine environment. Runoff from the construction and operation of highways can be a source of pollution to coastal waters. Individual states in the US have established regulatory programs to protect surface waters for their designated uses. Protecting near shore waters is particularly important in the State of Hawaii where beach water quality is critical to the tourism-based economy. Diffuse pollution from storm runoff is found to have a great impact on surface water quality (Novotny, 1999; Kim et al., 2005). State and federal regulatory agencies are increasing their efforts to quantify and control the sources of non-point source pollution. Limited water quality monitoring data for storm runoff from the construction and operation of highway H-3 on Oahu are available (Wong, 2005; Presley, 2001; Presley 2002; Young and Ball, 2004; Young and Ball, 2005). Such data are not widely available for all areas of the state, although the Hawaii Department of Health (HDOH) and the Clean Water Branch are trying to develop and implement TMDLs for various streams. The current research was undertaken to obtain additional data on storm runoff water quality.

The State of Hawaii Department of Transportation (HDOT) has included infiltration trenches as a Best Management Practice (BMP) option to reduce pollution caused by stormwater runoff. HDOT guidelines state that the implementation of BMPs is needed to reduce sediment and associated pollutant loads to streams and the ocean (State of Hawaii, 2007a, 2007b). In the standard trench design, highway runoff first passes through swales or buffer strips where most coarse materials and some contaminants are removed. This water then enters the trench and infiltrates through the trench bottom and sides, into the surrounding subsurface. While passing through the soil surrounding the trench, sediments and other pollutants (such as heavy metals, oil and grease, bacteria, and nutrients) are removed.

This project attempts to identify potential sites for the construction of stormwater infiltration trenches on the island of Oahu. Soils around Oahu were analyzed for their ability to absorb pollutants from highway runoff, and column studies were carried out in the laboratory to further help select the best locations to install infiltration trenches as a BMP to reduce coastal pollution.

2. Purpose and Scope

One of the goals of the project was to investigate the suitability of soils adjacent to highways on Oahu for the placement of infiltration trenches. However, the ultimate goal was to implement the research findings in field settings for direct use by the Hawaii DOT.

Specific Objectives

1. To conduct laboratory, field, and modeling studies to determine:
 - the ability of selected soils on Oahu to infiltrate highway runoff and adsorb pollutants from runoff water
 - the adsorption capacities of the natural soil to remove pollutants from runoff water
 - the time needed for a trench of given size to drain a given volume of water

2. To develop suitability index criteria for sites using a Geographic Information System (GIS) framework to identify areas having relatively greater infiltration potential to infiltrate runoff and to retain pollutant retentions.

3. Site Locations and Soil Characterization

3.1. Oahu Highway Locations and Descriptions

There are three major freeways in the interstate system on Oahu (Figure 1). Access to the freeways is restricted through dedicated ramps. The system is comprised of 54.9 route miles (or 347.4 lane miles). In addition to the freeways there are many principal arterial roads termed state highways. The state highway system has 280.3 route miles (936.6 lane miles). Operation and maintenance of the freeways is generally the responsibility of the HDOT while other roads are generally maintained by the City and County of Honolulu.

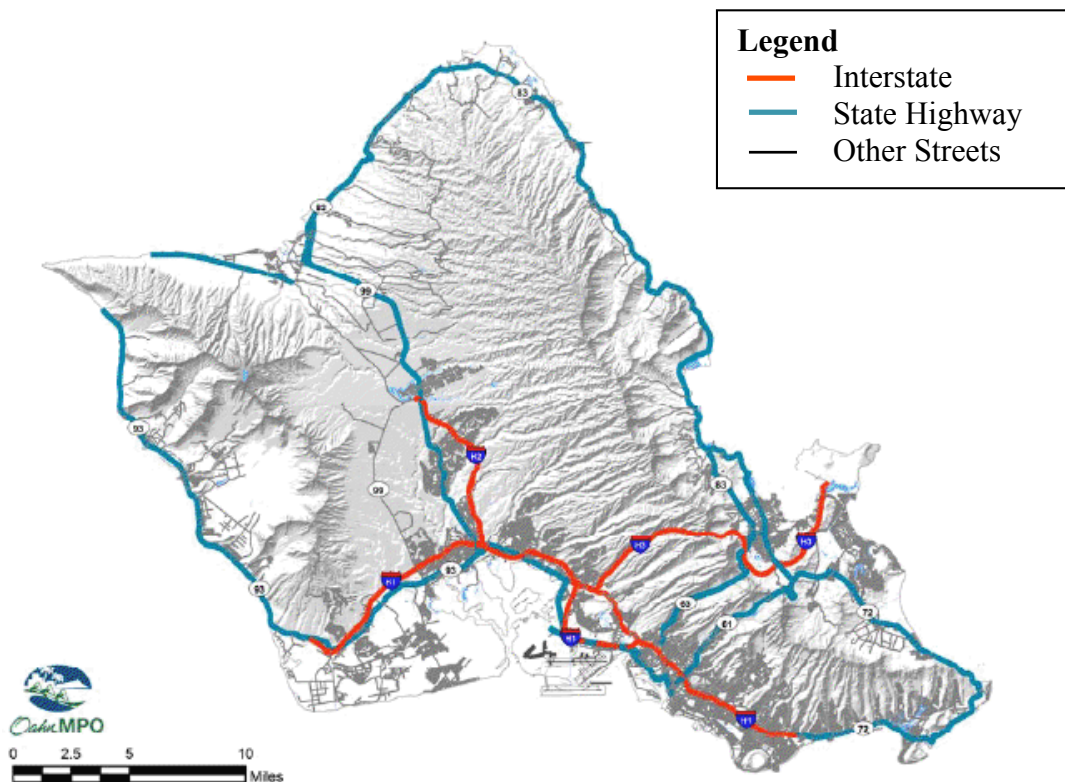


Figure 1. Oahu highway and state roadway system (Oahu Transportation System Inventory Report, 2009).

3.2. Identification of Sites for Study

The capacity of a trench to infiltrate runoff water and to remove pollutants in runoff is mainly dependent on the properties of the surrounding soil as water infiltrates through the trench bottom and sides. Two soil factors to be considered are infiltration capacity for water and adsorption capacity for pollutants. In this study, the factors were determined by conducting in situ

infiltration studies, a number of laboratory experiments, and column studies on soil samples obtained from selected sites (Figure 2).

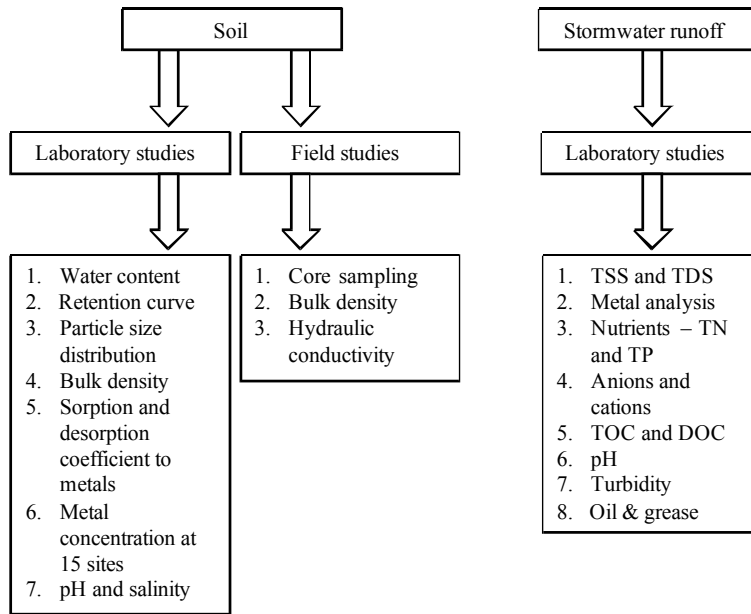
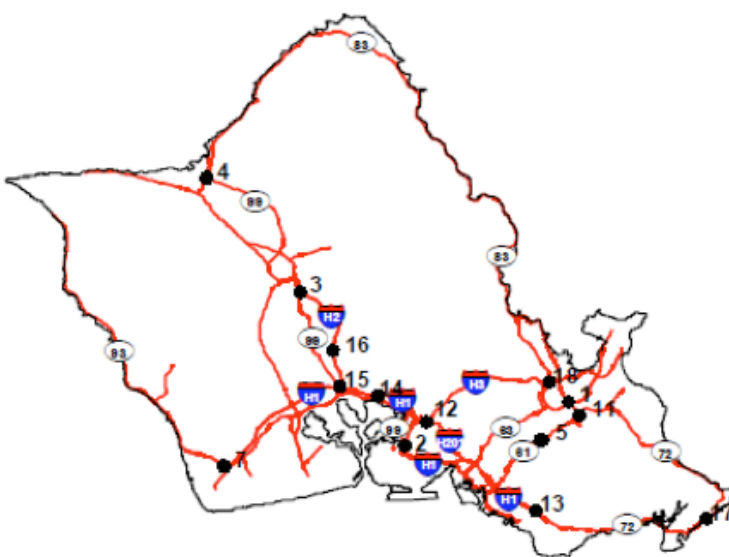


Figure 2. Summary of various analyses and tests.

We identified a total of 64 sites along Oahu’s highways where installation of infiltration trenches may be feasible. The general soil data for these locations were retrieved from satellite and soil survey maps (Foote et al., 1972). After eliminating locations with unsuitable conditions (e.g., lack of sufficient space, stony or fill land soils, constructed coastal areas filled with gravel, coral stone and debris) we found that investigating the soil from the remaining locations provided the information needed for the majority of soils along Oahu’s highways (Figure 3).



Label	Site names
1	H3–Kamehameha IC
2	H1–Kamehameha Hwy.
3	H2–Kahelu IC
4	Kamehameha–Waialua Beach Rd.
5	Pali from Ahi Pl. to the tunnel
7	H1–Kalaeloa Blvd., point 1
9	H1–Kalaeloa Blvd., point 3
10	Pali from Ahi Pl. to the tunnel
11	Pali–Kamehameha Hwy.
12	H3–H1 IC
13	H1–University Ave.
14	H1–Moanalua Rd.
15	H1–H2 IC
16	H2–Kauka Blvd.
17	Sandy Beach Park
18	Likelike–Kahekili Hwy.

Figure 3. Selection of sampling sites for potential of infiltration trenches.

3.3. In Situ Measurement of Hydraulic Conductivity, Bulk Density, and Infiltration Rate

Direct measurement of soil hydraulic conductivity can be determined at or below saturation using tension infiltrometers (Perroux and White, 1988). Different suction pressure was applied on the top of the soil surface and the infiltration rate was measured. Tension infiltration experiments are usually conducted to measure near-saturated and saturated hydraulic conductivity (Reynolds and Elrick, 1991; Clothier et al., 1992).

Therefore, after excavating a hole at each site according to the procedure followed in Reynolds et al. (2000), hydraulic conductivity was measured in the field using a tension infiltrometer at different depths. The results were compared to the information available in Foote et al. (1972). In addition, disturbed and undisturbed soil samples were taken from the excavated holes for various laboratory experiments using an auger or a core sampler. Bulk density and infiltration rates were measured at depths between one and three feet. Measurements were taken in the topsoil, after removing the turf, and in the subsoil at two or three depths at each location. The actual measurement depths at each site varied depending on the hardness of the soil, the ease of (manual) excavation, and the presence of clean soil (i.e., no gravel or boulders that might alter infiltration rates). Bulk density was measured by determining the water content, volume, and dry weights of undisturbed cores. Undisturbed soil cores (60 mm long and 57 mm in diameter) were used to determine the bulk density. Soil hydraulic conductivity was estimated from tension infiltrometer data at the sites using standard procedures (Reynolds et al., 2000). The measured soil properties are shown in Table 1. The hydraulic conductivities measured in this study were generally higher than those given by USDA/UH (1973). This was probably due to differences in measurement methodology. We measured hydraulic conductivity by in situ tension infiltrometry, whereas the USDA/UH (1973) method estimated hydraulic conductivity based on soil structure, soil porosity, and data from a limited number of conductivity tests made on undisturbed cores.

Table 1. Comparison of soil data measured for this study with data from literature.

Soil type	Bulk density (g/cm ³)		Water content at field capacity (%)		K (mm/h)	
	Yost et al. (1994)	This study	Yost et al. (1994)	This study	USDA/UH (1973)	This study
Kaneohe silty clay	ND	1.02	ND	43	51–160	184
Kawaihapai clay loam	1.27	1.16	36	32	16–51	26
Kaena clay	0.46	1.39	44	36	1.5–16	135
Makiki clay loam	ND	1.37	ND	35	51–160	351
Molokai silty clay loam	1.12	1.12	31	37	16–51	56
Waipahu silty clay	1.17	1.15	37	35	5–51	151
Alaeloa silty clay	ND	1.09	ND	32	51–160	38
Makalapa clay	ND	1.42	ND	58	1.5–5	412
Helemano silty clay	1.19	1.15	35	26	51–160	248
Waialua silty clay	1.23	1.40	36	45	16–51	217
Lolekaa silty clay	0.96	0.91	39	38	51–160	180
Honouliuli clay	1.49	1.50	41	40	5–16	485
Koko silt loam	ND	1.23	ND	37	16–51	71
Hanalei silty clay	0.88	1.06	50	48	16–51	736

Note: ND = not determined.

3.4. Measurement of Soil Water Retention in the Laboratory

The water holding capacity of soil is described by its retention curve. Retention curves show the relationships between volumetric water content and pressure potential at equilibrium. The soil water retention curve is a function of soil type. The shape of a retention curve is closely related to textural and mineralogical composition, organic content, soil structure, and volumetric water content.

Soil water retention curves were measured in the laboratory using undisturbed 100 cm³ soil samples. First, the soil samples were fully saturated and then the samples were drained applying different pressures. The measurements of water retention curves for the studied soils were made within the range of pressure from 60 to 600 cm during the drying process (Klute, 1986). Standard pressure chambers (Soil Moisture Equipment Corp., Santa Barbara, California, USA) were used. Soil hydraulic parameters were derived from the retention data using the parameter optimization program RETC (van Genuchten et al., 1991). Water retention and hydraulic conductivity were described using the van Genuchten approach (van Genuchten, 1980):

$$\theta(h) = \theta_r + \frac{\theta_s - \theta_r}{\left[1 + |\alpha h|^n\right]^m} \quad h < 0 \quad (1)$$

$$\theta(h) = \theta_s \quad h \geq 0 \quad (2)$$

where θ_r and θ_s are the residual and saturated water contents (cm³/cm³), respectively; α is an empirical parameter (cm⁻¹) whose inverse is sometimes referred to as the air entry value, n is a fitting constant reflecting the steepness of the retention curves, $m = 1 - 1/n$, and l is an empirical pore connectivity factor frequently set to 0.5 following Mualem and Klute (1986). Their values were estimated by fitting the retention and conductivity models to the observed data using RETC. A list of locations investigated, together with the measured and estimated soil hydraulic parameters, are shown in Table 2 and Appendix B. The results were used as input parameters for modeling scenarios.

3.5. Evaluation of Salinity and pH in Soils Along Oahu Highways

Salinity and pH were measured for fourteen different soil-types at sites along Oahu highways (Table 3). Electrical conductivity (EC), a measure of salinity, was measured directly in soil solutions consisting of 5 g dry soil and 15 ml deionized water. The pH of the soil was measured in a 1:1 paste prepared by adding 5 g dry soil to 5 ml deionized water. The pH varied between 4.3 and 8.4 with an average of 6.4. The electrical conductivity of the soils was generally low (<700 μ S/cm).

Table 2. Measured bulk density (BD), saturated water content (θ_s), estimated saturated hydraulic conductivity (K_s), residual water content (θ_r), and van Genuchten parameters (α , n , l) for soils along Oahu highways.

Location	Soil type	Texture ¹	Depth (cm)	BD (g/cm ³)	K_s (mm/h)	θ_s (%)	θ_r (%)	α (mm ⁻¹)	n	l
H3–Kamehameha IC	Kaneohe	Uniform	30- 50	1.10	184	52	0	0.0027	1.09	6
H3–H1 IC	Kawaihapai	Non-Uniform ²	25- 45	1.20	26	53	0	0.0019	1.23	0.5
			45- 65	1.06	15	46	0	0.0018	1.27	0.5
Likelike H1 IC	Kaena	Uniform	30- 35	1.40	136	50	0	0.0028	1.17	0.5
H1–University Ave.	Makiki	Uniform	45- 55	1.39	1,327	51	0	0.0093	1.16	0.5
			60- 70	1.37	351	53	0	0.0023	1.15	6.5
H1–Moanalua Rd.	Molokai	Uniform	10- 20	1.23	50	44	15	0.0023	1.24	6
			20- 40	1.21	56	50	28	0.0018	1.30	9
H1- H2 IC	Waipahu	Uniform	20- 40	1.29	151	54	0	0.002	1.22	0.5
Pali–Kamehameha Hwy.	Alaeloa	Uniform	40- 60	1.14	38	48	29	0.016	1.48	2
H1- Kamehameha Hwy.	Makalapa	Uniform	25- 45	1.52	412	65	36	0.004	1.11	8
H2–Kauka Blvd.	Helemano	Uniform	15- 25	1.04	1,396	41	0	0.007	1.14	5
			30- 40	1.15	248	43	0	0.005	1.19	4
Kamehameha- Waialua Beach Rd.	Ewa	Uniform	30- 40	1.48	217	54	0	0.001	1.15	2
Pali from Ahi Pl. to the tunnel	Lolekaa	Uniform	30- 50	0.93	180	44	20	0.002	1.35	47
	Fill (mixed)	Uniform	30- 50	1.22	35	53	20	0.002	1.25	7
H1–Kalaeloa Blvd., point 1	Honouliuli	Uniform	30- 50	1.51	100	46	20	0.002	1.63	0.5
H1–Kalaeloa Blvd., point 2 ³			35- 55	1.51	889	56	9	0.006	1.12	6
H1–Kalaeloa Blvd., point 3			25- 45	1.51	467	52	0	0.002	1.12	0.5
Sandy Beach Park	Koko	Non-Uniform ⁴	30- 50	1.23	71	47	20	0.002	1.25	0.5
Likelike–Kahekili Hwy.	Hanalei	Uniform	25- 35	1.23	5,904	63	0	0.007	1.03	0.5
			40- 50	1.06	736	43	6	0.004	1.06	6

Note: K_s , θ_r , α , n , and l were estimated by the RETC program of van Genuchten et al. (1991) using van Genuchten/Mualem ($m = 1 - 1/n$) model.

¹According to *Soil Survey of the Islands of Kauai, Oahu, Maui, Molokai, and Lanai, State of Hawaii* (1972).

²It is given that the subsoil (55–138 cm) is sandy loam and has a higher conductivity.

³More soil samples were collected and more infiltration measurements were made in this point than the other two points in this location; thus, it is more representative.

⁴The texture is silt loam from the surface to 64 cm depth but clay loam from 64 to 104 cm depth.

Table 3. Measured pH and electrical conductivity for soils along highways on Oahu.

No.	Sampling site	Soil type	pH (-)	EC (μ S/cm)
1	H3–Kamehameha intersection	Kaneohe silty clay	6.6	54
2	H3–H1 intersection	Kawaihapai clay loam	6.7	156
3	Likelike H1 intersection	Kaena clay	7.6	181
4	H1–University Ave.	Makiki clay loam	7.3	169
5	H1–Moanalua Rd.	Molokai silty clay loam	5.3	143
6	H1- H2 IC	Waipahu silty clay	5.5	151
7	Pali–Kamehameha Hwy.	Alaeloa silty clay	6.7	65
8	H1- Kamehameha Hwy.	Makalapa clay	8.4 ¹	183
9	H2–Kauka Blvd.	Helemano silty clay	4.3	88
10	Kamehameha–Waialua Beach Rd.	Ewa silty clay loam	6.7	57
11	Pali from Ahi Pl. to the tunnel (B)	Lolekaa silty clay	6.1	138
11	Pali from Ahi Pl. to the tunnel (C)	Lolekaa silty clay	4.8 ²	143
12	H1–Kalaeloa Blvd.	Honouliuli clay	7.0	235
13	Sandy Beach Park	Koko silt loam	7.9	658
14	Likelike–Kahekili Hwy.	Hanalei silty clay	5.5	165

Note: EC = electrical conductivity.

¹Soil is gravelly.

²Sampling point was surrounded by forest trees (Eucalyptus). Forest soils normally have a lower pH as compared to other soils.

Batch sorption tests were carried out for Cd, Co, Cr, Ni, and Pb. Three solutions containing different concentrations of all these metals together and a blank were prepared using filtered stormwater runoff for the tests. The tests were carried out by placing 0.5 g of sieved soil or charcoal into a plastic bottle containing 100 mL of each heavy metal solution and shaken for 24 hours. After shaking and allowing the mixtures to settle for some time, approximately 30 ml of solution was placed in centrifuging bottles and centrifuged at 7,500 rpm for 20 minutes to produce a clear supernatant solution. About 10 mL of each solution was extracted and acidified with nitric acid to a pH less than 2. The solutions were then analyzed for the heavy metals using inductively coupled plasma-mass spectrometry (ICP-MS). The detection limits ranged from 0.01 to 1 ng/mL. The equilibrated concentrations and amount adsorbed per mass of soil/coal were plotted and fitted to the linear sorption isotherm model. The sorption distribution coefficient K_d was determined from the slope of the fitted line. These batch sorption experiments determined the heavy metals retention capacity for the soils under examination.

Table 4. Distribution coefficient (K_d) of heavy metals on sample soils, charcoal, and various bio-chars.

Soil ID	Location	Soil series (map symbol) ¹	Heavy metals				
			Cd	Co	Cr	Ni	Pb
S1	H3–Kamehameha IC	Kaneohe silty clay (KgB)	1.7	994	166.7	959	325.5
S5	H3–H1 IC	Kawaihapai clay loam (KIA)	904	821	68.1	699	229.3
S6	Likelike H1 IC	Kaena clay (KaB)	766	375	45.2	241	136.4
S7	H1–Univ. IC	Makiki (MIA)	4.9	1.5	120.4	1.2	831.6
S9A	H1–Manualua Rd. IC	Molokai silty clay loam (MUB and MUC)	259	100	118.1	108	167.2
S10	H1- H2 IC	Waipahu silty clay (WzA and WzB)	160	80	7.2	73	67.8
S12	Pali–Kamehameha Hwy.	Alaeloa silty clay (AeE)	564	243	154.5	205	308.5
S18	H2–Kauka Blvd. IC	Helemano silty clay, HLMG	551	477	374.3	481	144.5
S21	H2–Kahelu IC	Wahiawa silty clay (WaA)	786	575	637.4	597	271.3
S24	Kamehameha–Joseph Leong– Waialua Beach Rd. JCT	Ewa (Eac)	524	297	87.4	209	155.1
S35B	Pali from Ahi Pl. to the tunnel	Lolekaa silty clay (Loc)	1.2	720	206.1	731	221.8
S35C	Pali from Ahi Pl. to the tunnel	Lolekaa silty clay (Loc)	148	59	87.5	64	71.1
S46	H1–Kalaeloa Blvd.	Honouliuli (HxA)	836	750	90.1	579	168.3
S57	along Kalaniana'ole (see maps)	Koko silt loam (KsB)	2,688	869	19.4	552	290.8
S62	Likelike & Kahekili Hwy.	Hanalei silty clay (HnB)	564	243	154.5	205	308.5
CC	Charcoal		530	87	8.5	93	25.2
CHK	Chicken Litter Char		8.2	1.6	11.4	873	23.5
PNT	Peanut Hull Char		577	61	4.2	1.3	7.7
PIN	Pine Pellet Char		360	71	4.3	132	10.1

¹ Foote et al. (1972).

3.6.2. Measurements of Desorption Coefficient of Soil

Adsorption and desorption of metals is strongly dependent on pH (Landner and Reuther, 2004; Bourg, 1988). Soil pH is potentially significant with respect to leaching of adsorbed metals from soil. However, factors other than pH can significantly affect the adsorption/desorption of trace metals. For example, Christensen (1984) found that a tenfold increase in Ca^{++} concentration in water reduced the adsorption of Cd by a factor of three on sandy loam.

Adsorption/desorption reactions are usually faster than precipitation/dissolution reactions and they can thus be the predominant removal mechanism during periods of high heavy metal input in soil (Bourg, 1988). A test of Cd sorption in two Danish soils, under otherwise identical conditions, showed full adsorption reversibility for loamy sand but partial reversibility in a sandy loam (Christensen, 1984). The strongest irreversibility was observed in samples with high carbonate content.

Another factor that affects removal of metals is competition for adsorption sites. For example, the presence of competing metals reduced the sorption of metals, especially Cd, in an orthic luvisol (Schmitt and Sticher, 1986). Christensen (1985) also found a strong decrease of Cd adsorption in the presence of competing metals in sandy loam and loamy sand.

Aside from adsorption competition from other metals, the mobility of trace metals can be influenced by the presence of certain ions or compounds. However, other studies found that the adsorption of trace metals decreased when chloride was present (Bourg, 1988).

It should be noted that besides soil texture, there are many other factors (such as cation exchange capacity, organic carbon, pH) that affect sorption to soils. Some important characteristics of soils for the retention of metal pollutants are:

1. pH
2. Content of hydrous oxides of Fe and Mn
3. Organic matter content
4. Oxidation/ reduction potential
5. Surface properties (cation-exchange capacity)
6. Quantity and flow rate of water that travels through the soil

3.6.2.1. Evaluation of potential soil leaching using synthetic precipitation leaching procedure (SPLP) batch test

Leaching potential tests were conducted for selected soils collected along highways on Oahu according to the HDOH established guidance (HDOH, 2008). In these tests, 1.5 g of dry soil were placed in 30 ml of buffered deionized water (pH = 5.4) and the mixture was agitated for eighteen hours. The pH of the mixtures was adjusted to 4 and the amount of metals leaching out of soils was measured. The mixtures were centrifuged for fifteen minutes and the supernatant of two replicates were extracted, mixed, and sent to the Agricultural Diagnostic Service Center (ADSC) of the University of Hawaii (UH) for detection of heavy metals using an inductively coupled plasma optical emission spectrometer (ICP-OES) system.

The ratio of the mass of contaminant that remains sorbed to a soil compared to the mass that goes into solution is defined as the desorption coefficient for that soil/contaminant combination (HDOH, 2008). According to HDOH guidance, if the desorption coefficient (DC) value is greater than twenty then the contaminant is considered immobile and no further action is required to address leaching hazards. If the DC value is less than twenty then the estimated concentration of the contaminant in leachate, and ultimately in groundwater, is compared to target groundwater action levels and the need for further action is evaluated (HDOH, 2008).

In our study, the DC values calculated were greater than twenty for all soil/metal combinations except for cadmium in the soils from Sandy Beach Park and H1–Kalaeloa Boulevard IC (Table 5). This indicated that the adsorption capacity of the majority of soils along Oahu highways is high enough to make metal contaminants immobile as per HDOH guidance. However, two soils need further investigation since their cadmium DC values were 15 (Honouliuli at H1–Kalaeloa Boulevard) and 12 (Koko silt loam at Sandy Beach Park).

Table 5. Desorption coefficients for soils along Oahu highways based on SPLP.

Location	As	Cd	Co	Cr	Cu	Ni	Pb	Se	Zn
H3–Kamehameha	ND	63	2,024	734	ND	556	ND	329	ND
H3–H1	ND	25	1,761	3,973	ND	358	ND	ND	ND
Likelike H1	ND	37	1,214	744	ND	451	ND	136	ND
H1–University Ave.	ND	51	628	122	ND	517	1,035	184	ND
H1–Moanalua Rd.	ND	44	118	1,284	ND	145	232	120	ND
H1–H2	ND	26	200	536	ND	273	199	92	ND
Pali–Kamehameha	ND	37	288	519	ND	186	3,658	93	ND
H2–Kauka Blvd.	871	31	101	1,535	ND	195	121	153	ND
H2–Kahelu	687	36	151	2,149	ND	179	129	127	ND
Kamehameha–Waialua Beach Rd.	558	41	719	2,120	ND	3,365	126	81	ND
Pali from Ahi Pl. to the tunnel (b)	728	27	278	388	ND	355	170	129	ND
Pali from Ahi Pl. to the tunnel (c)	614	23	342	225	ND	443	195	157	ND
H1–Kalaeloa Blvd.	94	15	330	422	ND	265	46	37	ND
Sandy Beach Park	103	12	180	255	ND	366	54	40	ND
Likelike–Kahekili Hwy.	195	21	185	557	ND	125	76	44	ND

Note: ND = no metal was detected in solution.

4. Highway Runoff Water Quality on Oahu — Measurement and Analysis

4.1. Stormwater Runoff Sampling

Runoff from the H3 freeway was collected at two different locations, Kaneohe heading traffic and Honolulu heading traffic (at the field office of DOT contractor Parsons Brinkerhoff in Halawa Valley, 99-1070 Halawa Valley St. Aiea, HI 96701; shown in Appendix C). The runoff collected was used in column experiments and batch sorption tests to determine the adsorption capacities of soils for highway contaminants. The runoff was analyzed for pH, dissolved organic carbon (DOC), zeta potential, metals, total dissolved solids (TDS), total suspended solids (TSS), ions, cations, particle size distribution of sediment, and oil and grease (O&G) (Tables 6 and 7). The pH measured in the H3 runoff during May 2008 was similar to the H3 runoff during 2000–2008 (Tables 6 and 7) and the H1 runoff during 2006–2008.

Table 6. Concentration of different constituents (mg/L) in runoff from H3 and Honolulu tap water for comparison, collected at two locations on Parsons Brinkerhoff's site on Halawa Valley Street, May 2008.

Soil properties	Container A	Container B	Average	Tap Water
TDS	473.2	455.2	464.2	
TSS ¹	3,234.5	3,390	3,312.25	
DOC	57.54	44.76	51.15	
NO ₃ -N	<0.2	<0.2	<0.2	
NO ₂ -N	<0.2	<0.2	<0.2	
NH ₄ -N	6.9	4.2	5.55	
Total Nitrogen	7.14	4.67	5.91	
Dissolved P	<1	<1	<1	
Fluoride	0.14	0.18	0.16	0.03
Chloride	52.82	53.58	53.20	85.84
Nitrite	<0.2	<0.2	<0.2	<0.2
Bromide	0.11	0.12	0.11	<0.2
Nitrate	<0.2	<0.2	<0.2	2.24
Phosphate	<1	<1	<1	<1
Sulfate	26.53	22.77	24.65	14.97
Lithium	<0.02	<0.02	<0.02	<0.02
Sodium	39.71	39.61	39.66	59.75
Ammonium	6.90	4.20	5.55	<0.1
Potassium	6.02	6.48	6.25	2.64
Magnesium	8.26	8.29	8.28	12.21
Calcium	89.19	82.58	85.88	12.35
O&G			8.8	
TPH			8.8	

Note: Tap water was sampled at UH on October 16, 2008; Container A = Kaneohe heading traffic, Container B = Honolulu heading traffic.

¹Containers were placed at the outlet of two drainage pipes and runoff was collected continuously during three weeks. It may have caused an accumulation of sediments, and thus, disproportionately higher TSS.

Table 7. Concentration of heavy metals (µg/g) in sediments in runoff from H3, collected at two locations at Parsons Brinkerhoff's site on Halawa Valley Street, May 2008.

Metal	Container A	Container B	Average
As	22.6	26.77	24.7
Cd	2.08	3.65	2.9
Cr	117.5	114	115.8
Cu	280.9	268.1	274.5
Ni	69.04	72.42	70.7
Pb	62.12	79.73	70.9
Zn	636.8	824.7	730.8
Co	21.3	24.96	23.1
Se	30.71	46.45	38.6

4.2. Analysis of Existing Water Quality Data of Highway Runoff on Oahu and in California

Extensive databases from the USGS and HDOT were analyzed. This included the *Stormwater Monitoring Report* (HDOT, Highways Division; 2008). The median, range and the maximum values are summarized in Table 8 and Appendixes E and F.

The median and maximum concentrations of fifteen constituents in runoff from Oahu highways were compared to concentrations in highway runoff in California. Results of this comparison are summarized in Table 8 and Appendixes D, E, and F. The concentrations in Oahu runoff were similar or lower than the corresponding concentrations in California except for TSS, Cr, and Cu. Table 8 shows a comparison of metals concentrations in the two runoffs.

The concentration of Cr in highway runoff on Oahu was higher than in California; and was the highest, of the nine metals tested, at three of the five locations investigated. Hawaii's volcanic parent rock represents a substantial natural source of Cr. The coarse-grained fractions of Hawaii soils contained significant quantities of primary igneous minerals (e.g., olivine and pyroxene), which are thought to be the principle sources of Cr in Hawaii soils (De Carlo and Anthony, 2002; De Carlo et al., 2004).

Based on the ratio of dissolved to total metal concentrations, the estimated maximum dissolved concentration of different metals in runoff from H1 and H3 is shown in Table 8.

Table 8. Estimated and measured maximum dissolved metal concentration ($\mu\text{g/L}$) in highway runoff on Oahu and California.

Constituent	Estimated			Measured	
	H1 at Kapiolani–King (2007–2008)	H3–Halawa (2000–2008)	H3 (1992–1998) ¹	California Highways (2000–2003)	H3 at PB (May 2008)
Cd	0.84	0.24		8.4	1
Cr	18.3	72.3	1.3	23.0	13
Cu	180.0 ²	81.0 ²	1.0 ³	130.0	0
Pb	47.5	5.0	0.6	480.0	0
Ni	30.4	39.1	2.0 ³	40.0	11
Zn	750.0	165.0	18.0	1,017.0	6

¹Monitoring period varied for different stations and number of samples was generally less than measurements during 2000–2008.

²Maximum occurred in the first week of November 2007.

³Measured.

4.3. Heavy Metal Concentration in Sediments in Runoff from H3 Drain Outlets

Heavy metal concentrations in dry sediments around the H3 drain outlet near Parsons Brinkerhoff's portable office building were compared to concentrations in fifteen soils along Oahu highways (Figure 5). Excluding Zn and Cu, the sediment around the H3 drain outlet had lower concentrations of metals than the soils (Figure 5). Higher Cu and Zn may be attributed to deposition by vehicles. Nixon and Saphores (2007) found that brake linings are a primary source of Cu in runoff from roadways. Also, recent literature suggests that particles from the abrasion

and wearing of tires can be found in runoff sediment (Sansalone and Buchberger, 1997) and may contribute to fine particulates and higher levels of Zn in runoff water.

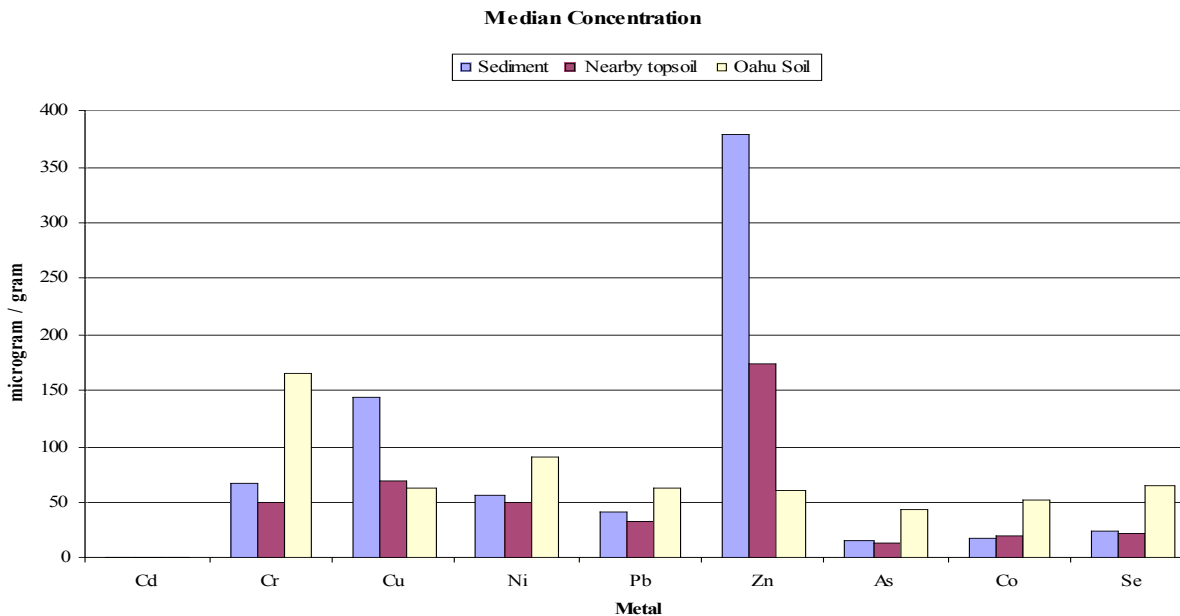


Figure 5. Median metal concentrations in the soils along Oahu’s highways (yellow), the sediments around the H3 drain outlet near Parsons Brinkerhoff’s portable office building (blue) and the topsoil nearby the Parsons Brinkerhoff’s site (red). Soil along the highways was sampled at fifteen different sites whereas the sediment was sampled at five different points.

A comparison of the concentrations of cations and anions in H3 runoff with tap water collected from the University of Hawaii campus is included in Appendix F.

4.4. Zeta Potential of H3 Runoff

Suspended particles in runoff carry a charge if they are in the colloidal range. Similarly charged particles in solution repulse each other. Zeta potential is a measure of the degree of repulsion. Zeta potential is the electro kinetic potential in a colloidal system. Colloids with high zeta potential (negative or positive) will resist aggregation (i.e., settling) while colloids with low zeta potentials have a higher tendency toward coagulation or flocculation (Brookhaven Instruments Corporation, 2002). According to the *ASTM Standard Methods* (1985), a zeta potential from 0 to ± 5 means rapid coagulation, ± 10 to ± 30 means incipient instability, and greater than ± 30 means stability. Non-colloid particles were removed from runoff samples using 1.2 μm filters, and then the zeta potential of the particles in filtrate from the H3 runoff were measured (Table 9). Our measurements indicated that the zeta potential varied between 10 and 20 mV. Therefore, the colloids in the H3 stormwater were classified as “incipiently unstable” according to the *ASTM Standard Methods* (1985) and would have a moderate propensity to coagulate.

Table 9. Zeta potential in runoff from H3 during different storm events.

Storm event	Surface charge (mV)
April 28 to May 20, 2008	-9
Feb 11 to Feb 15, 2009	-16
Feb 18 to Feb 19, 2009	-11
Feb 24 to Feb 25, 2009	-20
Feb 26 to March 2, 2009	-14
March 2 to March 23, 2009	-20.5
March 23 to March 25, 2009	-10.3
May 15 to May 18, 2009	-13
Total average	-14

4.5. Particle Size Distribution of H3 Runoff

Smaller (e.g., colloidal) particles can facilitate the transport of metals when the metals bind to them. These particles generally carry charge (measured by zeta potential) and because of that the metals bind to them. We analyzed particle size distribution (PSD) of pollutants in H3 runoff in the size ranging from 1 to 1000 nm. Particles can be divided into colloidal (1–1000 nm) and non-colloidal (1–1000 μm). The results showed the proportion of colloidal particles varied between samples and storm events but was in a narrow size range for each event (Appendix H). Conversely, non-colloidal particles showed a broader size distribution with the largest fraction occurring between 10 and 100 μm (Appendix I).

5. Development of Site Suitability Map for Sitting Infiltration Trenches

BMPs are implemented for land at various locations (including highway segments) to mitigate negative impacts on surface water of diffuse pollution loading from stormwater runoff. This study focuses on one such practice—infiltation trenches. Infiltration trenches are one of several BMPs that the HDOT could implement in areas with pervious soils, limited space, and high land value.

Performance of infiltration trenches is found to be highly dependent on a number of site-specific conditions, including the hydraulic properties of surrounding soils, the soil’s capacity to attenuate pollutants, and design factors such as contributing drainage area and geographic location (Zhen et al., 2004; Perez-Pedini et al., 2005). Therefore, site suitability can be assessed considering all these factors. The following section provides a general description of how a suitability map can be developed based only on site constraints, using a geographic information system (GIS).

Several states have established various design criteria for infiltration trenches including site constraints and feasibility based on a guidance manual prepared by the US Environmental Protection Agency (US EPA, 1999; CASQA, 2003; DOH, 2007; CWP, 2010) (Appendix J Table 1). However, selecting the best locations for infiltration trenches based on these guidelines is not

easy when trying to simultaneously satisfy all the necessary conditions such as topography, land use, and proximity to water bodies.

Previous studies (Noh and Lee, 2003; Chen et al., 2010; Sener et al., 2010) have shown that GIS spatial overlay analysis is a robust tool useful in solving multi-criteria problems such as site suitability analysis and risk/vulnerability assessment. In spatial overlay analysis, multiple spatial GIS data layers, including the major factors affecting site feasibility or vulnerability, are merged into a single map (superposition of thematic layers) based on a relative ranking system. The relative ranking system combines weights (assigned to individual layers) and ratings (assigned to object classes in the layers) to compute a numerical value (or index) that produces a depiction of any area of interest in terms of suitability or vulnerability potential.

For this study, a two-level screening method (Figure 6) was employed to assess site feasibility for the location of infiltration trenches. This filtering process included both larger scale and smaller scale analyses to identify candidate sites because a successful feasibility analysis requires rapid initial site screenings, and later, detailed investigation of candidate sites identified by the initial screening. Figure 6 indicates the initial site selection determined by the overlay analysis using thematic layers (as discussed earlier) and an in-depth verification of the feasibility of candidate sites based on the results from both laboratory soil clogging experiments and numerical simulation by the HYDRUS-2D model, respectively (discussed in the following sections).

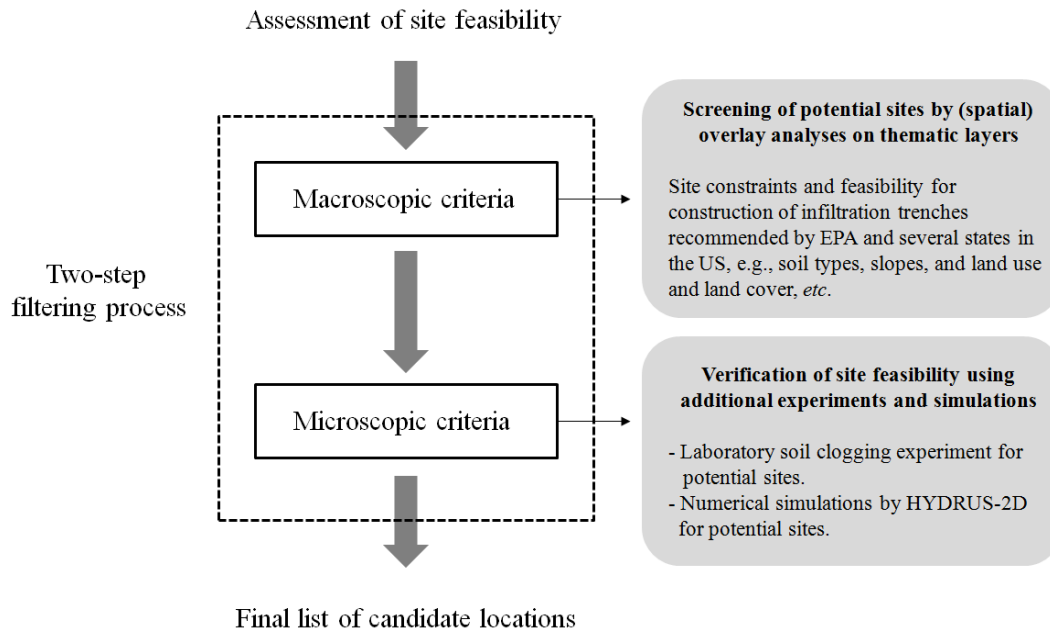


Figure 6. Two-level screening approach to identify candidate locations for implementing infiltration trenches.

In the initial site screening for infiltration trench sites, a total of four different overlay approaches were used to examine the effect of taking different approaches on site suitability determination. The overlay analyses included (1) two types of Analytic Hierarchy Processes (AHP) employed by Saaty (1980) and Sener et al. (2010) that differ in the assigned weights due to difference in

the rankings of important thematic layers by analyst (referred to as human preferences or subjective judgments); (2) Rank Order Centroid (ROC) analysis, used by Noh and Lee (2003); and (3) fuzzy logic, combining fuzzy membership and fuzzy overlay used by Joss et al. (2008). Both AHP and ROC, which slightly differ only in terms of weighting systems, assess site suitability by means of a weighted sum (or overlay) technique from weight and rating values.

This study mainly used seven thematic layers—including topography, land use, and proximity to public supply wells—from among the various criteria for site selection adopted by several states and the EPA in assessing site suitability for infiltration trenches (Appendix J Tables 1 and 2). Figure 7 shows our final site suitability index map as determined by one of the AHP processes (Appendix J Figure 4) using the seven layers. Most suitability maps developed from other overlay analyses were run repeatedly, indicating similar locations (except for two sites) as the best places for siting infiltration trenches (Appendix J Figure 4a). Figure 7 shows the best locations to install infiltration trenches according to this analysis.

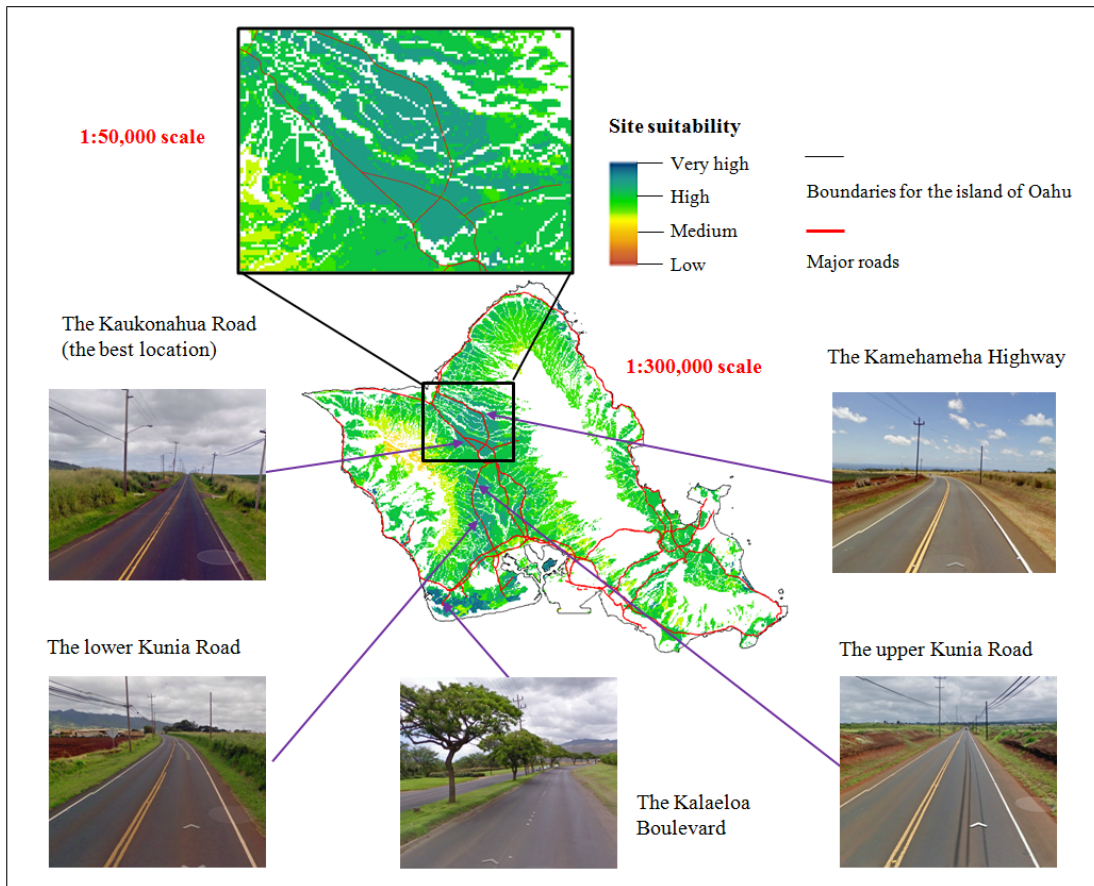


Figure 7. Best locations for implementing infiltration trenches on the island of Oahu. The final site suitability map is based on one of the results from an Analytic Hierarchy Process in Appendix J Figure 4. See Appendix J Figure 5 for higher resolution site suitability maps.

A series of site suitability maps were developed based on different overlay approaches. The results showed that applying different overlay approaches had a significant impact on site suitability determination (Appendix J Figure 4). In particular, both fuzzy logic and user preferences had large effects on the determination of site suitability, whereas only small differences were observed between the AHP and ROC analyses. Among the suitability maps created, we found that the site suitability map based on the results of the AHP analyses (shown in Appendix J Figure 4a) was superior, with respect to suitability scores calculated from the overlay/weightings, and because it indicated a greater number of suitable sites compared to the other analyses (total number of arrows indicated in each map). In conclusion, different overlay approaches may result in significantly different results, and it is recommended that various overlay approaches be employed and compared to improve the accuracy of the site suitability maps. Further study to determine which layers (e.g., rainfall in the area, pollutant attenuation capacity of soils) should be considered for inclusion in site suitability analysis is warranted.

6. Column Studies to Evaluate Clogging Potential

6.1. Introduction

Infiltration trenches are typically designed and emplaced using soil data from literature. Literature-reported hydraulic conductivity values are often based on the passage of clean water through soil. Hydraulic conductivity is a function of the number, size and continuity of the soil pores. If the fluid is not able to enter or leave these pores, hydraulic conductivity will be greatly reduced. There are certain processes that influence the usable pore volume or reduce the infiltration rate and cause soil clogging. These can include physical, chemical or biological processes. All of these processes probably occur to some degree in a typical subsurface infiltration system (i.e., a trench). Physical clogging is caused by accumulation of fine particles in pore throats or the formation of a cake layer at the surface of the soil. Once fine particles get lodged in pore throats, more and more particles get entrapped and this causes a reduction in hydraulic conductivity. Similarly, the formation of a cake layer on the soil surface will severely reduce hydraulic conductivity. Chemically induced clogging can occur due to the formation of insoluble precipitates in pore spaces. The growth of microorganism and their byproducts in pore spaces can also lead to clogging. A detailed description of clogging processes and other literature relating to clogging studies are presented in Appendix K. Information we obtained from these clogging studies will be useful in elucidating the long-term performance of stormwater infiltration trenches.

We conducted three types of clogging experiments: one involving four undisturbed soil cores (representing four of the fifteen soils) for shorter durations (one day) and simulating the filling and draining process of trenches, and the other, longer duration (1 month and more) clogging experiment with one soil. The soils used in the clogging study were taken from potential sites where trenches can be built (based on site suitability criteria and validation from our field experiments). Results of this study will show to what extent the hydraulic conductivity of the soil might be reduced by infiltrating stormwater from the H-3 highway, an elevated freeway not impacted by runoff from surrounding soils. In reality, more clogging can be expected if runoff from surrounding land joins runoff coming from highways.

6.2. Experimental Procedure

To simulate different conditions in an infiltration trench during storm events, we performed three types of experiments in the laboratory: a) intermittent flow experiments, b) one-step outflow experiments and c) long term infiltration-outflow experiments. The intermittent flow experiments were carried out to simulate intermittent rainfall events with continuous saturation of the soil. The one-step outflow experiments were designed to simulate a fully drained infiltration trench after a rain event. The long-term infiltration – outflow experiments were designed to study the effect of clogging under continuously saturated conditions in an infiltration trench such as over a prolonged period of rain. Details of these experiments are presented below.

6.2.1. Intermittent Flow Experiment

The intermittent flow experiments were conducted on four columns. The columns were periodically wetted and drained to imitate intermittent rainfall events. The columns were initially filled with stormwater runoff. Then, drainage was initiated by opening effluent valves at the bottoms of the columns. Unit head loss was monitored using a stopwatch while the water drained out of three columns. This process was repeated three times; on day zero, day three and day nine, at each of three different inflow rates (50, 100, and 125 ml/min). The hydraulic conductivity of the columns was calculated using Darcy's law. The reason for doing this experiment was to examine the effect of more rapid filling of the trenches as related to clogging.

6.2.2. One-Step Outflow Experiment

Using the same columns, similar experiments were subsequently conducted by setting the effluent level below the soil core. This resulted in free outflow and unsaturated conditions in the soil. The purpose of this experiment was to simulate a fully drained infiltration trench with unsaturated surrounding soil (a situation analogous in the field to a trench having water table significantly below its bottom). A peristaltic pump was used to supply a constant flow of stormwater and ensure full saturation of the column. Once the overflow level was reached the pump was stopped. Initially the column was filled with water and then a valve at the bottom was opened to allow the sample drain. Head losses during the one-step outflow experiment were monitored using 0.95 mm manometer tubes. The tubes were connected to the lowest ports located in soil and the unit head loss was monitored using a stopwatch. The effluent tubes were inserted at the bottom of the columns to ensure free outflow. Calculation of the outflow rate was achieved by weighing the effluent. Pressure heads were recorded every 60 seconds and balance data every five or ten seconds depending on the velocity of water flow. The experimental procedure was repeated three times for each column at zero, three, and six days with the same inflow rate and same settings for the effluent outlets.

6.2.3. Long Term Infiltration-Outflow Experiment

A long-term experiment was conducted for one column to simulate a long rainfall event. A peristaltic pump was used to ensure constant flow through and continual saturation of the column for a period of 25 and 49 days. The effluent was collected using a fraction collector. Calculation of the outflow rate was achieved by weighing the effluent. Pressure heads were monitored using microtensiometers.

6.3. Soil Sampling

6.3.1. For the Intermittent Flow and One-Step Outflow Experiments

Eight of the twelve soil orders occurring in the world are found on Oahu (Hue et al., 2006). We chose to sample the four primary orders; Oxisol, Andisol, Ultisol and Inceptisol that occur on Oahu from sites believed to be suitable for infiltration trenches. The specific locations were: North Shore (between Mahinaai St. and Oloho St. on Farrington Highway), Kunia (Upper Kunia Road after Hauula St.), Sandy Beach (8080 Kalaniana'ole Highway) and Pali (intersection of Pali Highway and Nuuanu Pali Dr.). Sampling locations are shown in Figure 8.

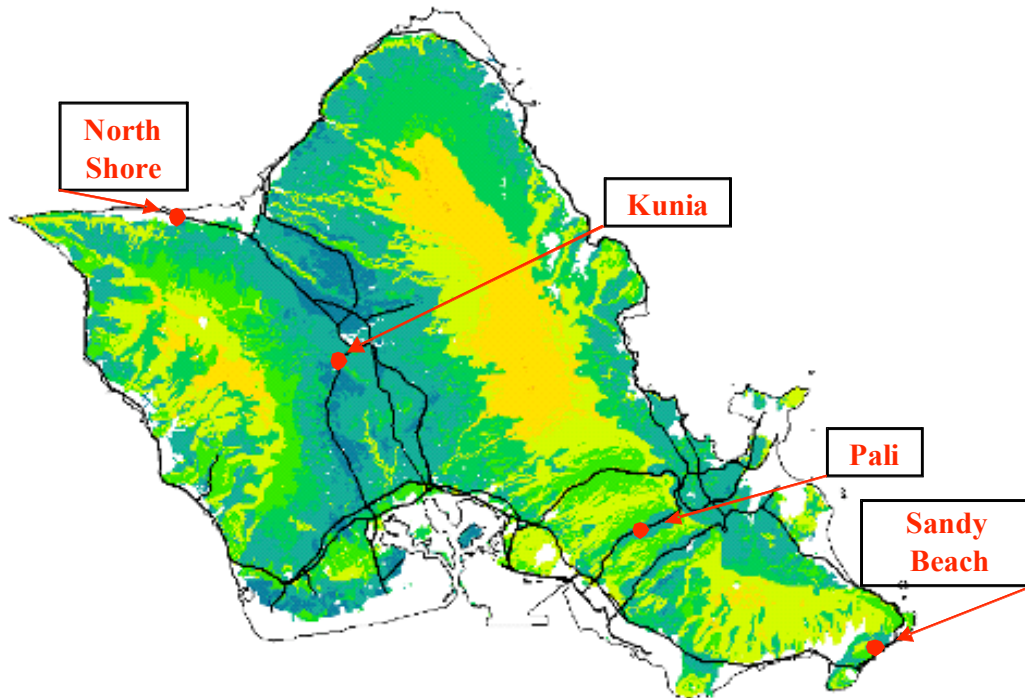


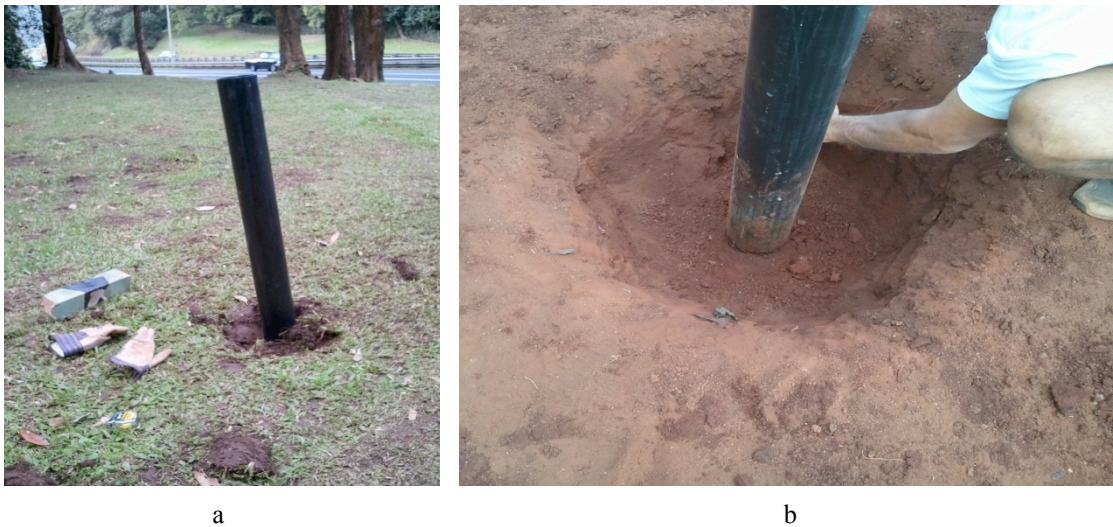
Figure 8. Locations of column sampling.

When collecting a sample, the area was cleared of debris such as leaves, twigs and litter, and then leveled. Because we needed undisturbed core samples and previous efforts to transfer core samples from the collection cylinder to PVC columns in the lab often disturbed the samples excessively, we drove the 125 cm long columns themselves into the soil (Figure 9).

6.3.2. For the Long Term Infiltration-Outflow Experiment

Two cores from Sandy Beach in East Oahu) were obtained by driving coring tubes into soil at least 1 m below ground surface. The soil from Sandy Beach is of the Koko silt loam series (KsB) (Foote et al., 1972), a mixture of silt, sand and clays, with a light reddish brown color. Attempts to obtain cores of Poamoho soil proved futile as the soil was too compacted to drive the columns into (Figure 10). The soil cores for this experiment were transferred into columns into long PVC columns in the laboratory using a press. The transferred soil cores were covered with gravel and

saturated with DI water containing 1 mmol CaCl_2 . Two long-term infiltration-outflow experiments were conducted on one of the columns from Sandy Beach.



a b
Figure 9. Collecting soil cores for column laboratory studies.



Figure 10. Collected soil cores from Poamoho.

6.4. Collection of Highway Storm Runoff

Laboratory experiments with synthetic and semi-artificial storm runoff have been reported in earlier studies (e.g. Mays, 2010, Hsieh and Davis, 2005). Hatt et al. (2007) discussed the general advantages and disadvantages of using artificial and real stormwater. Natural storm runoff is used when the physical, biological and chemical characteristics have to be truly representative, but handling and maintaining constant conditions are more difficult. Synthetic storm runoff is used to achieve greater consistency but is unnatural in composition. Semi-artificial stormwater made by using tap water and sediment from a stormwater pond sieved a certain particle size and amended with selected chemicals is a compromise between using real and synthetic stormwater.

To better address naturally occurring conditions on Oahu storm runoff was used in our experiments. Stormwater runoff from rain events was collected from an H3 storm drain near the Animal Quarantine Station in Halawa (Figure 11a, b). Characteristics of highway runoff are shown in Table 10. The stormwater was applied at the top of the soil columns. Before being introduced into the columns the runoff was filtered through a sieve with a mesh diameter of 850 μm to remove debris and prevent clogging of tubing.

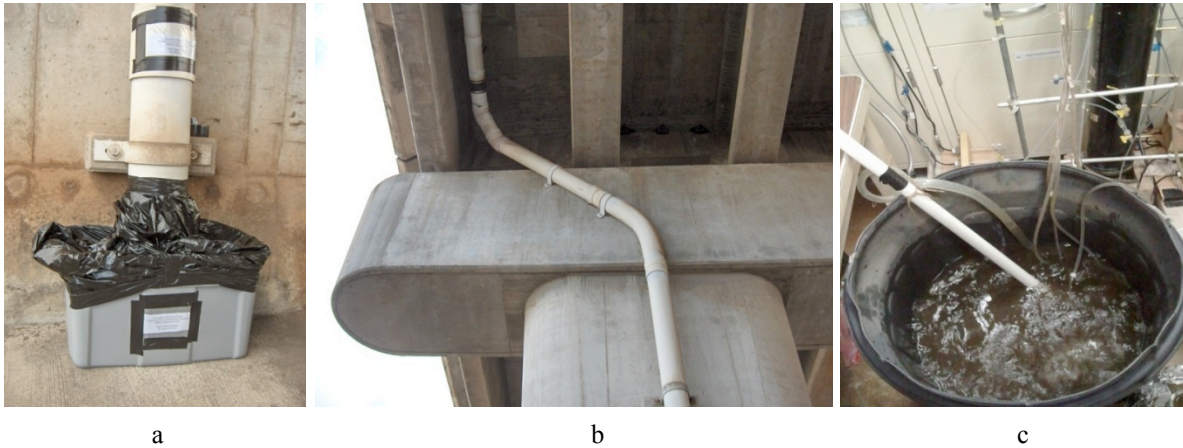


Figure 11. Collection of stormwater at H3; (a), (b), and (c) aeration of stormwater runoff dosed into columns.

Table 10. Characteristics of highway runoff water used in clogging experiment.

Constituents	Unit	H3–Halawa Highway runoff	
		Average	Range
pH	–	6.9	6.8–7.1
TSS	mg/L	72.4	1.5–155.0
TDS	mg/L	195.4	152.0–280.0
O ₂	mg/L	5.6	3.7–7.8
TU	NTU	18.8	2.8–33.6
Chloride	mg/L	26.11	10.5–43.9
Nitrate	mg/L	1.77	0.26–3.2
Phosphate	mg/L	0.8	0.04–0.13
Calcium	mg/L	30.9	22.41–43.49
Sodium	mg/L	20.53	9.82–31.47
Potassium	mg/L	0.97	0.69–1.44
Ni total	mg/L	3	1.0–5.3
Cu total	mg/L	20.8	9.1–39.0

6.5. Experimental Setup Design

6.5.1. Intermittent Flow and One-Step Outflow Experiments

We used a semi-automated setup for a) the intermittent flow experiments and b) the one-step outflow experiments (see Gardner, 1956; Kool et al., 1985). Four PVC columns (125 cm height,

10 cm diameter) with soil in the bottom 25 cm were instrumented in the laboratory (Figure 12). Thirteen cm of coarse sand (~ 0.7 mm mean diameter) was added on top of the soil, followed by 80 cm of pea gravel (2–4 cm diameter). The instrumentation included microtensiometers consisting of stainless steel cups (316L stainless steel, series 6500, Mott Corporation) inserted into the gravel, sand, and soil at various levels to monitor pressure heads in the composite columns. All of the tensiometers were connected to pressure transducers (236PC 15GW, Honeywell Microswitch) and connected via multiplexor (AM 416 Relay Multiplexor, Campbell Scientific) to a data logger (CR10X, Campbell Scientific). Highway runoff inflow was set at a constant rate (from 1.4 to 1.7 cm/min) using a peristaltic pump. The outflow was measured using buckets placed on load cells (AND GP 20K). The effluent was collected from the bucket to measure chemical parameters. 0.5 mm diameter manometer tubes filled with water were used to monitor head loss in the columns. These were connected to the side of each column at sampling ports located just above the soil. The effluent tube from the bottom of each column was raised to this level to ensure that the soil always remained saturated during the intermittent flow experiment. During the “flow” phases excess water went to an overflow port located 5 cm above the gravel layer. The experimental setup is shown in Figures 12 and 13. This experiment was designed to simulate the situation where a trench receives intermittent pulses of stormwater but the soil surrounding the trench remains essentially saturated. This situation could be expected to arise in areas of Oahu where the soil does not drain rapidly and there are frequent rainfall events.

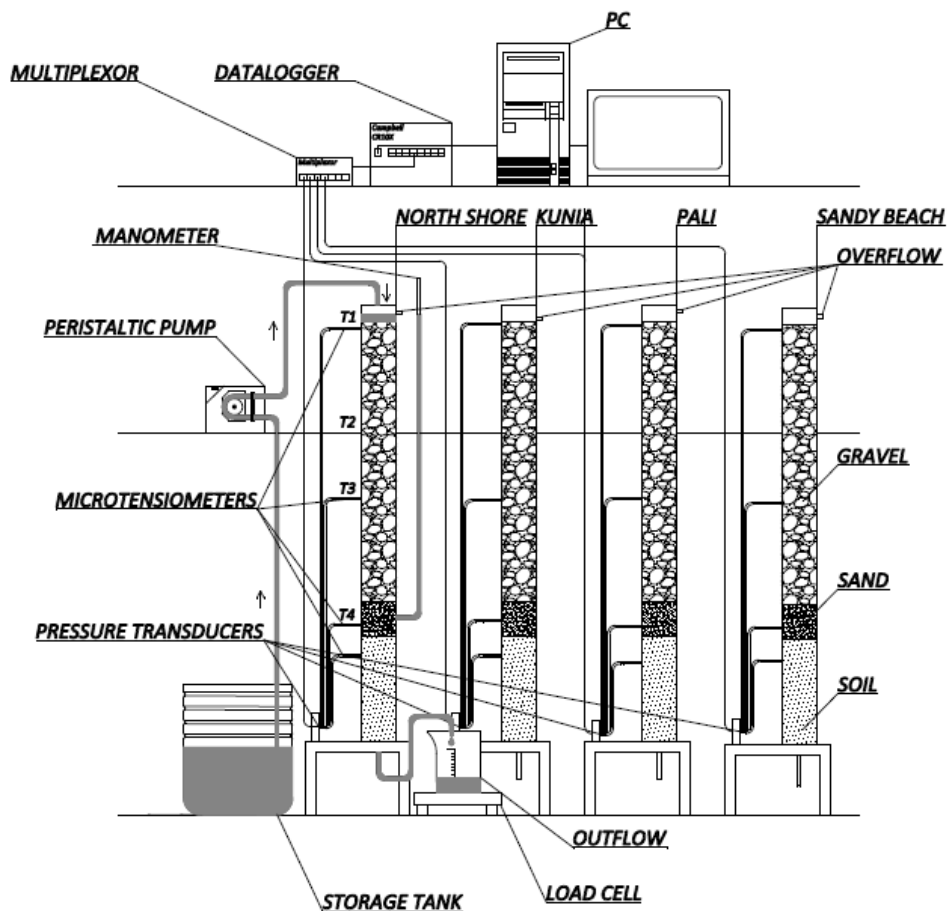


Figure 12. Schematic of the experimental setup for four columns.



Figure 13. Laboratory setup of four columns connected to data-logger for intermittent and one-step outflow experiment.

6.5.2. Long Term Infiltration-Outflow Experiment

The experimental setup consisted of columns containing 25 cm of undisturbed soil core covered by a 0.97-meter gravel layer to simulate conditions comparable to those in infiltration trenches (Figures 14 and 15). Pressure transducers connected to microtensiometers were inserted in the soil cores to allow monitoring of hydraulic head loss while clogging occurred. A constant water level was maintained by means of an overflow drain located near the top of the column. Input water consisting of highway runoff was continuously stirred in order to maintain homogenous concentrations of particulates and other contaminants. This water was fed into the top of the columns for a period of 25 and 49 days. The flow rate was calculated by weighing the outflow. Each experiment was terminated when the outflow asymptotically approached zero. Tensiometers placed in the soil were connected to a data logger that recorded every five seconds. A complete characterization of influent and effluent quality parameters, including pH, turbidity, particle size distribution (PSD), total dissolved solids (TDS), dissolved organic carbon (DOC), total organic carbon (TOC), anions, cations was done. However, TSS was deemed to be the main parameter defining clogging since the TSS capture mechanisms in infiltration trenches are important for making design and maintenance recommendations. TSS is usually the target pollutant for stormwater BMPs.

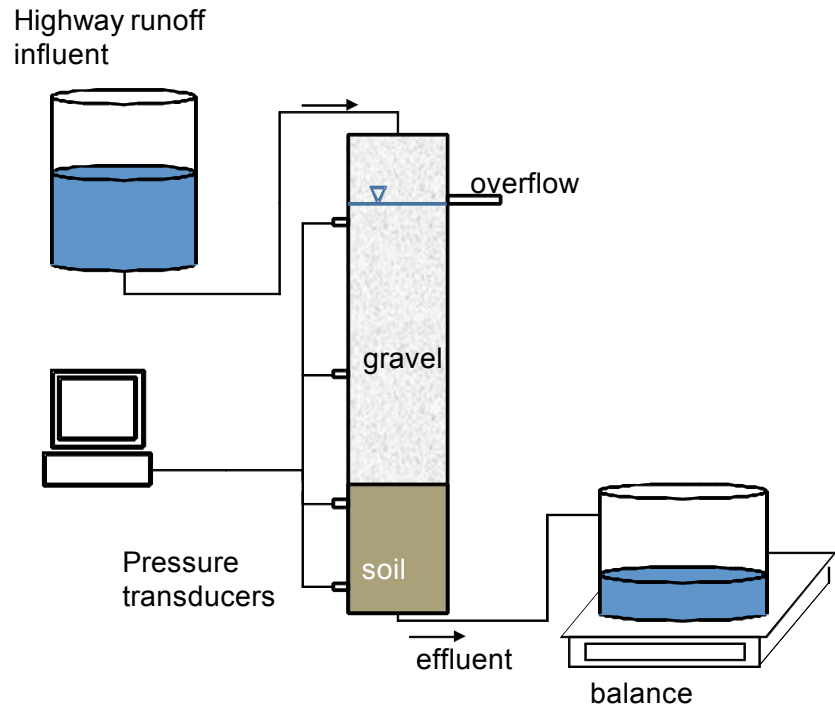


Figure 14. Schematic view of experimental setting.

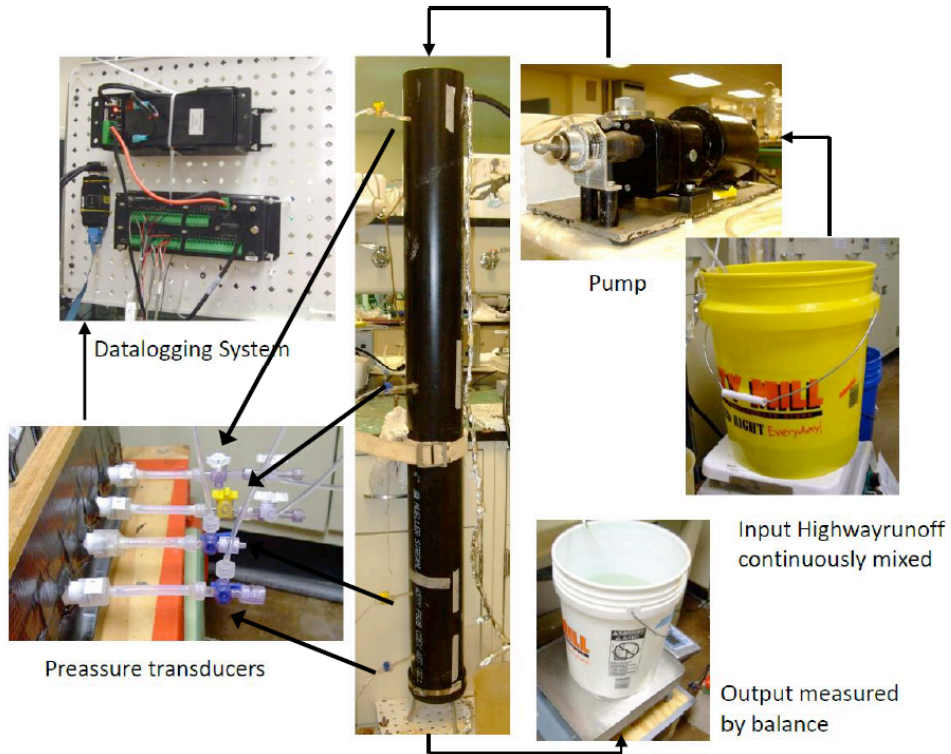


Figure 15. Experimental setup to measure reduction of hydraulic conductivity in soil column.

6.6. Results and Discussion

6.6.1. Intermittent Flow Experiments

6.6.1.1. Hydraulic performance

Two different phenomena were observed when the columns were subjected to flow/no flow cycles. Upon reestablishing flow through the columns on day three, the microtensiometer data indicated that the deposited particles had been drawn down to the gravel-sand-soil or sand-soil interfaces.

Flux data indicated clogging occurred in the column. Physical evidence of a clogging layer and the effluent flow rate profile indicate that loss of hydraulic conductivity was due primarily to a cake layer formed at the top of the gravel layer by the deposition of suspended solids over time. Sandy Beach soil is derived from volcanic ash - dominated by fine particles (68 % silt and 20% clay), and the suspended solids in natural stormwater are predominantly particles of sizes similar to this. Because of this, self-filtration due to deposition of these similarly sized particles may have caused clogging in this column. While the Sandy Beach column clogged the most, the least clogging occurred in the Pali soil compared to the other three columns (Table 11). Kunia soils are highly weathered and have high clay and metal oxide content. It is expected that these soils will clog rapidly. It has been shown that clogging occurs in soils rich in clay minerals due to the deposition and leaching of fines (Frenkel et al., 1978; Pupisky et al., 1979; Pignon et al., 2000; Santiwong et al., 2008).

Table 11. Summary of K values during intermittent flow experiments.

Column	Flow rate (ml/min)				Decrease in K in 9 days (%)
	50	100	125	Average	
NS-0d	114.3	111.5	123.9	116.5	
NS-3d	115.5	103.5	99.9	106.3	
NS-9d	109.4	120.2	78.2	102.6	12
SB-0d	84.8	67.6	30.6	61.0	
SB-3d	34.6	30.2	28.9	31.3	
SB-9d	31.9	27.0	42.7	33.9	44
K-0d	124.1	130.2	72.9	109.0	
K-3d	88.5	95.1	81.3	88.3	
K-9d	83.9	86.2	42.7	70.9	35
P-0d	125.2	112.7	137.6	125.2	
P-3d	137.0	117.7	107.3	120.7	
P-9d	117.4	112.7	114.6	114.9	8

The changes in hydraulic conductivity during the flow/no flow cycles are shown in Figure 16 and summarized in Table 11.

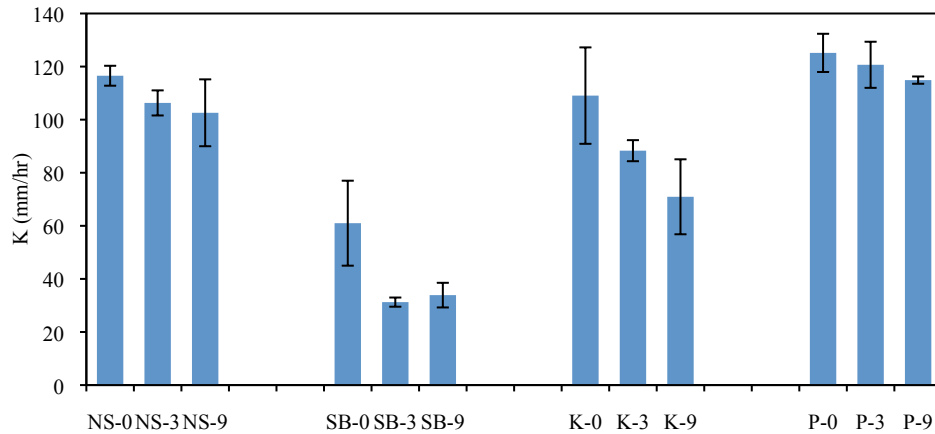


Figure 16. Average hydraulic conductivity values during intermittent flow experiments in four columns. (NS = North Shore, SB = Sandy Beach, K = Kunia, P = Pali; error bars represent standard deviation)

There was visible cake formation on the top of the gravel layer due to the accumulation of particulates and sediment from the stormwater influent, which caused reduction in hydraulic conductivity indicative of physical clogging. The Sandy Beach and Kunia cores had the greatest reductions in hydraulic conductivity. The clogging layer that formed atop the Sandy Beach column is shown in Figure 17a and Figure 17b.

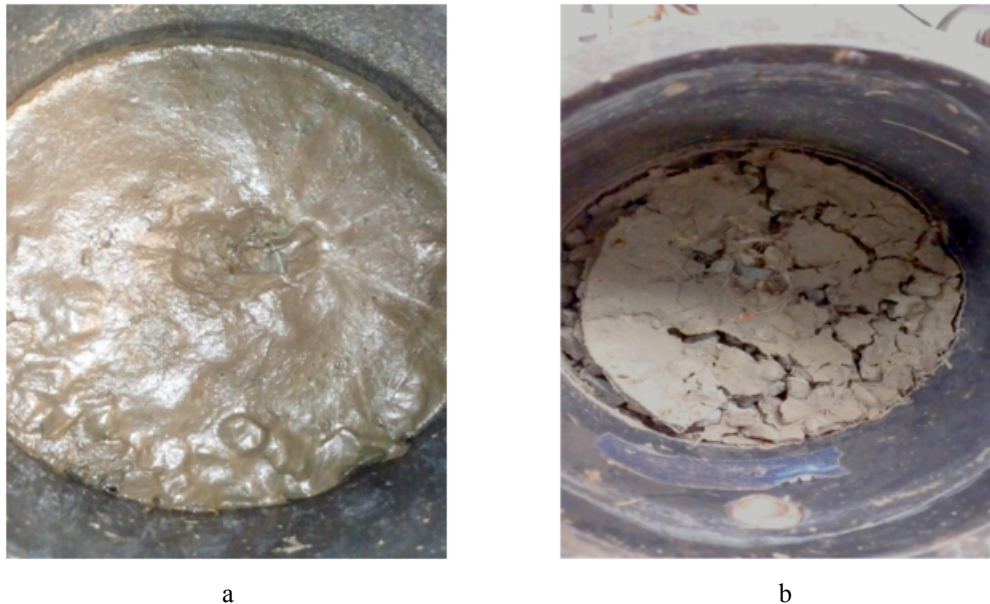


Figure 17. Clogging layer during (a) the wet cycle, and (b) after nine days of drying.

6.6.1.2. Pollutant removal efficiency

Four metals – total Fe, Zn, Al and Mn were analyzed (shown in Appendixes N, Q, T, and W) to ascertain the pollutant removal capability of the soils during intermittent flow. All the soils

removed Fe to about the same extent from 0.086 mg/L in the influent to less than 0.01 mg/L (81%) in the effluent within the first three days of the start of intermittent flow.

Kunia soil has high concentrations of clay minerals (kaolinite) and iron/aluminum/manganese oxides. In our experiments the Kunia soil column effluent had a high concentration of Mn (0.29 mg/L), about 49 times higher than the 0.06 mg/L measured in the influent (Appendix N). Leaching of Mn from this soil has been studied by various researchers (Golden et al., 1993; Hue et al., 2001). After being subjected to just three days of flow/no flow cycles, the concentration in the effluent dropped to 0.005 mg/L. Some studies have shown that reduction of Mn (IV) to Mn (II) occurs when soil columns are subjected to intermittent flow. Intermittent flow of soil increases the solubility of Mn (Fujimoto et al., 1946; Goldberg et al., 1984). The later decrease in Mn concentration in the effluent may have been due to the presence of organic matter or clay minerals to which the soluble Mn could have attached and complexed in this soil .

It was found that there were no changes in Al or Zn concentrations in any of the soil columns except for Zn in the Pali column (Appendixes N, Q, T, and W). The location where the Pali sample was taken receives high rainfall, far exceeding the evapotranspiration rate, and hence leaching of nutrients has occurred in the soil. At the end of flow cycle on day three, it was observed that the Zn concentration in the effluent was 50% that in the influent. Finally at the 9th day of intermittent flow the effluent concentration of Zn was similar to the influent concentration. For Mn in the Pali column, the effluent concentration slightly increased from 0.06 mg/L to 0.08 mg/L after three days of drying, which subsequently decreased to 0.036 mg/L and 0.034 mg/L at days three and nine respectively we believe because of the previously mentioned reasons.

The Sandy Beach and North Shore, soils removed 82% of Mn in the influent and intermittent flow did not cause significant changes in the Mn removal capacity (Appendixes T and Q).

For all the soils we studied there were higher concentrations of some anions and cations analyzed in the effluent stormwater. For example chloride concentration in the effluent from the Kunia soil was 141 mg/L compared to only 54 mg/L in the inflow stormwater. Similarly sodium measured 77 mg/L in the column effluent compared to 33 mg/L in the influent. These values indicate that ions that are already present in the soil, probably due to agricultural practices, could leach from the soils with stormwater.

Solids removal was observed in all the columns. The removal of solids was consistently between 85 % and 95%. Turbidity was used to measure solids removal. There was an increase in the dissolved solids eluting from the column. In some columns the effluent TDS was higher (Kunia, Sandy Beach) (see Appendixes L and R), while in others (North Shore, Pali) (Appendixes O and U), the TDS was lower than the influent during the intermittent flow. It is believed that the higher TDS seen was due to the leaching of ions from the soils after non-flow periods.

6.6.2. Results of One-Step Outflow Experiment

One-step outflow experiments (e.g. Gardner, 1956; Kool et al., 1985)—where the inflowing water was stopped and the columns allowed to drain were conducted in the same columns as the intermittent flow experiments were done. Our laboratory experiments simulated infiltration in one dimension similar to experiments conducted by Hatt (2007); Hatt et al., (2008); Li and Davis (2008a).

Each column was wetted periodically. Drying periods took place between each wetting period. The intention was to mimic natural conditions in an infiltration trench in an area where the ambient water table is below the infiltration trench. The columns were filled to the top and subsequently allowed to empty. At first, collected highway storm runoff was pumped into each column at a constant flow rate to fill the columns until water flowed out the overflow outlet. The experimental run was then started by opening the effluent valves at the bottoms of the columns. The volume of effluent was monitored using a bucket placed on a balance. The outflow rate was calculated from the weight of the effluent. The head losses were recorded using pressure transducers and observed from manometer readings. For all runs, changes in pressure head, weight of outflow, unit head losses, and water quality parameters (TSS, TDS, TN, TOC, DOC, anions and cations) were measured. A summary is given in Appendixes HH and II.

Using manometer readings to determine the loss of hydraulic head and the rate of outflow, it was observed that flow velocity was reduced between the different materials in the columns (sand, gravel, soil) for all columns (see Figure 18). Cake layers forming on the surfaces of the columns retarded flow. A similar retardation effect was observed at the gravel/sand interfaces. The decrease of outflow rate at the gravel/sand interfaces may have been due to the deposition of particles in pores, different material properties or the presence of entrapped air (Faybishenko, 1995). When the soil was repeatedly drained and re-saturated over a short period of time, air could have become trapped in pores. On the other hand, if a less permeable layer was present, the air might have been confined behind it. In our case, we believe that when the sand layer became clogged by fine particles it behaved like a less permeable layer. Table 12 shows the time duration of all runs. Extremely slow drainage was observed during the 2nd and 3rd runs for the Sandy Beach column. Slightly slower drainage was also observed in the North Shore column during the 2nd and 3rd runs in contrast to the Kunia and Pali columns where the 2nd and 3rd runs were accelerated.

Table 12. Duration of the experiments.

Column	Run Time (min)		
	1	2	3
North Shore	9.0	10.5	10.7
Kunia	17.8	9.5	9.7
Pali	7.7	8.7	7.6
Sandy Beach	49.6	72.8	73.2

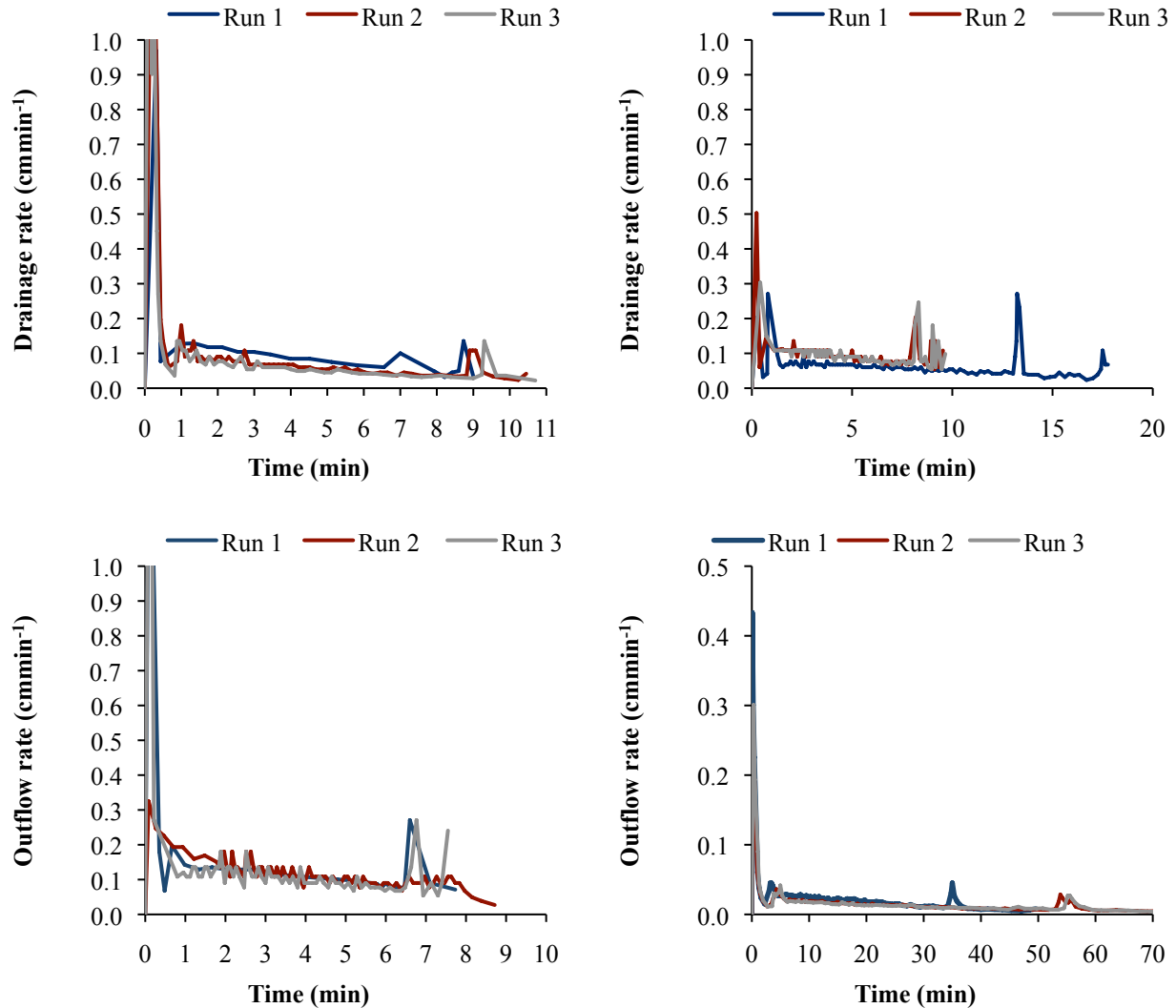


Figure 18. Outflow rates for the 1st, 2nd, and 3rd runs of wet/dry cycles of the North Shore, Kunia, Pali and Sandy Beach.

Appendix Y shows the hydraulic heads at four points along the column over time for the North Shore, Kunia, Pali and Sandy Beach soil columns respectively. The hydraulic head in the gravel (T1) for the North Shore column did not show significant change. A slight decrease of hydraulic head was observed in the gravel (T1) in the Kunia, Pali and Sandy Beach columns. After the water level declined, hydraulic heads approached zero or slightly positive pressure indicating wet or saturated conditions. In the case of the second tensiometers inserted in gravel (T2), after a gradual decline corresponding to the decreasing water level, the values reached zero or a slightly positive pressure, except for the Sandy Beach column. The Sandy Beach column showed development of a slight negative pressure. Siriwardene et al. (2007) found that sediment particles less than six μm in diameter are the main driver in the development of clogging layers. They also found that larger particles are able to reach the gravel/sand interface. Delayed responses were seen at tensiometers T2, T3 and T4 during the 2nd and 3rd runs in the North Shore and the Sandy Beach columns.

Appendixes Z, AA, BB, and CC show the changes in pH in all columns. Measurements of pH in the influent and the effluent showed that there were changes in pH during all runs. It was observed that the pH of the effluent decreased compared to the influent. Influent pH ranged from 7.38 to 7.63 and the effluent pH ranged from 6.43 to 7.46. Changes in pH can be attributed to dissolution of calcite or exchange of H^+ ions from solution to matrix (Blume et al., 2002).

Conductivity is a numerical expression of the ability of an aqueous solution to carry an electrical current (ASTM, 1985). It is dependent on the presence of ions, their total concentrations, and aqueous temperature (ASTM, 1985). Appendixes Z, AA, BB, and CC show the electrical conductivity of the influent and the effluent for all columns. In the Pali, Kunia and Sandy Beach columns, the electrical conductivity of the effluent was always higher than it was in the influent. The highest conductivity was obtained after the 1st run and decreased during the 2nd and 3rd runs. In the North Shore column electrical conductivity of the effluent increased with respect to the influent with each run. A possible explanation could be that an abrupt change in soil solution caused particle release (Blume et al., 2002).

Turbidity expressed in terms of nephelometric turbidity units (NTUs) was recorded for the influent and effluent for all columns. The columns were highly efficient at particle removal (Appendixes Z, AA, BB, and CC). The turbidity of the influent was in the range of 60 to 174 NTU corresponding to 90–347 mg/l of TSS. The wide range of influent turbidity was mainly due to inconsistent aeration of the solution in a storage tank. The turbidity and total suspended solids were reduced by up to 1.7 NTU as the solution infiltrated through the columns. It is evident that the turbidity and concentration of total suspended solids decreased rapidly in all runs.

Initially, clogging cakes formed on the surface of the gravel (see Figure 17). Similar observation of layers forming on column surfaces was made by Li and Davis (2008a). The decrease of the infiltration rate due to deposition of sediment in the voids between filter media particles was also observed by Kandra et al. (2010). The reduction of turbidity clearly indicates deposition of suspended solids in our columns.

6.6.3. Long Term Infiltration-Outflow Experiment

Two infiltration-outflow column experiments were conducted for the Sandy Beach soil (East Oahu). Figure 19 shows the hydraulic conductivity during the first and second infiltration-outflow experiments for the Sandy Beach soil. The hydraulic conductivity decreased during both the first and second infiltration-outflow experiment (conducted over 25 and 49 days respectively). The hydraulic conductivity was reduced by 56 percent within 25 days during the first experimental run. The inflow of water was temporarily stopped between the first and second runs and the caked old gravel was replaced with new gravel and the sediment trapped in each layer was measured. Hydraulic conductivity of the core during the second run was slightly improved by the replacement of the gravel (see Figure 19), but declined again in a few days approximately within five pore volumes. During the 49 days of the second experiment, during which time 53 pore volumes were passed through, a 75% reduction of hydraulic conductivity occurred, reducing the initial flow rate of 0.4 m/d to 0.1 m/d.

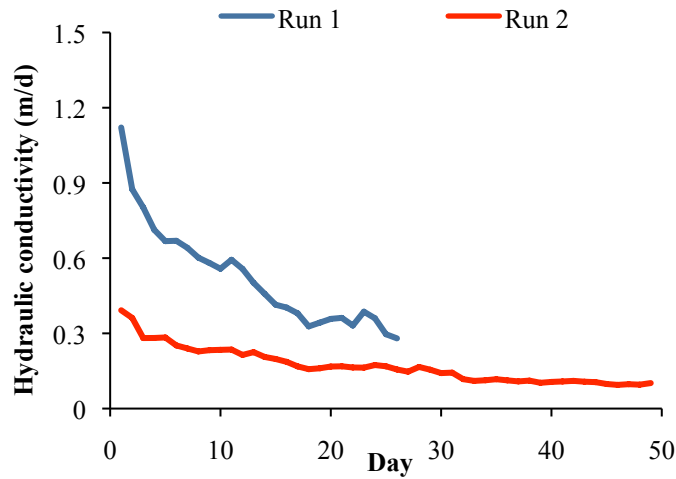


Figure 19. Results of clogging column experiments (in Sandy Beach soil) and soil clogging experiments; shows decreasing hydraulic conductivity for Run 1 (first run) during 25 days, and Run 2 (second run) during 49 days.

Appendix KK shows the inflow and effluent concentrations of: electrical conductivity, turbidity, TDS and TSS for 49 days of the experiment. Input and output measurements of electrical conductivity and TDS show a similar trend Appendix KK. A decrease in ionic strength of infiltrating water is known to cause particle release, since higher salt concentrations correspond to increased attraction forces and augment attachment between soil matrix and fine particles. This particle release can either lead to an increased permeability due to washing out the particles, or to a decrease, when pore necks are blocked by fine particles (Blume et al., 2002). High removal efficiency for both target pollutants can be seen. The removal efficiency increased with the duration of the experiment. After fourteen days turbidity was reduced below 1 NTU irrespective of influent turbidity (Appendix KK).

At the end of the first experimental run, 27 cm of gravel was removed in three discrete layers, and the sediment that had collected on each layer was removed and measured. From these measurements (Figure 20, Table 13), it was found that 60 percent of the removed sediment was trapped in the top layer of column (within a depth of 7 cm), and only 7 % of the total sediment settled at a depth greater than 15 cm. The total 27 cm of gravel contained 2919.4 g of gravel (dry mass) and 58.6 g of particles (dry mass).

Figures 21 and 22 shows the development of clogging layer on the top of the gravel.

Table 13. Characteristics of highway runoff water used in clogging experiment.

Layer	Layer thickness (cm)	Sediment per layer (g/cm)	Sediment per gram of gravel (g/g)
1	0–7	4.97	0.0497
2	8–15	2.45	0.0251
3	16–27	0.35	0.0029

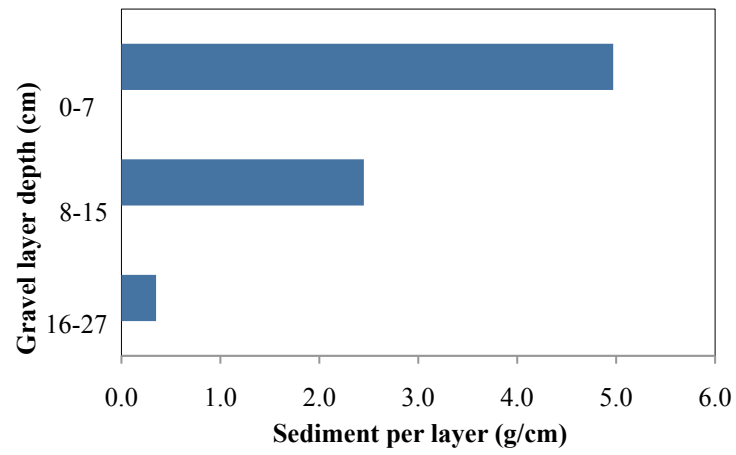


Figure 20. Accumulation of sediment in gravel layer.



Figure 21. Image of development of a clogging layer in soil column.



Figure 22. Cracked clogging layer after five days of column during dry cycle.

In the second run, clogging of the tubing caused by the particles in the influent stopped the pump from operating several times. Free drainage of the column was induced. After installation of a new peristaltic pump it was possible to obtain results after 49 days of operation without flow interruption.

Influent and effluent concentrations of anions and cations indicate that leaching of ions from the soil occurred. Appendix LL shows the observed concentrations. Sampling of the effluent only started one day after restarting the column because a sampling volume of approximately one liter was required to get a significant concentration of TSS. The last sample was collected during drainage of the column when no water was being fed in. Concentrations below detection level are shown as zero. Nitrate concentrations in the influent exceeded effluent concentrations indicating ongoing nitrate reduction. The nitrate concentration in the effluent was found to be reduced after twelve days of flow. Over a period of five days (Sept 12th –Sept 16th 2011) input concentrations averaged 8.5 mg/L, while effluent concentrations below 0.5 mg/L. Input oxygen concentrations were high because the reservoir of influent was constantly stirred. Neither nitrite nor ammonia was found in the influent.

7. Modeling of Water Movement from a Potential Trench Site Along Oahu's Highways

- The scope of this modeling study is to conduct predictive simulations of water movement from an infiltration trench under wetting and drying conditions and various operational conditions of the trench.
- The location of the water table with respect to trench bottom and the height of water in the trench were used to determine time needed to drain a given volume of water.
- Numerical models are particularly helpful for comparing systems with complex geometries, and initial and boundary conditions.

Water flow in trenches is predominantly three-dimensional (3D) and it includes saturated and unsaturated zones depending on the location of the water table and the amount of water entering the trench. Unsaturated flow simulations in 3D are difficult and time consuming. It is sufficient to analyze the infiltration process using two-dimensional (2D) numerical models for variably saturated flow in a porous medium. The S 2D model (Vogel et al., 2000), the predecessor of the HYDRUS 2D (Simunek et al., 2006) was used for our simulation of the operation of the trench. This code is based on two-dimensional form of Richards' equation for water flow. The governing equation is solved numerically using the finite element method. The model is also capable of predicting transport of water-dissolved chemical species. However, this option was not used in this modeling effort as all the heavy metals under study (i.e., Cd, Co, Cr, Ni, Pb) showed strong sorption properties in the laboratory batch experiments on Oahu soils.

7.1. Simulation of Infiltration for Different Soils

For simulation, we used a hypothetical gravel-filled trench 100 cm deep and 100 cm wide. Because of symmetry, only half of the trench was considered since the center line of the trench is an axis of symmetry. All calculations are based on unit length of the trench (since it is a 2D

simulation). The depth and width of the 2D simulated flow domain (the soil surrounding the trench) are 300 and 250 cm, respectively (Figure 23), representing a one cm thick vertical slice through the system. A total of fourteen different soil types were obtained from a soil survey we conducted along highways on Oahu (Table 14).

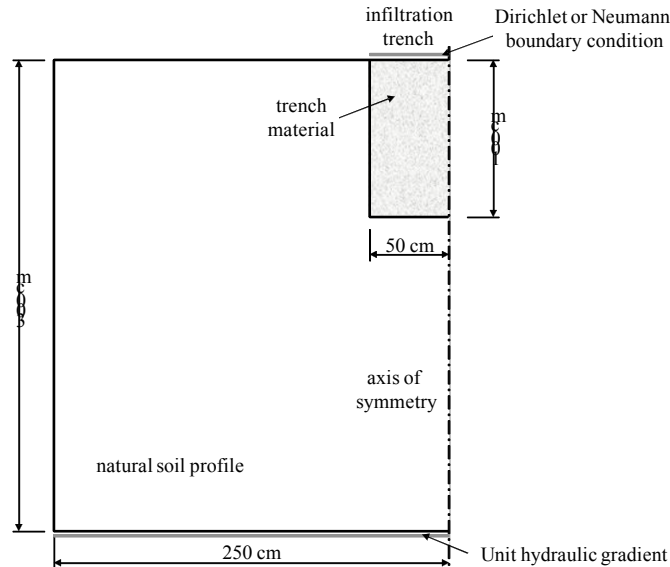


Figure 23. Dimensions of flow domain.

We assumed homogeneous soil profiles surrounding the trench. Soil hydraulic functions (retention curve and hydraulic conductivity) were described using a modified van Genuchten model (Vogel and Cislérova, 1988; Vogel et al., 2001), available in the HYDRUS model. Assuming the water table was some depth below the trench, the initial pressure in soil was set to -150 cm in the whole computational domain. The domain was divided into 23,501 triangular finite elements. The finite element mesh was refined along the vertical and horizontal boundaries of the trench where high water fluxes are expected. An important assumption for the simulations is the water level in the trench. In reality, the level of water in an actual trench is not fixed but fluctuates in response to runoff events. The simulation was done assuming the trench to be running full, 100 cm deep. The boundary condition defined the hydrostatic pressure from 0 cm at the top to 100 cm at the bottom. It means that the trench is filled fully with water. It is important to note that the setting of the boundary conditions for the trench is a simplification of a real system. Free drainage condition was used for the lower boundary of the simulated domain. All other boundaries of the domain were treated as no-flow boundaries (Neumann condition).

Water storage capacity of the gravel of the full infiltration trench was set to $0.40 \text{ m}^3/\text{m}^3$ assuming 40 % total porosity. For modeling the symmetrical half, considering a unit length of 1 cm of the trench, the maximum total water storage capacity in this half for complete filling is 2 liters of water. This volume gets rapidly filled during a storm event since the gravel has high saturated hydraulic conductivity. According to HDOT guidelines (State of Hawaii, 2007a), trenches are required to fully de-water their entire water volume within 48 hours after a storm event. The emptying time is primarily influenced by the properties of the surrounding soil, not by the gravel

material. Thus, the time required to drain the trench of 2 L water volume was determined for each soil.

Table 14. Soil hydraulic characteristics of fourteen different soil types used in the simulations.

Location	Soil type	K_s (cm h ⁻¹)	θ_r (-)	θ_s (-)	α (cm ⁻¹)	n (-)	l (-)	h_s (cm)
H3–Kamehameha IC	Kaneohe	18.4	0.00	0.52	0.027	1.09	6	-2.27
H3–H1 IC	Kawaihapai	1.5	0.00	0.46	0.018	1.27	0.5	-2.06
Likelike H1 IC	Kaena	13.6	0.00	0.50	0.028	1.17	0.5	-1.67
H1–University Ave.	Makiki	35.1	0.00	0.53	0.023	1.15	6.5	-1.10
H1–Moanalua Rd.	Molokai	5.6	0.28	0.50	0.018	1.30	9	-2.73
H1–H2 IC	Waipahu	15.1	0.00	0.54	0.020	1.22	0.5	-1.18
Pali–Kamehameha Hwy.	Alaeloa	3.8	0.29	0.48	0.160	1.48	2	-0.39
H1–Kamehameha Hwy.	Makalapa	41.2	0.36	0.65	0.040	1.11	8	-1.23
H2–Kauka Blvd.	Helemano	24.8	0.00	0.43	0.050	1.19	4	-1.87
Kamehameha–Waialua Beach Rd.	Ewa	21.7	0.00	0.54	0.010	1.15	2	-2.49
Pali from Ahi Pl. to tunnel	Lolekaa	3.5	0.20	0.53	0.020	1.25	7	-1.76
H1–Kalaehoa Blvd., point 1	Honouliuli	10.0	0.20	0.46	0.020	1.63	0.5	-2.96
H1–Kalaehoa Blvd., point 2	Honouliuli	88.9	0.09	0.56	0.060	1.12	6	-2.56
H1–Kalaehoa Blvd., point 3	Honouliuli	46.7	0.00	0.52	0.020	1.12	0.5	-1.39
Sandy Beach Park	Koko	7.1	0.20	0.47	0.020	1.25	0.5	-2.07
Likelike–Kahekili Hwy.	Hanalei	73.6	0.00	0.43	0.040	1.06	6	-3.67

Note: Measured saturated water content θ_s , estimated saturated hydraulic conductivity K_s , residual water content θ_r , and van Genuchten fitting parameters (α , n , l) for soils along highways Oahu. Fitting parameters α , n , and l were estimated using the RETC program of van Genuchten et al. (1991). Air-entry value h_s was estimated according to Vogel et al. (2001).

Table 15 shows simulated times required for infiltration of stormwater. The simplified selection of the boundary condition for the trench leads to shorter simulated times than would be seen in reality, i.e. the assumption of a completely full trench during the simulations would be fulfilled only in large runoff events. All soils, except for the Kawaihapai soil at the H3-H1 interchange, which had the smallest value of, saturated hydraulic conductivity, showed infiltration times less than two hours (Table 15). HDOT guidelines (State of Hawaii, 2007b), recommend that soils should have infiltration rates higher than 0.52 inch/hour (1.3 cm/hour) to be suitable for construction of infiltration trenches. The Kawaihapai soil is close to this limit (1.5 cm/hour, Table 14). The shortest infiltration time was seen for Honouliuli soil at H1–Kalaehoa Boulevard, point 2. The differences in infiltration times between this and the Kawaihapai soils are primarily caused by differences in the saturated hydraulic conductivity (K_s) of the two soils (Table 14).

Table 15 is further supplemented by Figure 24, where total cumulative flux (bottom and sidewall contributions) through the trench for all simulated soils is shown. Graph shows needed time to empty the trench of given size and volume of 2 L.

The bottom and sidewall contributions to total cumulative flux from the infiltration trench for Kawaihapai soil are depicted in Figure 25.

Pressure head distribution in the simulated domain for the two soils (Honouliuli point 2 and Kawaihapai) after infiltration of 2 L volume of stormwater is depicted in Figure 26.

Table 15. Simulated times required for infiltration of 2 L of stormwater.

Location	Soil Type	Infiltration time (min)
H3–Kamehameha IC	Kaneohe	19.01
H3–H1 IC	Kawaihapai	208.03
Likelike H1 IC	Kaena	20.80
H1–University Ave	Makiki	8.73
H1–Moanalua Rd	Molokai	62.46
H1–H2 IC	Waipahu	17.48
Pali–Kamehameha Hwy	Alaeloa	72.43
H1–Kamehameha Hwy	Makalapa	9.39
H2–Kauka Blvd	Helemano	10.83
Kamehameha–Waialua Beach Rd	Ewa	15.63
Pali from Ahi Pl to the tunnel	Lolekaa	90.18
H1–Kalaeloa Blvd, point 1	Honouliuli	24.24
H1–Kalaeloa Blvd, point 2	Honouliuli	3.32
H1–Kalaeloa Blvd, point 3	Honouliuli	7.19
Sandy Beach Park	Koko	46.83
Likelike–Kahekili Hwy	Hanalei	5.32

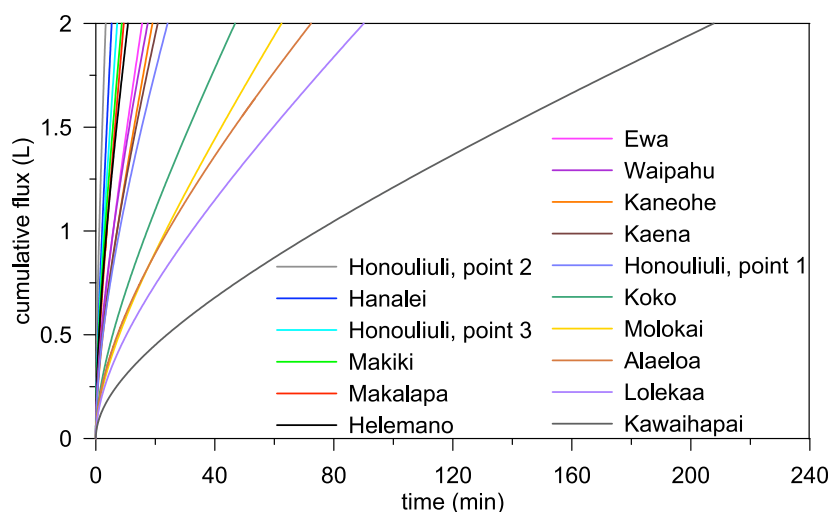


Figure 24. Cumulative flux through the trench for the simulated soils.

Our simulation indicated that all the sampled Oahu soils, except Kawaihapai, would require less than two hours draining our hypothetical trench filled with stormwater. Therefore, these soils are potential candidates for construction of infiltration trenches as a possible BMP.

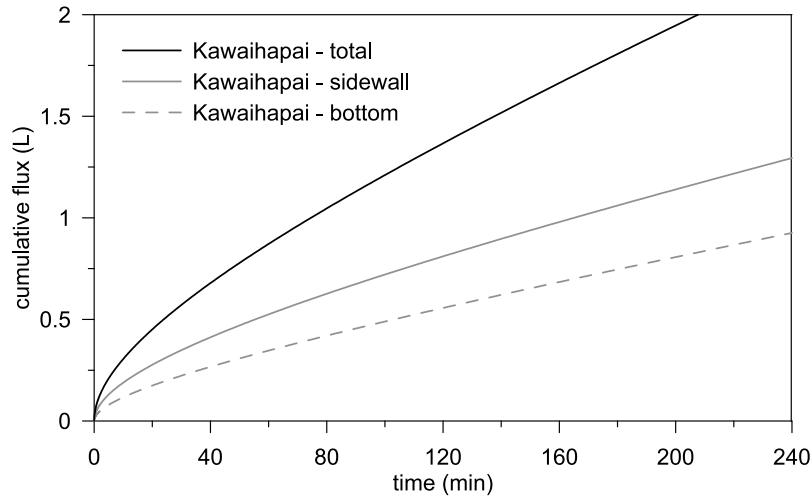


Figure 25. Cumulative flux through the sidewall and bottom of the trench for Kawaihapai soil.

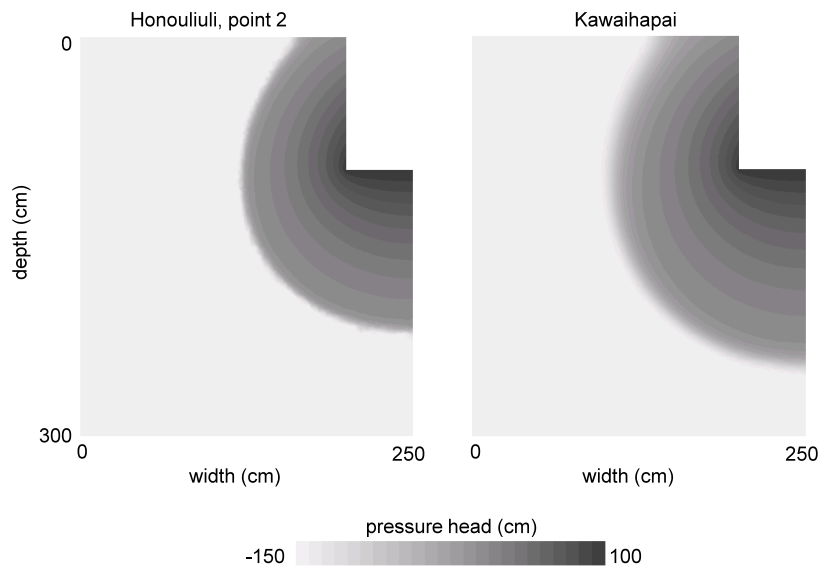


Figure 26. Pressure head distributions in simulated domain for two soils after infiltration of 2 L volume of stormwater. Dark grey represents high saturation with water; light grey represents dry soil.

7.2. Modeling of Trench Operation

In this numerical analysis, the infiltration trench was considered to be 100 cm deep and 100 cm wide and the specific location of Sandy Beach soil was chosen. The location was selected due to nearness to the ocean, exposition to frequently use main road and suitable soil properties. As with the previous modeling runs, only half of a trench was used since the center line of the trench is an axis of symmetry. The depth and width of the 2D simulated flow domain were 300 and 250 cm, respectively (Figure 26). The S2D model was used (Vogel et al., 2000). Five different scenarios were considered with different initial and boundary conditions. The purpose of

modeling different cases was to demonstrate the impact of different regimes/conditions on-site operation of infiltration trenches. The soil parameters were obtained from soil survey along highways on Oahu for Sandy Beach location ($\theta_s = 0.47 \text{ cm}^3/\text{cm}^3$, $K_s = 170 \text{ cm/d}$). The trench material was represented by a highly permeable gravel ($\theta_s = 0.60 \text{ cm}^3/\text{cm}^3$, $K_s = 10000 \text{ cm/d}$). Soil hydraulic functions (retention curve and hydraulic conductivity) were described using a modified van Genuchten model (Vogel and Cislerova, 1988; Vogel et al., 2001). Initial conditions differed between the study cases. Depending on the study case, two different boundary conditions were used for the surface boundary of the infiltration trench. Surface boundary conditions were: (i) Specified pressure head (representing inflow into the trench) and (ii) Neumann flux (representing no inflow into the trench) (Table 16). Free (gravity) drainage condition (unit hydraulic gradient) was used for the lower boundary of the simulated domain (3 m depth). All other boundaries of the domain were treated as no-flow boundaries (Neumann condition).

Table 16. Review of modeled cases with different conditions.

Case	Inflow	Water table	Outflow	Dimensions of the infiltration trench
I.	Representing inflow into the trench	Near soil surface	Free drainage condition	100 cm wide 100 cm depth
II.	Representing inflow into the trench	On the trench bottom	Free drainage condition	100 cm wide 100 cm depth
III.	Representing no inflow into the trench	On the trench bottom	Drainage process	100 cm wide 100 cm depth
IV.	Representing no inflow into the trench	2 m below the bottom of the infiltration trench	Drainage process	100 cm wide 100 cm depth
V.	Representing inflow into the trench	2 m below the bottom of the infiltration trench	Cyclic changes of filling and drying	100 cm wide 100 cm depth

The domain was divided into 22644 triangular finite elements (Figure 27). The finite element mesh was refined along the vertical and horizontal boundaries of the trench where high water fluxes were expected. The clogging of the bottom of the infiltration trench was not assumed. We investigated five different cases to simulate varied conditions in infiltration trenches. The first case represented a fully filled trench with the water table near the surface of the surrounding area. This represents conditions after long term rainfall when the soil profile is fully saturated and the infiltration trench is continuously supplied with runoff. In the second case the simulated water table was held at the bottom of the infiltration trench and the trench remained full of water during the simulation. This represents the same condition as in case I after a period of drying. In the third case the trench was initially filled and then the water level was allowed to drop at time $t=0$ with no further addition of water until it reached the bottom of the trench. This simulates an isolated rainfall event resulting in a single filling of the trench. In the fourth case the water table was kept significantly below the bottom of the trench imitating dry season conditions, without rainfall events. The infiltration trench was filled with water at time $t=0$ and allowed to drain completely drained within two days. This simulates a single rainfall event with initial filling of the trench and discontinuation of rain before commencement of emptying. Our fifth simulation involved three repetitions of this fourth case.

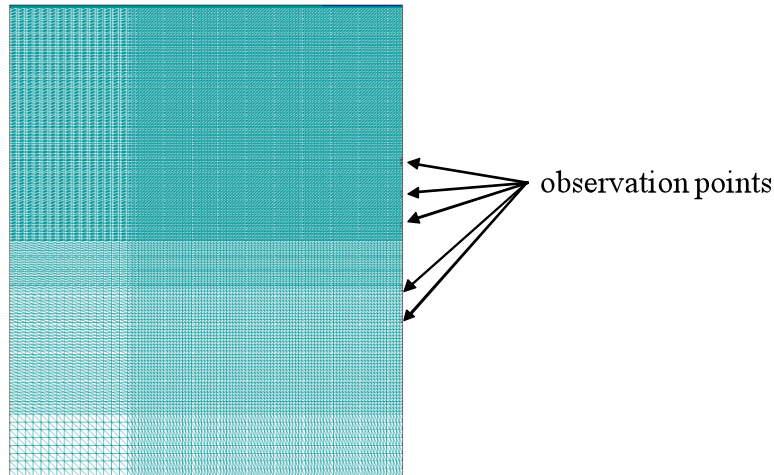


Figure 27. 2D flow domain.

7.2.1. Case Study I

This case study was designed to predict water movement through the infiltration trench in a setting with the water table near the soil surface. The infiltration trench was initially assumed to be full of water. The trench was continuously supplied with water from the top of the infiltration trench (Figure 28).

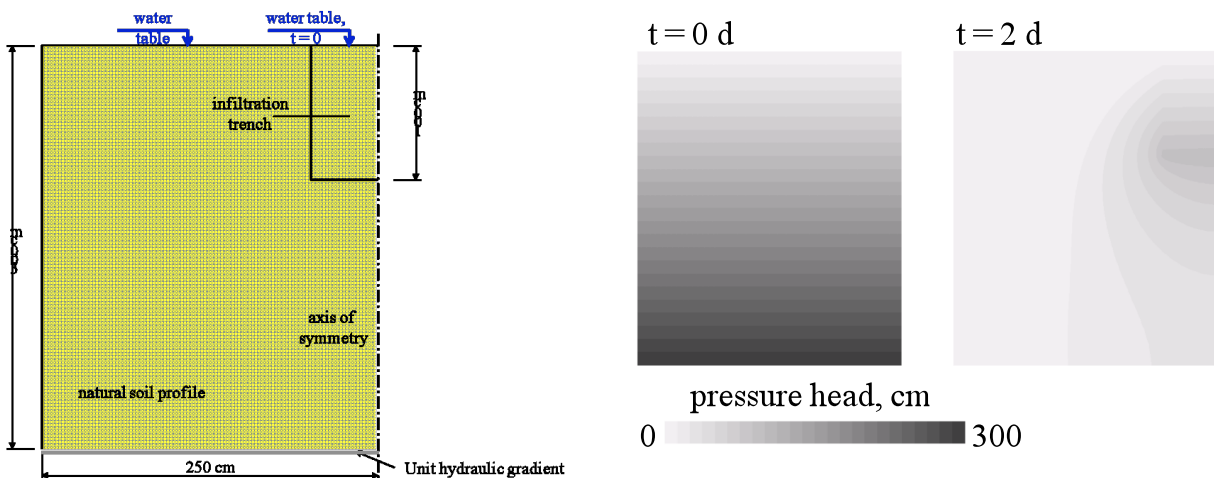


Figure 28. Water table and pressure heads in the infiltration trench during case study I. Dark grey represents high saturation with water; light grey represents dry soil.

In Figure 28, the initial condition as well as simulated pressure head distribution after two days of continuous water supply to the trench is shown. Figure 29 presents pressure head development at selected observation depths below the trench bottom and fluxes into the trench and for three m depth. This case study reached steady state relatively quickly (inflow to the trench was identical to the outflow to the simulated domain).

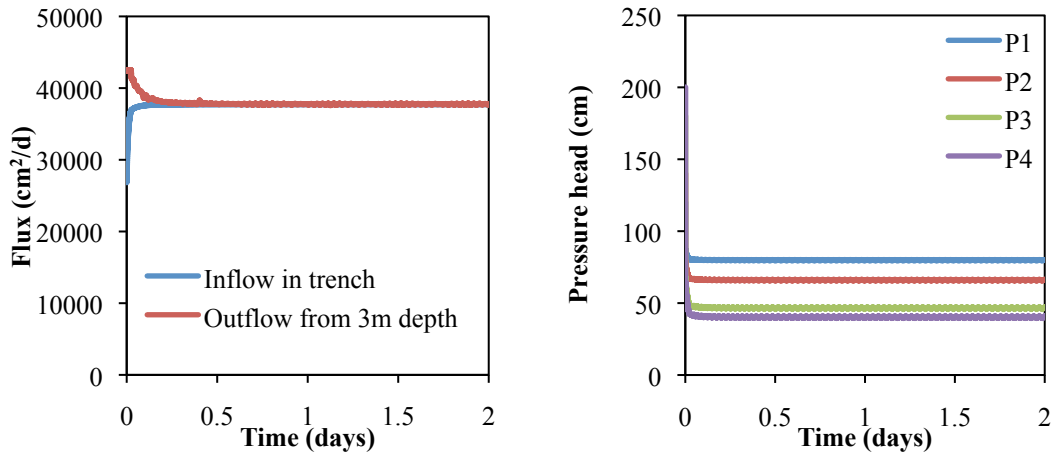


Figure 29. Fluxes and pressure heads at 20, 40, 80, and 100 cm below the infiltration trench bottom during case study I.

7.2.2. Case Study II

The water table in this case study was set at the trench bottom. A continuous supply into the trench was assumed. In Figure 30, the initial condition and simulated pressure head distribution after two days of continuous water supply to the infiltration trench are shown. Figure 31 shows pressure head development at selected observation depths below the trench bottom and fluxes into the trench and from three m depth in the simulated domain. Similarly to case study I., steady state was reached relatively quickly.

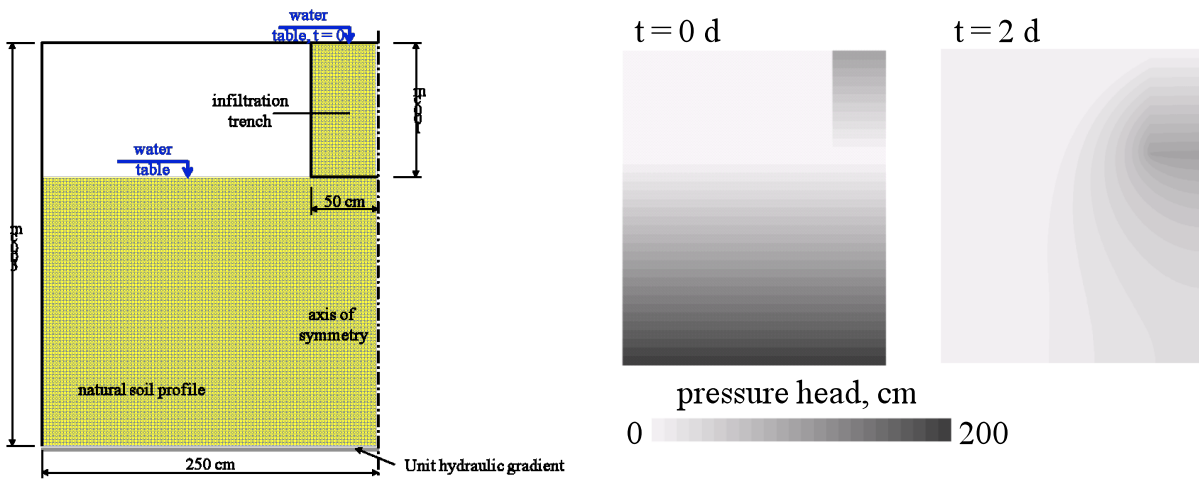


Figure 30. Water table and pressure heads in the infiltration trench during case study II. Darker color indicates greater pressure head.

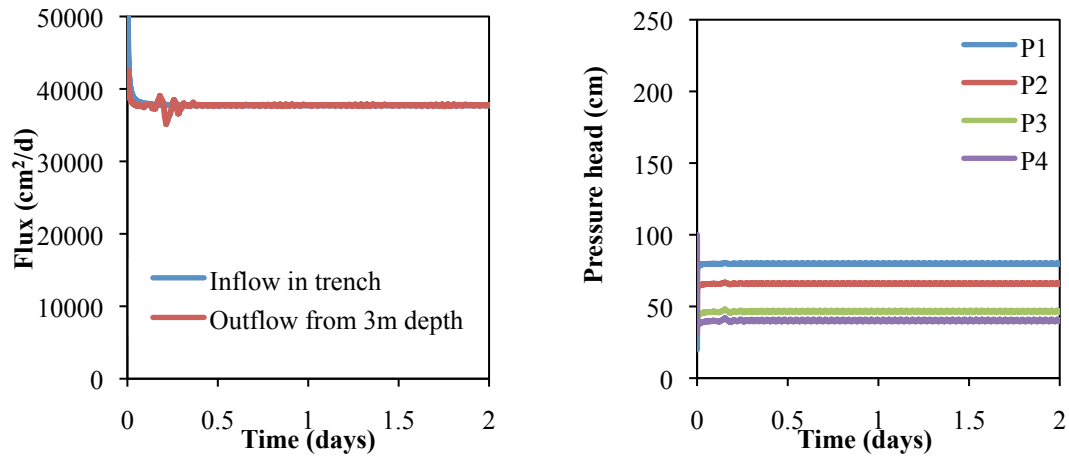


Figure 31. Fluxes and pressure heads in 20, 40, 80, and 100 cm below the infiltration trench bottom during case study II.

7.2.3. Case Study III

In this case study the water table was set at the bottom of the trench (as in case study II.). The trench was filled with water at the beginning (Figure 32). The trench was allowed to drain – the top boundary condition of the trench was no flow.

Water level in the trench started dropping from full at time $t = 0$ d and drained entirely in less than two days (Figure 32). In Figure 33, simulated pressure heads at selected observation depths below the trench and fluxes into the trench and from 3 m depth are depicted. Obviously, there was no inflow to the infiltration trench. The outflow from the simulated domain reflected drainage from both the natural soil and the infiltration trench. Simulated pressure heads showed a declining trend at two depths below the trench bottom.

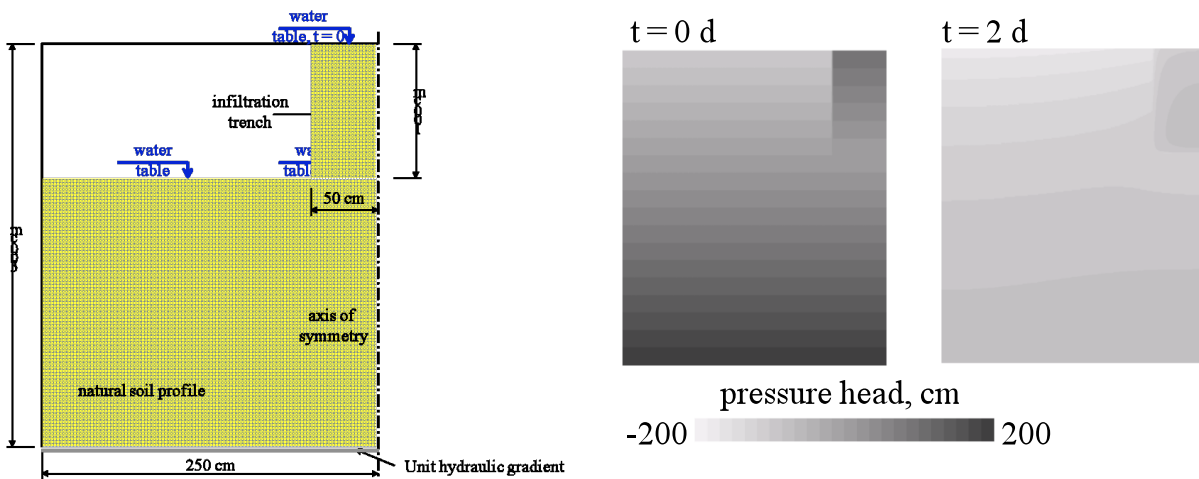


Figure 32. Water table and pressure heads in the infiltration trench during case study III. Darker color indicates greater pressure head.

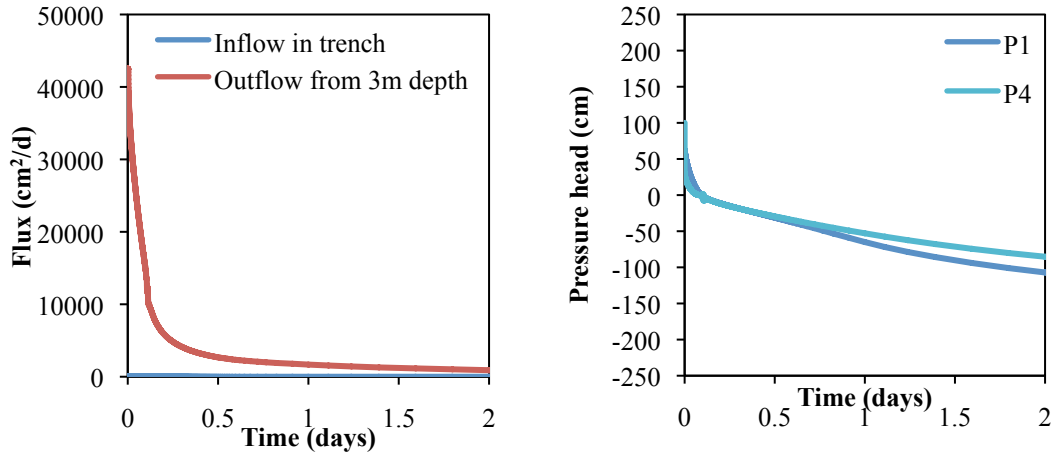


Figure 33. Fluxes and pressure heads in the infiltration trench during case study III.

7.2.4. Case Study IV

In this case study, the water table was set to two m below the bottom of the trench. The trench was full at $t = 0$ d (Figure 34). The trench was allowed to drain. In this simulation the water in the trench drained within two days (Figure 34). In Figure 35, simulated pressure heads at selected depths below the trench and flux from three m depth are depicted. As in case study III, the outflow from the simulated domain reflected drainage from both the soil and the infiltration trench. At first, outflow decreased significantly, which could be associated with drainage of water initially residing between the bottom of the trench and water table. Then, an increase of outflow was predicted, representing drainage of water from the initially saturated trench. After that, a gradual decline of outflow flux is seen (Figure 35). The drainage mechanism is also documented by simulated pressure heads at two depths below the trench bottom (Figure 35).

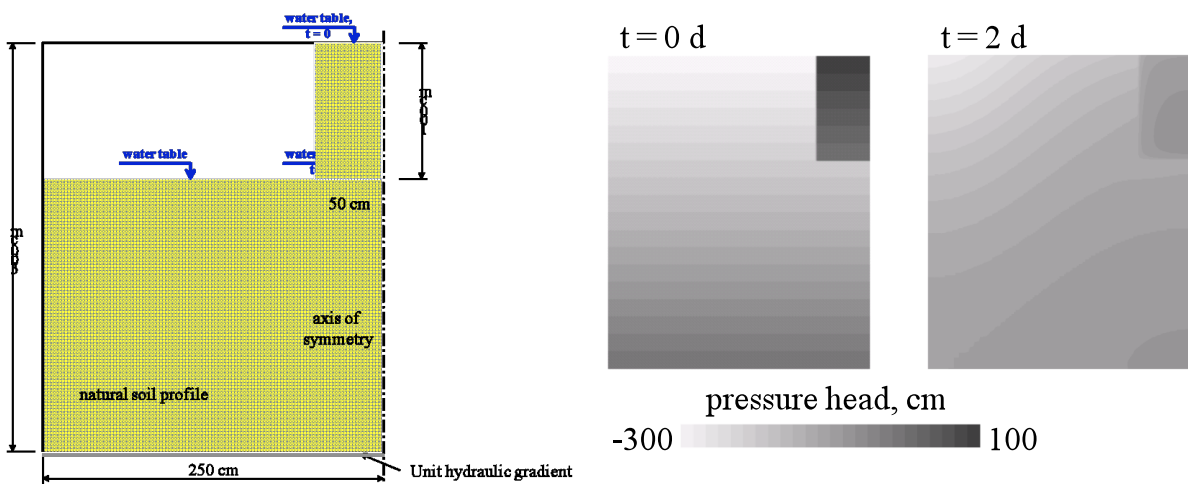


Figure 34. Water table and pressure heads in the infiltration trench during case study IV. Darker color indicates greater pressure head.

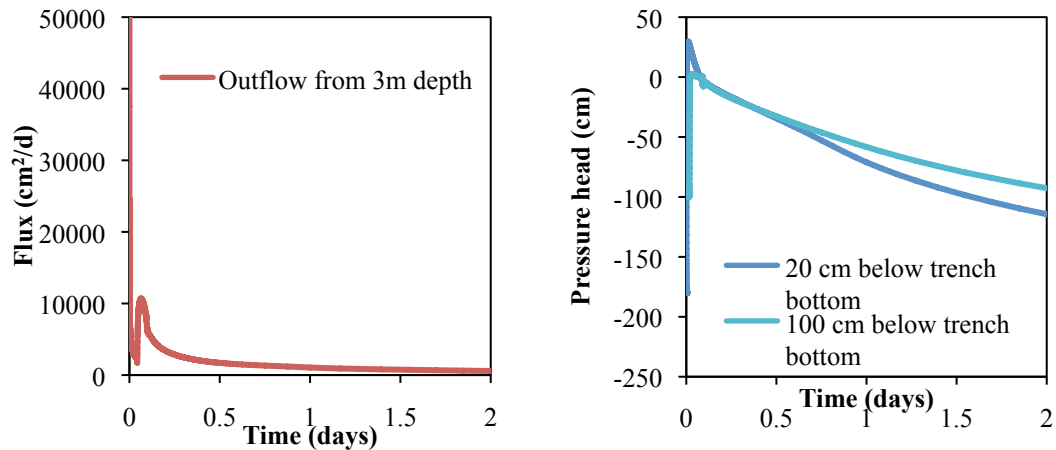


Figure 35. Fluxes and pressure heads in the infiltration trench during case study IV. Darker color indicates greater pressure head.

7.2.5. Case Study V

In this case study, the water table was set to two m below the bottom of the trench (as in case study IV.). The infiltration trench was full at $t = 0$ d, the trench was allowed to drain for two days (case study IV, in Figure 35). The infiltration trench was then supplied with water for two days up to the top of the trench. After that the top boundary condition of the trench was changed to no flow. Filling and draining of the trench switched until $t = 12$ days (three draining phases and three filling phases) of the infiltration trench were considered.

Figure 36 shows simulated pressure heads at the times, filling/drying took place. In Figure 37, simulated pressure heads at two depths below the trench and soil water fluxes are depicted. This figure reveals the cyclic functioning of the trench filling and draining as imposed on the top boundary condition. The simulated inflow and outflow as well as pressure head fluxes reached steady state during filling phases of the trench. During draining phases of the trench, gradual decline of the flux was predicted (Figure 37).

8. Drainage Time and Size of the Infiltration Trench

Best Management Practices (BMPs) Manuals (or Handbooks) differ from state to state, so individual states have different criteria for infiltration trenches.

The Stormwater Permanent Best Management Practices Manual for Hawaii (Department of Transportation, Highways Division, 2007) set out the criteria for infiltration trenches which include; the porosity of the trench's material ($n = 0.4$), rainfall intensity (0.4 inches per hour), site area, runoff coefficient, location, water table, trenches should be drained within 48 hours.

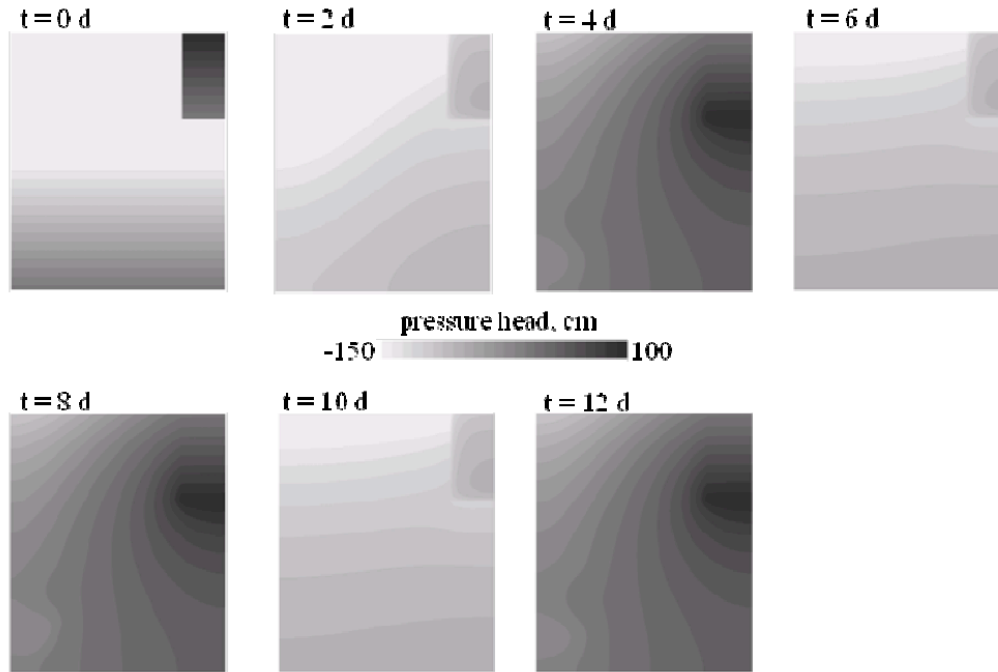


Figure 36. Pressure heads in the simulated domain at selected times (case study V). Darker color indicates greater pressure head.

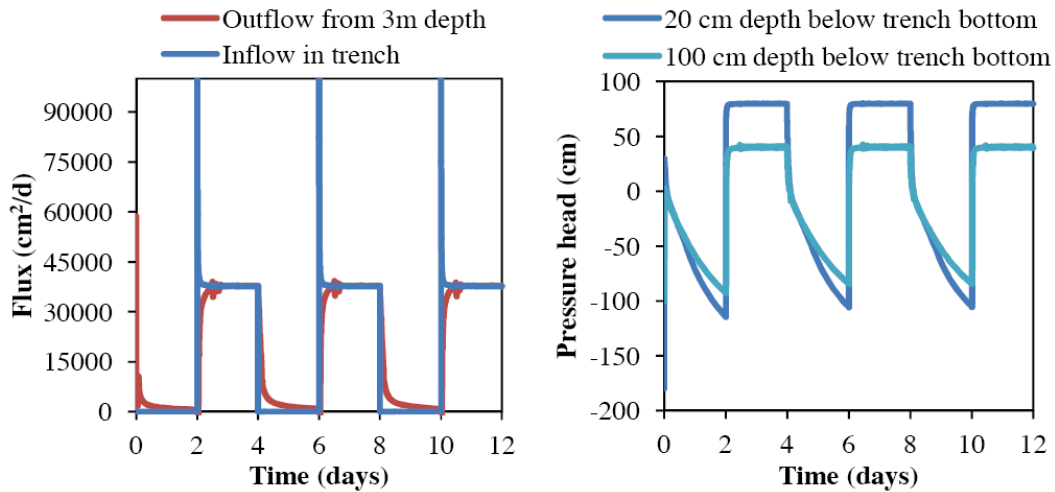


Figure 37. Fluxes and pressure heads in the infiltration trench during case study V.

In order to predict the time for a trench to fully drain we used the S 2D model. For a given size infiltration trench we assumed five conditions for the infiltration trench operation. Saturated water content $\theta_s = 0.47 \text{ cm}^3/\text{cm}^3$ and saturated hydraulic conductivity $K_s = 170 \text{ cm/d}$ were considered for soil from the Sandy Beach location. The trench material was represented by highly permeable gravel with saturated water content $\theta_s = 0.60 \text{ cm}^3/\text{cm}^3$ and saturated hydraulic conductivity $K_s = 10,000 \text{ cm/d}$. The time to reach steady state flow was 350 min for case study I

and 457 min for case study II. For case study III, IV and V the infiltration trench emptied within 48 hours. Results are given in Table 17.

Table 17. Review of modeled cases with different conditions and given time to reach steady state flow or no flow.

Case	Time to reach steady state flow or no flow
I	350 min
II	457 min
III	Fully drained within 2 days
IV	Fully drained within 2 days
V	Cyclic functioning of the trench filling and drying within 12 days

9. Summary of Findings

9.1. Capabilities of Selected Natural Soils to Infiltrate Stormwater and Adsorb Pollutants from Runoff Water

- Infiltration capacity of several soils was measured by retention curve. Hydraulic conductivity ranging between 26–485 mm/h for fourteen soils at different sites on Oahu was measured in the field. Water content (from 26–58 %) and bulk density (0.91–1.5 g/cm³) were determined from small undisturbed soil samples.
- Soils from sixteen sites were examined for heavy metal concentration. Results showed that all the soils contained arsenic, cobalt, chromium and selenium at detectable concentrations.
- Calculated desorption coefficient values were greater than 20 for all soil/metal combinations except for cadmium in the soils collected from Sandy Beach Park and H1–Kalaehoa Boulevard IC. This indicates that the adsorption capacity of the majority of soils along highways on Oahu is high enough to retain heavy metals in stormwater runoff.

9.2. Stormwater Runoff from the Highway

- Collected runoff, rather than metal-spiked water was used in column experiments to determine the adsorption capacities of the soils for highway contaminants.
- Dissolved metal concentrations in H3 runoff exceeded the groundwater EAL (Environmental Action Levels, HDOH, 2008) for all heavy metals except for copper and zinc. Interestingly, copper and zinc were the metals that showed the highest concentration in the sediments around the H3 drain outlets.

9.3. Site Suitability Index Using GIS

- A site suitability index map was developed by applying spatial analysis techniques with multiple GIS layers to identify potential sites suitable for infiltration trenches.

- GIS overlay analysis was found to be an effective tool to develop site suitability maps. Some areas were found to be highly suitable for implementing infiltration trenches on Oahu.
- Different analysis techniques (i.e., weighting schemes and overlay analyses) significantly affected the site suitability maps, and thus, various approaches should be compared to improve the accuracy of overlay analysis.
- GIS overlay analysis applied in this study only describes the site suitability in terms of geographic context.
- This overlay analysis should be evaluated with other general models such as receiving water quality models (Hydrological Simulation Program - Fortran, HSPF or System for Urban Stormwater Treatment and Analysis Integration, SUSTAIN) and vadose zone models (HYDRUS- 1, 2, or 3D). Further studies are needed to demonstrate the positive effects of infiltration trenches on downstream water quality, although this subject is beyond the scope of this study.

9.4. Laboratory Experiments

- A one dimensional experiment to imitate water flowing through an infiltration trench was carried out for four soil samples. Different experimental procedures included long – term saturated infiltration, and flow/no flow cycling was applied to measure the saturated hydraulic conductivity. Real highway stormwater runoff was used in these experiments.
- A cake layer formed on top of the gravel surface that was placed atop the soil cores resulting in declines of the outflow rate.
- Decreasing hydraulic conductivity values were observed during the flow/no flow cycles and the long-duration experiment.
- The gravel has a great potential to remove or retain sediment particles, which was demonstrated by the analysis of the total suspended solids and measurements of turbidity.
- All soils showed high capacity to remove Fe during flow/no flow cycles.

9.5. Modeling

- Two-dimensional HYDRUS and S2 D models based on Richards' equation were used to demonstrate the impact of different regimes/conditions on on-site functioning of infiltration trenches. Soil hydraulic functions (retention curve and hydraulic conductivity) were described using modified a van Genuchten model.
- Several different study cases were examined with different initial and boundary conditions.
- For scenarios where the water table was near the soil surface or below the bottom of the infiltration trench with continuous supply of water into the infiltration trench was assumed, a steady state condition was reached relatively quickly (in 0.1 day from the initiation of drainage).
- Simulated infiltration trenches could be drained within two days when the water table was set at the bottom of the infiltration trench or two m below the bottom of the trench

and there was not a continuous supply of water during the draining period. Drainage from both the soil and the infiltration trench was successfully simulated.

Two dimensional models used in this study were found to be capable of predicting the water regime in an infiltration trench assuming no clogging developed during infiltration. These models do not have the ability to simulate dynamic clogging; hence do not simulate probable reductions in hydraulic conductivity with time. Modification of the computational code should be done to simulate dynamic clogging.

10. References

- AMEC Earth & Environmental, Inc. 2008. Northeast Tennessee Water Quality BMP Manual, Chapter 4.3.7: Design and Maintenance of Structural BMPs, Infiltration Trench. AMEC Earth & Environmental, Inc., Knoxville, TN.
- Antal, M. J., Mochidzuki, K., Paredes, L. S.. 2003. Flash Carbonization of Biomass. *Ind. Eng. Chem. Res.*, 2003, 42 (16), pp 3690–3699. DOI: 10.1021/ie0301839.
- Association, A.P.H. 1994. Water Environment Federation (1998) Standard methods for the examination of water and wastewater, Washington, DC.
- ASTM Standard. 1985. Zeta Potential of Colloids in water and waste water, ASTM Standard D 4187-82, American Society for Testing and Materials.
- Atlanta Regional Commission (ARC). 2001. Georgia Stormwater Management Manual, Volume 2: Technical Handbook, Infiltration Trench. ARC, Atlanta, GA.
- Baveye, P., Vandevivere, P., Hoyle, B.L., DeLeo, P.C., de Lozada, D.S.. 1998. Environmental impact and mechanisms of the biological clogging of saturated soils and aquifer materials. *Crit. Rev. Environ. Sci. Technol.*, 28(2): 123-191.
- Blume, T., Weisbrod, N., Selker, J.S., 2002. Permeability changes in layered sediments: Impact of particle release. *Ground Water*, 40(5): 466-474.
- Storm Water Permanent Best Management Practices Manual, State of Hawaii Department of Transportation Highways Division. 2007.
- Bourg, A.C.M. 1988. Metals in aquatic and terrestrial systems: sorption, speciation, and mobilization. In: Salomons, W. & Förstner, U. (Eds). *Chemistry and Biology of Solid Waste - Dredged Material and Mine Tailings*. Springer-Verlag.
- Bright, T.M., Hathaway, J. M., Hunt, W. F., Asce, M. de los Reyes, F. L., and Burchell, M. R. 2010. Impact of Storm-Water Runoff on Clogging and Fecal Bacteria Reduction in Sand Columns. *Journal of Environmental Engineering*, 136(12): 1435-1441.
- Brookhaven Instruments Corporation, 2002. ZetaPlus, Zeta Potential Analyzer, Instruction Manual., Holtsville, NY.
- California Stormwater Quality Association (CASQA). 2003. California Stormwater BMP Handbook, New Development and Redevelopment, Infiltration Trench (TC-10). CASQA, Menlo Park, CA.

- Center for Watershed Protection (CWP). 2010. New York State Stormwater Management Design Manual, Appendix C.2 Construction Specifications for Infiltration Practices. CWP, Ellicott City, MD.
- Chen, Y, Yu, J, Khan, S. 2010. Spatial sensitivity analysis of multi-criteria weights in GIS-based land suitability evaluation. *Environmental Modeling and Software* 25(12): 1582-1591.
- Christensen, T.H. 1984. Cadmium soil sorption at low concentrations: I. Effect of time , cadmium load, pH and calcium. *Water, Air and Soil Pollutant.* 21: 105-114.
- Christensen, T.H. 1985. Heavy metal competition for soil sorption sites at low concentrations. *Proc. Internat. Conf. Heavy Metals in the Environment*, Sept 1985, Athens, 2: 394-397.
- Clark, S. and R. Pitt. 2009. Storm-water filter media pollutant retention under aerobic versus anaerobic conditions. *Journal of Environmental Engineering* 135(5): 367-371.
- Clothier, B.E.; Kirkham, M.B. and McLean, J.E. In situ measurement of the effective transport volume for solute moving through soil. *Soil Sci. Soc. Am. J.*, 56: 733-736, 1992.
- Cook, F.J., Kelliher, F.M., McMahan, S.D., 1994. Changes in infiltration and drainage during waste-water irrigation of a highly permeable soil. *Journal of Environmental Quality*, 23(3): 476-482.
- Center for Watershed Protection (CWP). 2010. New York State Stormwater Management Design Manual, Appendix C.2 Construction Specifications for Infiltration Practices. CWP, Ellicott City, MD.
- De Carlo, E. H., Anthony, S. S. 2002. Spatial and temporal variability of trace element concentrations in an urban subtropical watershed, Honolulu, Hawai'i. *Applied Geochemistry*, 17, 475–492.
- De Carlo, E. H., V. L. Beltran, and M. S. Tomlinson. 2004. Composition of water and suspended sediment in streams of urbanized subtropical watersheds in Hawai'i. *Applied Geochemistry*, 19, 1011–1037.
- Department of Transportation (DOH). 2007. Storm Water Permanent BMP Manual, Infiltration Trench. DOT, Highways Division, Honolulu, HI.
- Faybishenko, B. A. 1995. Hydraulic behavior of quasi-saturated soils in the presence of entrapped air - laboratory experiments. *Water Resources Research* 31(10): 2421-2435.
- Foote, D.E., Hill, S.N. and Stephens, F. 1972. Soil Survey of The Islands of Kauai, Oahu, Maui, Molokai and Lanai, State of Hawaii. USDA- Soil Conservation Service & The University of Hawaii- Agricultural Experiment Station, 232 p.
- Frenkel, H., Goertzen, J. and Rhoades, J. 1978. Effects of clay type and content, exchangeable sodium percentage, and electrolyte concentration on clay dispersion and soil hydraulic conductivity. *Soil Science Society of America Journal*, 42(1), 32-39.
- Fujimoto, C.K. and Sherman, G.D. 1946. The Effect of Drying, Heating, and Wetting on the Level of Exchangeable Manganese in Hawaiian Soils¹. *Soil Sci. Soc. Am. J.*, 10(C), 107-112.
- Gardner, W. R. 1956. Calculation of capillary conductivity from pressure plate outflow data. *Soil Sci. Soc. Am. Proc.* 20: 317-320.

- Goldberg, S.P. and Smith, K.A. (1984) Soil Manganese: E Values, Distribution of Manganese-54 among Soil Fractions, and Effects of Drying. *Soil Sci. Soc. Am. J.*, 48(3), 559-564.
- Golden, D., Dixon, J. and Kanehiro, Y. 1993. The manganese oxide mineral, lithiophorite, in an oxisol from Hawaii. *Soil Research*, 31(1), 51-66.
- Haselbach, L.M.. 2010. Potential for Clay Clogging of Pervious Concrete under Extreme Conditions. *Journal of Hydrologic Engineering*, 15(1): 67-69.
- Hatt, B. E., T. D. Fletcher, and Deletic, A. 2007. Treatment performance of gravel filters media: Implications for design and application of stormwater infiltration systems. *Water Research* 41(12): 2513-2524.
- Hatt, B. E., T. D. Fletcher, and Deletic, A. 2008. Hydraulic and pollutant removal performance of fine media stormwater filtration systems. *Environmental Science & Technology* 42(7): 2535-2541.
- HDOH, Highways Division. 2008. Storm Water Monitoring Report – Waste Load Allocation in Kapaa, Kaelepulu, Waimanalo and Ala Wai Watersheds 2007–2008. Prepared by Oceanit, Honolulu, Hawaii.
- HDOH, 2008. Environmental Action Level, Evaluation of Environmental Hazards at Sites with Contaminated Soil and Groundwater 1, User's Guide.
- Hossain, M. S. and N. G. Das (2010). "GIS-based multi-criteria evaluation to land suitability modelling for giant prawn (*Macrobrachium rosenbergii*) farming in Companigonj Upazila of Noakhali, Bangladesh." *Computers and Electronics in Agriculture* 70(1): 172-186.
- Hue, N.V., Vega, S. and Silva, J.A. 2001. Manganese toxicity in a Hawaiian Oxisol affected by soil pH and organic amendments. *Soil Science Society of America Journal*, 65(1), 153-160.
- Hue, N.V, Uehara, G., Yost, R.S. and Ortiz, M. 2006. Distribution of Soil Orders in Hawaii. http://hilo.hawaii.edu/academics/cafnrm/research/documents/hawaii_soils706.pdf
- Institute for Transportation (IT). 2009. Iowa Stormwater Management Manual, Version3, 2E-2 Infiltration Trenches. IT, Iowa State University, Ames, IA.
- Joss, BN, Hall, RJ, Sidders, DM, Keddy, TJ. 2008. Fuzzy-logic modeling of land suitability for hybrid poplar across the Prairie Provinces of Canada. *Environmental Monitoring and Assessment* 141(1-3): 79-96.
- Kandra, H. S., McCarthy, D., Deletic, A., Fletcher, T. D. 2010. Assessment of clogging phenomena in granular filter media used for stormwater treatment. Novatech.
- Kayhanian, M., Suverkropp, C., Ruby, A. & Tsay, K. 2007. Characterization and prediction of highway runoff constituent event mean concentration. *Journal of Environmental Management* 85: 279–295.
- Kim, L.-H., Kayhanian, M., Zoh, K.-D., Stenstrom, M.K. 2005. Modeling of highway stormwater runoff *Science of the Total Environment*, 348 (1-3), 1-18
- Klute. A. 1986. Water Retention: Laboratory Methods. In: A., Klute *Methods of Soil Analysis, Part 1 Physical and Mineralogical Methods*. Agronomy. American Society of Agronomy, Inc. Soil Science Society of America, Inc, Madison, Wisconsin, pp. 635-662.

- Kool, J. B., Parker, J. C., and M. Th. van Genuchten. 1985. Determining soil hydraulic properties from one step outflow experiments by parameter estimation: I. Theory and numerical studies, *Soils Sci. Soc. Am. J.*, 49, 1348-1354.
- Landner, L. and Reuther, R. 2004. *Metals in Society and in the Environment- A Critical Review of Current Knowledge on Fluxes, Speciation, Bioavailability and Risk for Adverse Effects of Copper, Chromium, Nickel and Zinc.* Kluwer Academic Publishers.
- Li, H. and A. P. Davis. 2008a. Urban particle capture in bioretention media. I: Laboratory and field studies. *Journal of Environmental Engineering-Asce* 134(6): 409-418.
- Li, H., Davis, A.P., 2008b. Urban particle capture in bioretention media. II: Theory and model development. *J. Environ. Eng.-ASCE*, 134(6): 419-432.
- McDowell-Boyer, L.M., Hunt, J.R., Sitar, N. 1986. Particle-transport through porous-media. *Water Resour. Res.*, 22(13): 1901-1921.
- Mays, D.C., Hunt, J.R., 2005. Hydrodynamic aspects of particle clogging in porous media. *Environ. Sci. Technol.*, 39(2): 577-584.
- Mays, D.C., Hunt, J. R. 2007. Hydrodynamic and Chemical Factors in Clogging by Montmorillonite in Porous Media. *Environ. Sci. Technol.*, 41(16): 5666–5671.
- Mays, D.C., 2010. Contrasting Clogging in Granular Media Filters, Soils, and Dead-End Membranes. *J. Environ. Eng.-ASCE*, 136(5): 475-480.
- Mualem, Y. and Klute, A. 1986. Hydraulic conductivity of unsaturated soils: prediction and formulas. *Methods of soil analysis. Part 1. Physical and mineralogical methods*, 799-823.
- Nixon, H. and Saphores, J.D.M. 2007. Impacts of motor vehicle operation on water quality - Clean-up Costs and Policies. *Transportation Research Part D.* 12(8):564-576.
- Nogaro, G., Mermillod–Blondin, F., Francois–Carcaillet, F., Gaudet, J. P., Lafont, M., Gibert, J. 2006. Invertebrate bioturbation can reduce the clogging of sediment: an experimental study using infiltration sediment columns. *Freshwater Biology*, 51, 1458–1473.
- Noh, J., Lee, K. M. 2003. Application of multiattribute decision-making methods for the determination of relative significance factor of impact categories. *Environmental Management* 31(5): 633-641.
- Novotny, V. 1999. Integrating diffuse/nonpoint pollution control and water body restoration into watershed management. *Journal of the American Water Resources Association*, 35 (4), pp. 717-727.
- Oberdorfer, J.A., Peterson, F.L.. 1985. Wastewater Injection - Geochemical and Biogeochemical Clogging Processes. *Ground Water*, 23(6): 753-761.
- Pavelic, P., P. J. Dillon, et al. 2011. Laboratory assessment of factors affecting soil clogging of soil aquifer treatment systems. *Water Research* 45(10): 3153-3163.
- Perez-Pedini, C., Limbrunner, J. F. et al. 2005. Optimal location of infiltration-based best management practices for storm water management. *Journal of Water Resources Planning and Management-Asce* 131(6): 441-448.
- Perroux, K.M. and White. 1988. I. Designs for disk permeameters. *Soil Sci. Soc. Am. J.*, 52: 1205-1215.

- Pfeiffer, S. R., Ragusa, S., Sztajn bok, P., and Vandavelde, T. 2000. Interrelationships between biological, chemical, and physical processes as an analog to clogging in aquifer storage and recovery (ASR) wells. *Wat. Res.* 34 (7): 2110–2118.
- Pignon, F., Magnin, A., Piau, J.M., Cabane, B., Aimar, P., Meireles, M. and Lindner, P. 2000. Structural characterisation of deposits formed during frontal filtration. *Journal of Membrane Science*, 174(2), 189-204.
- Pupisky, H. and Shainberg, I. 1979. Salt effects on the hydraulic conductivity of a sandy soil. *Soil Science Society of America Journal*, 43(3), 429-433.
- Presley, T.K. 2001. Rainfall, Streamflow and Water- Quality Data During Stormwater Monitoring, Halawa Stream Drainage Basin, Oahu, Hawaii, July 1, 2000 to June 30, 2001. USGS, Open-File Report 01- 256. Prepared by USGS & HDOT.
- Presley, T.K. 2002. Rainfall, Streamflow and Water-Quality Data During Stormwater Monitoring, Halawa Stream Drainage Basin, Oahu, Hawaii, July 1, 2001 to June 30, 2002. USGS, Open-File Report 02-319. Prepared by USGS & HDOT.
- Reynolds, W. D. and Elrick, D. E. 1991. Determination of Hydraulic Conductivity Using a Tension Infiltrometer, *Soil Sci. Soc. Am. J.* 55:633-639.
- Reynolds, W.D., Bowman, B.T., Brunke, R.R., Drury, C.F. and Tan, C.S. 2000. Comparison of tension infiltrometer, pressure infiltrometer, and soil core estimates of saturated hydraulic conductivity. *Soil Science Society of America Journal* 64(2), 478-484.
- Reddi, L.. 1997. Particle Transport in Soils: Review of Significant Processes in Infrastructure Systems. *J. Infrastruct. Syst.*, 3(2): 78.
- Reddi, L.N., Ming, X., Hajra, M.G., Lee, I.M.. 2005. Physical clogging of soil filters under constant flow rate versus constant head. *Can. Geotech. J.*, 42: 804–811.
- Saaty T.L. 1980. *The analytic hierarchy process*. McGraw Hill, New York.
- Santiwong, S.R., Guan, J. and Waite, T.D. 2008. Effect of ionic strength and pH on hydraulic properties and structure of accumulating solid assemblages during microfiltration of montmorillonite suspensions. *Journal of colloid and interface science*, 317(1), 214-227.
- Sansalone, J. J., and Buchberger, S. G. 1997. Partitioning and First Flush of Metals in Urban Roadway Storm Water. *Journal of Environmental Engineering*, 123 (2): 134–143.
- Schmitt, H.V. and Sticher, H. 1986. Long-term trend analysis of heavy metal content and translocation in soils. *Geoderma*, 38: 145-208.
- Sener, S, Sener, E, Nas, B, Karaguzel R. 2010. Combining AHP with GIS for landfill site selection: A case study in the Lake Beysehir catchment area (Konya, Turkey). *Waste Management* 30(11): 2037-2046.
- Simunek, J., M.Th. van Genuchten, and M. Sejna. 2006. *The HYDRUS Software Package for Simulating the Two- and Three-Dimensional Movement of Water, Heat, and Multiple Solutes in Variably-Saturated Media, Version 1.0*, PC Progress, Prague, Czech Republic.
- Siriwardene, N. R., Deletic, A., Fletcher, T. D. 2007. Clogging of stormwater gravel infiltration systems and filters: Insights from a laboratory study. *Water Research* 41(7): 1433-1440.

- State of Hawaii, Department of Transportation, Post-Construction Storm Water Management in New Development and Redevelopment, 2007a.
- State of Hawaii, Department of Transportation, Storm Water Permanent Best Management Practices Manual, 2007b.
- USDA/UH. 1973. Hawaii Online Soil Survey Manuscripts. http://soils.usda.gov/survey/online_surveys/hawaii/ [Access date: 6rd December 2012]
- USDA. Web of Soil Survey. 2012. <http://websoilsurvey.nrcs.usda.gov/app/HomePage.htm> [Access date: 3rd December 2012]
- US Environmental Protection Agency. 1999. Storm water technology fact sheet. Infiltration Trench. EPA 832-F-99-019. Office of Water, Washington, DC.
- Yost, R.S. 1994. Hawaii soil database for organic chemical leaching assessment. HITAHR, College of Tropical Agriculture and Human Resources, University of Hawaii, 1994.
- Young, S.T.M. and Ball, M.T.J. 2004. Rainfall, Streamflow and Water- Quality Data During Stormwater Monitoring, Halawa Stream Drainage Basin, Oahu, Hawaii, July 1, 2003 to June 30, 2004. USGS, Open-File Report 2004- 1275. Prepared by USGS & HDOT.
- Young, S.T.M. & Ball, M.T.J. 2005. Rainfall, Streamflow and Water- Quality Data During Stormwater Monitoring, Halawa Stream Drainage Basin, Oahu, Hawaii, July 1, 2004 to June 30, 2005. USGS, Open-File Report 2005- 1280. Prepared by USGS & HDOT.
- van Genuchten, M.T. 1980. A closed-form equation for predicting the hydraulic conductivity of unsaturated soils. *Soil Science Society of America Journal* 44(5), 892-898.
- van Genuchten, M.Th., Leij, F.J., Yates, S.R. 1991. The RETC Code for Quantifying the Hydraulic Functions of Unsaturated Soils, U.S. EPA Rep. 600/2-91/065. Environ. Protect. Agency, Washington, DC. 85 pp.
- Vogel, T., and M. Cislerova. 1988. On the reliability of unsaturated hydraulic conductivity calculated from the moisture retention curve, *Transport in Porous Media*, 3, 1–15.
- Vogel, T.: Modeling Flow and Transport in Dual Porosity Media. 2000. In *Proceedings of Workshop 2000*. Prague: CTU, vol. B, p. 589. ISBN 80-01-02229-3.
- Vogel, T., M.Th. van Genuchten, and M. Cislerova. 2001. Effect of the shape of soil hydraulic functions near saturation on variably-saturated flow predictions, *Advances in Water Resources*, 24, 133–144.
- Wong, M.F. 2005. Water quality in the Halawa, Haiku, and Kaneohe drainage basins before, during, and after H-3 Highway construction, Oahu, Hawaii, 1983-99: U.S. Geological Survey Scientific Investigations Report 2004-5002, 45 p.
- Zhao, L.F., Zhu, W., Tong, W. 2009. Clogging processes caused by biofilm growth and organic particle accumulation in lab-scale vertical flow constructed wetlands. *J. Environ. Sci.*, 21(6): 750-757.
- Zhen, X. Y., Yu, S. L., Lin, J. Y. 2004. Optimal location and sizing of stormwater basins at watershed scale. *Journal of Water Resources Planning and Management-Asce* **130**(4): 339-347.

Appendix

Appendix A. Google map locations of sites to investigate soil properties for infiltration capacity.

1) H-3 Kamehameha Hwy Intersection



2) H3 median near Kapaa above Kawainui Marsh



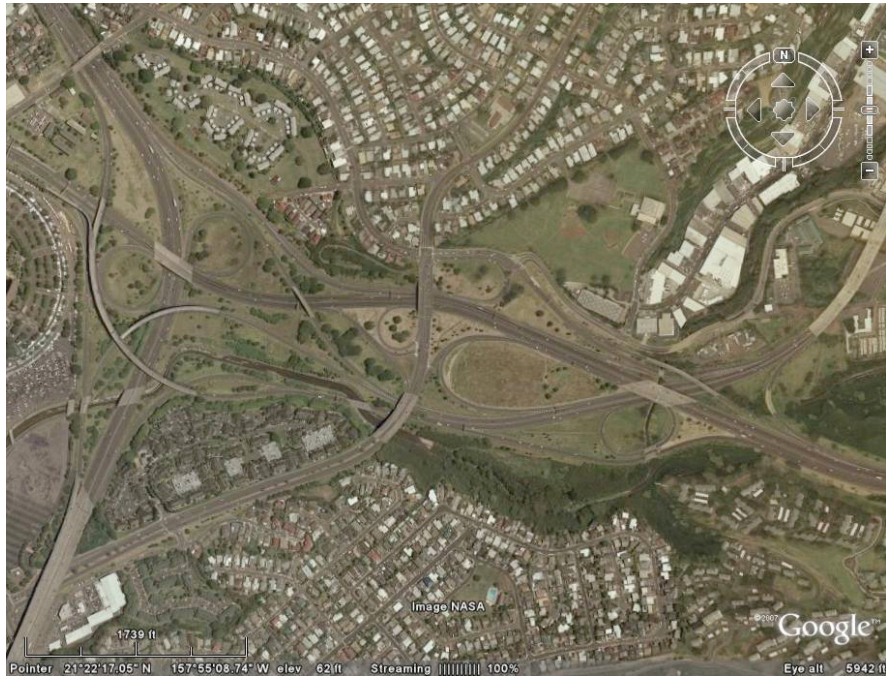
3) H3 Intersection with Kaneohe Bay Drive above Marine Corps Air Base



4) Median Strip in Kamehameha Hwy near junction with Likelike Hwy



5) H3: H1 Interchange.



6) LikeLike: H1 Junction



7) H1: University Intersection



8) H1 between Kaahumanu overpass and Bridge over stream



9) H1 Moanalua road Intersection

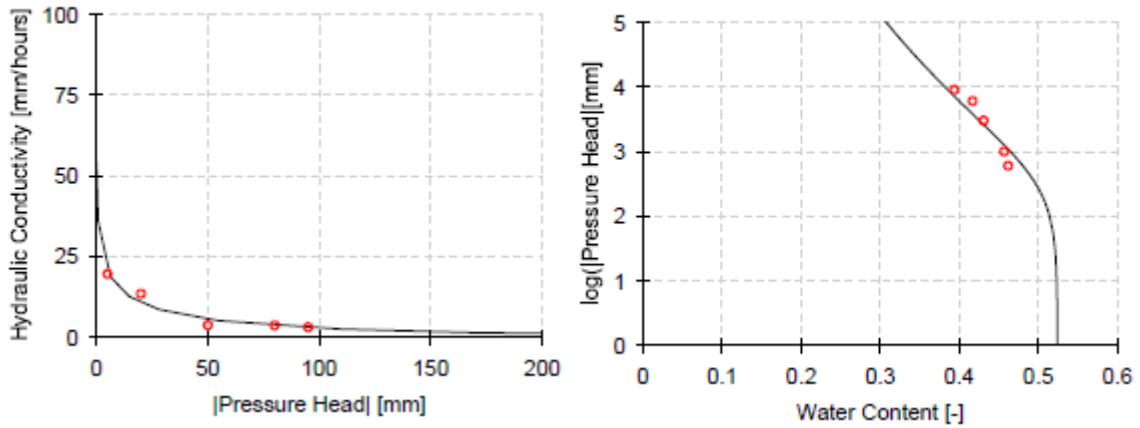


10) H1:H2 Intersection

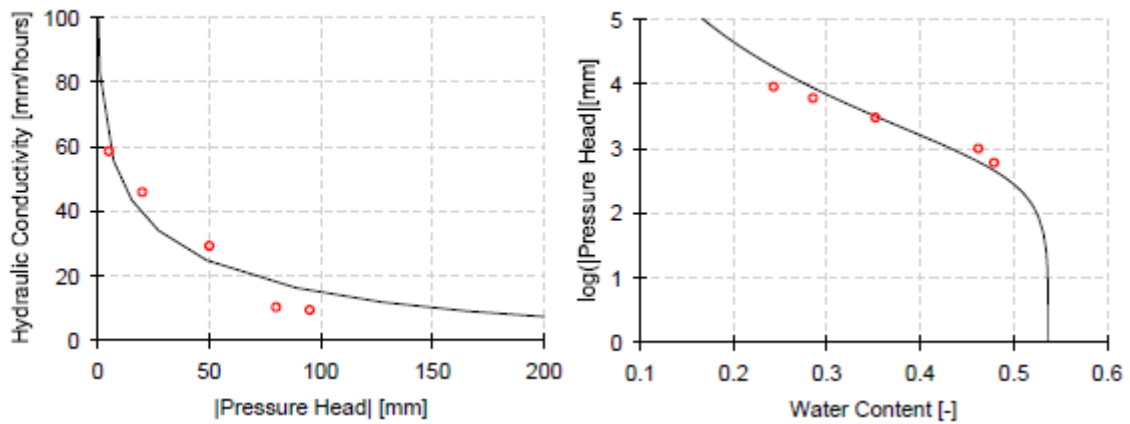


Appendix B. Measured and estimated hydraulic conductivity and retention curves.

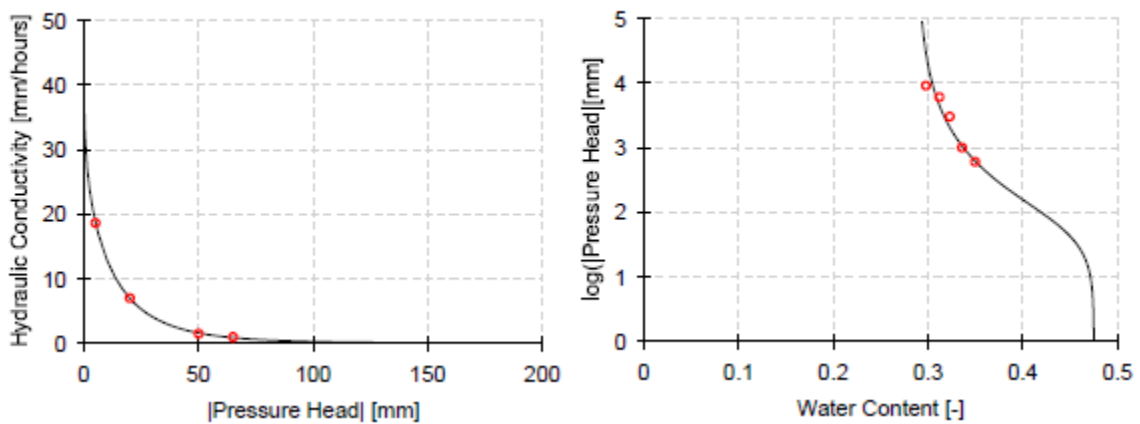
S1, 40 cm, H3 – Kamehameha IC, Kaneohe silty clay



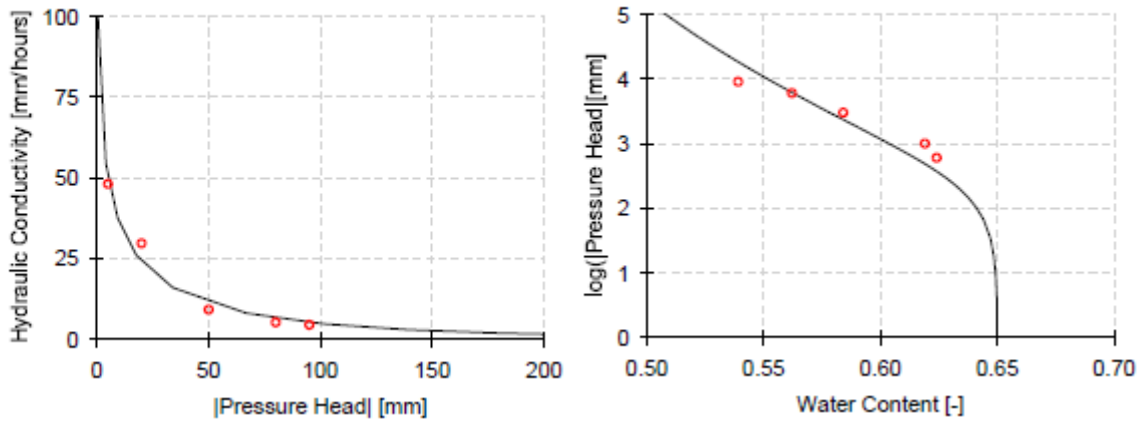
S10, 30 cm



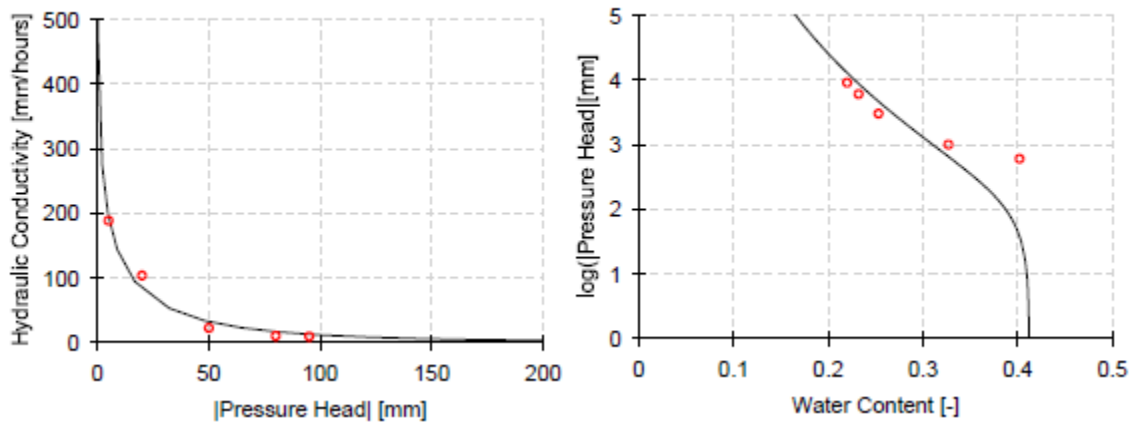
S12, 50 cm, Pali – Kamehameha, Alaeloa silty clay



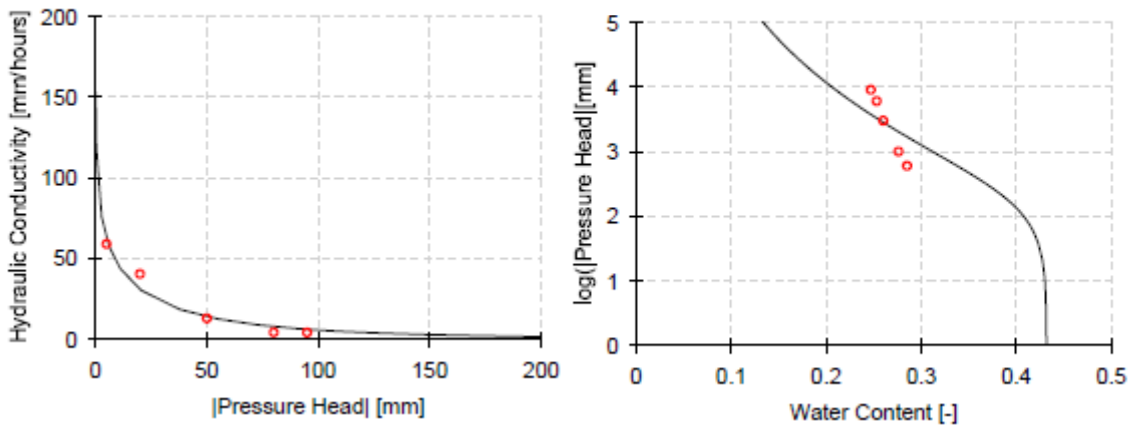
S 14, 35 cm, H1 – Kamehameha, Makalapa clay



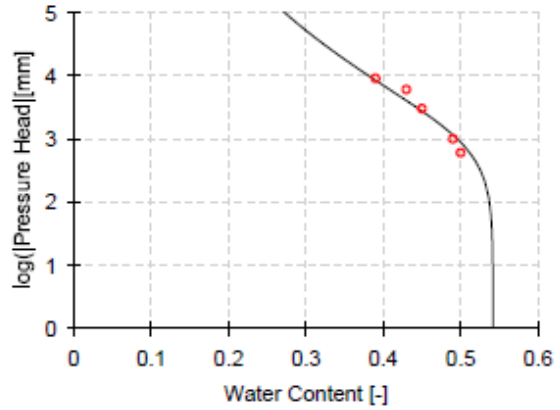
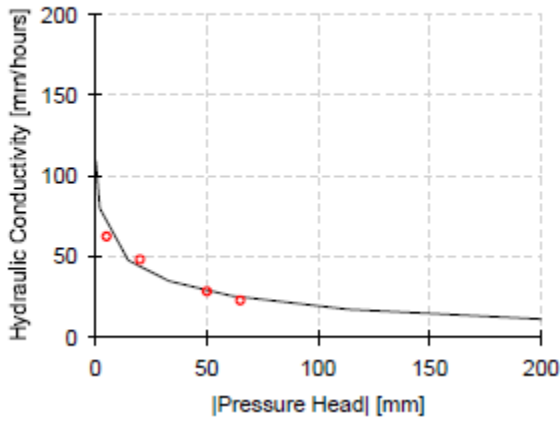
S18, 15 cm, H2 – Kauka Blv, Helemano silty clay



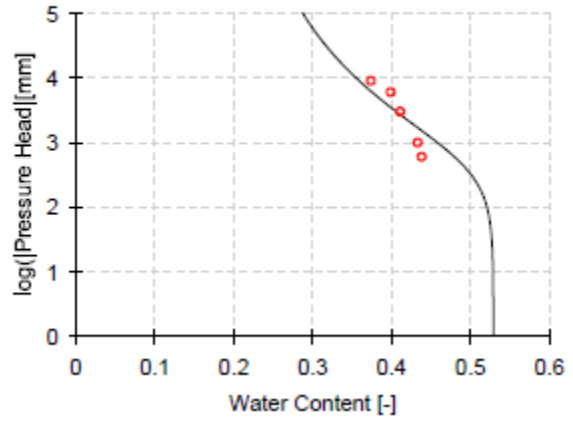
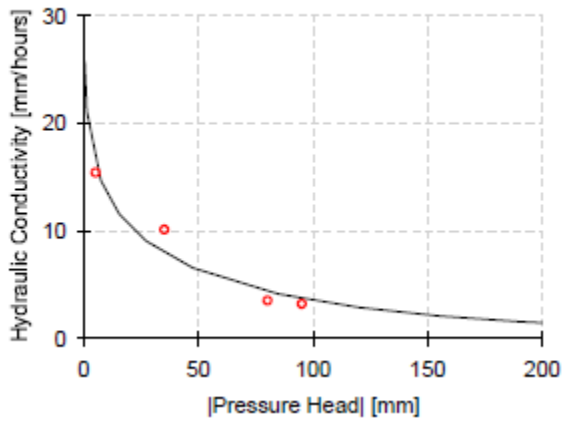
S18, 35 cm, H2 – Kauka Blv, Helemano silty clay



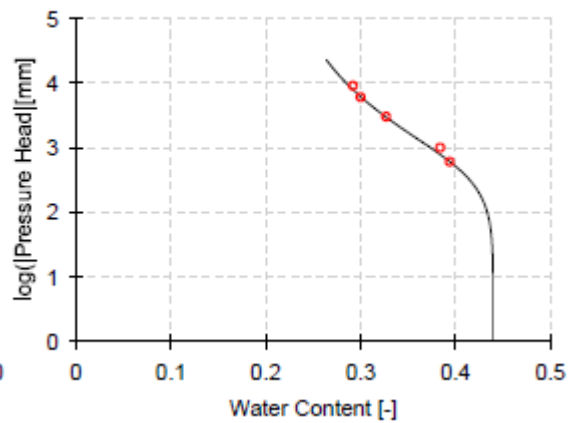
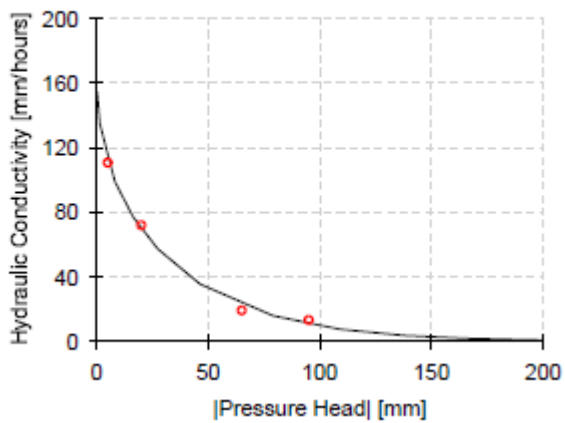
S24b, 30 cm, Kamehameha – Joseph Leong, Waialua silty clay



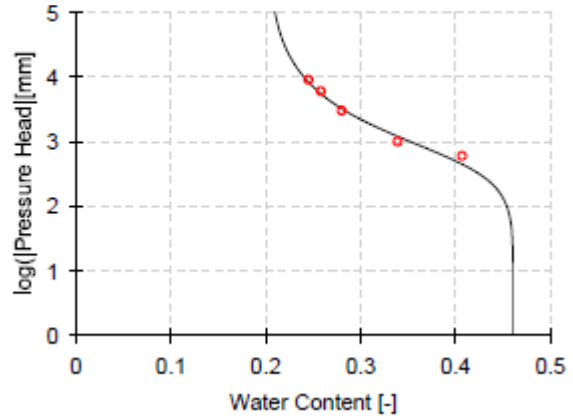
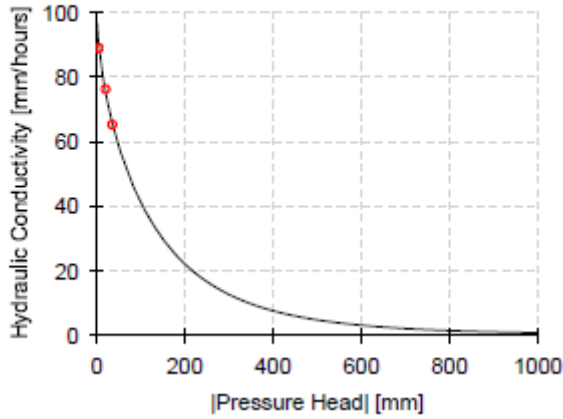
S35_B, 30 cm, Pali Hwy, Lolekaa silty clay



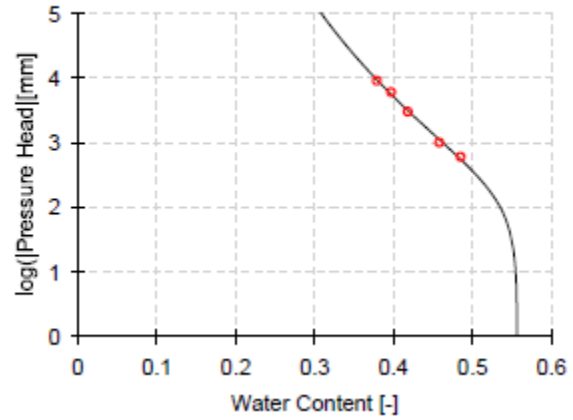
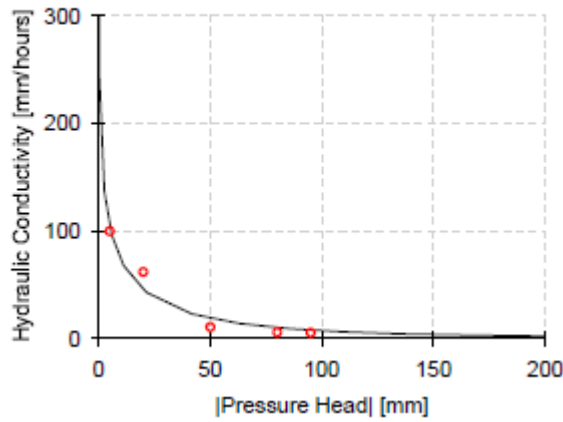
S35_C, 40 cm, Pali Hwy, Lolekaa silty clay



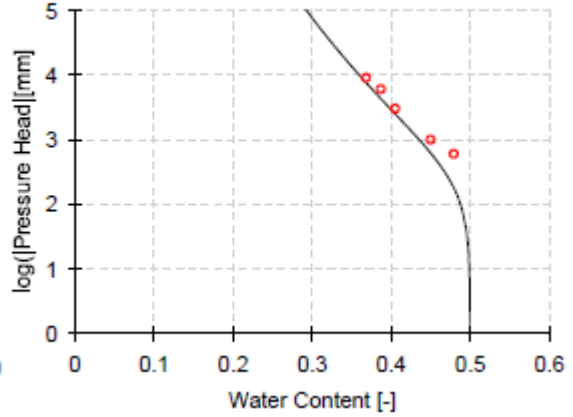
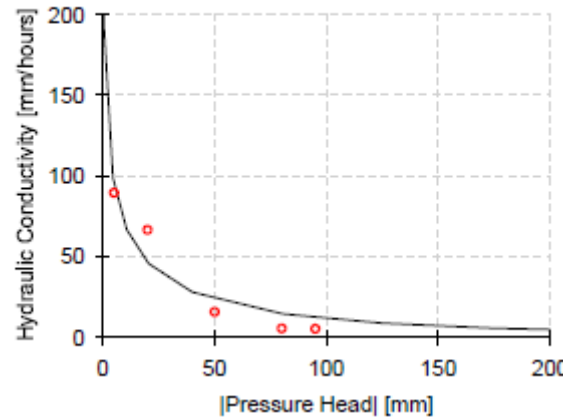
S46_A, 30 cm, Honouliuli



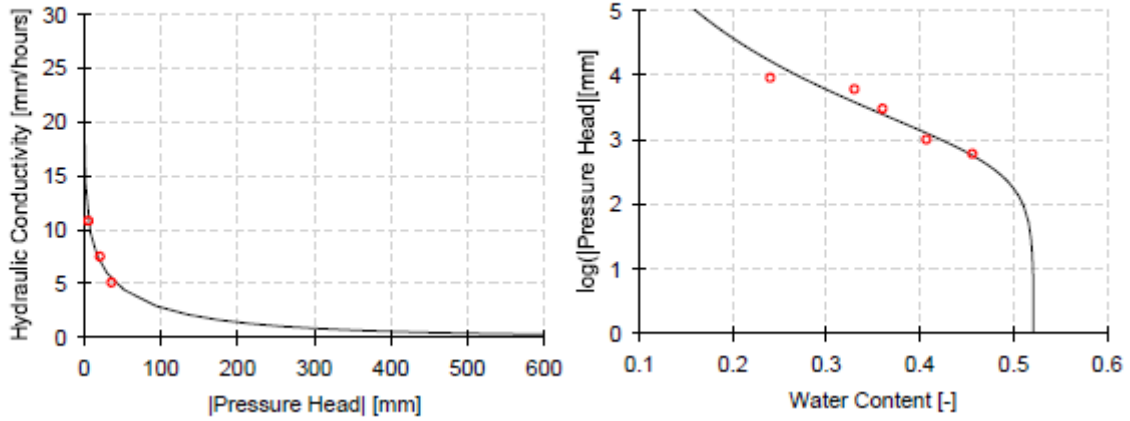
S46_B, 30 cm, Honouliuli



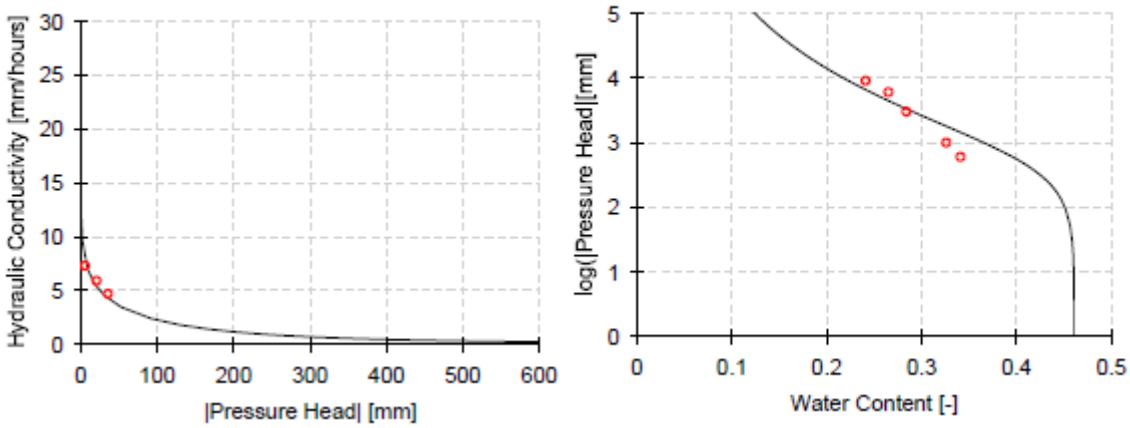
S46, median, 45 cm, H1 – Kalaeloa Blvd, Honouliuli



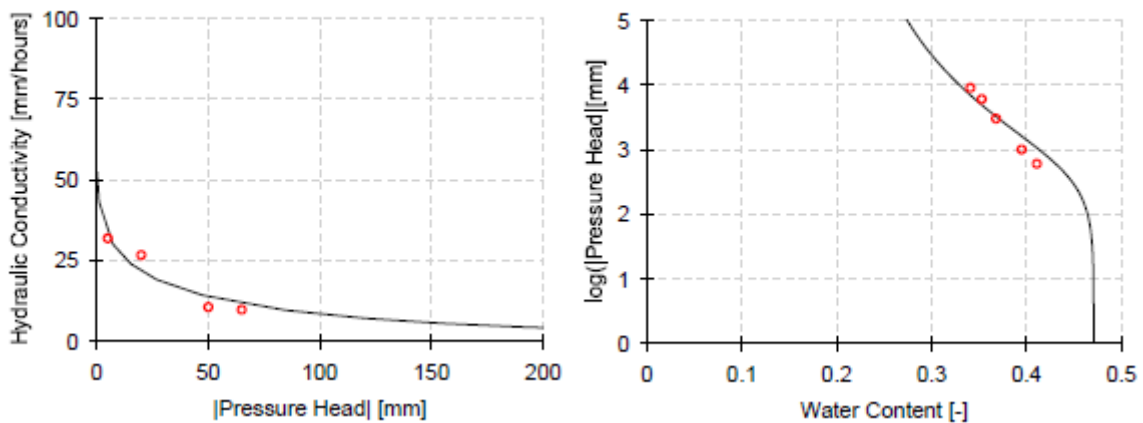
S5, 30 cm, H3 – H1 IC, Kawaihapai clay loam



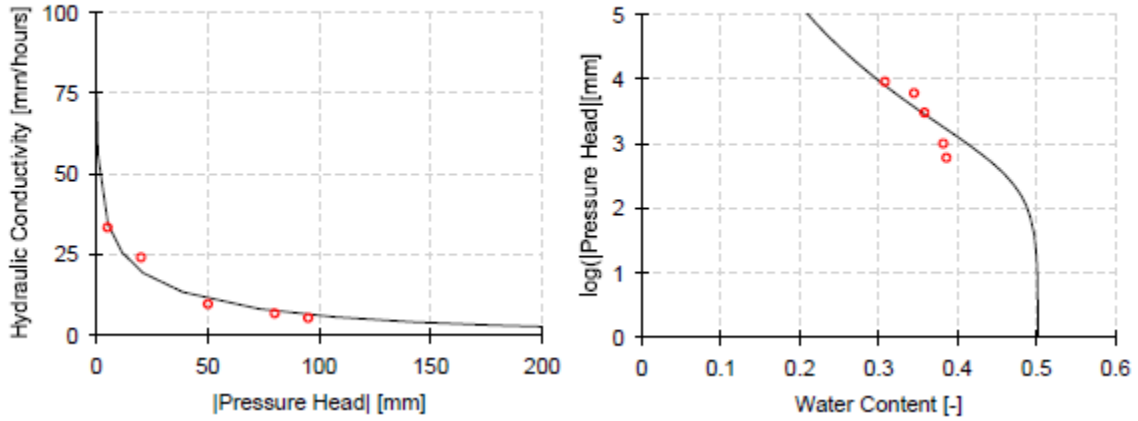
S5, 55 cm, H3 – H1 IC, Kawaihapai clay loam



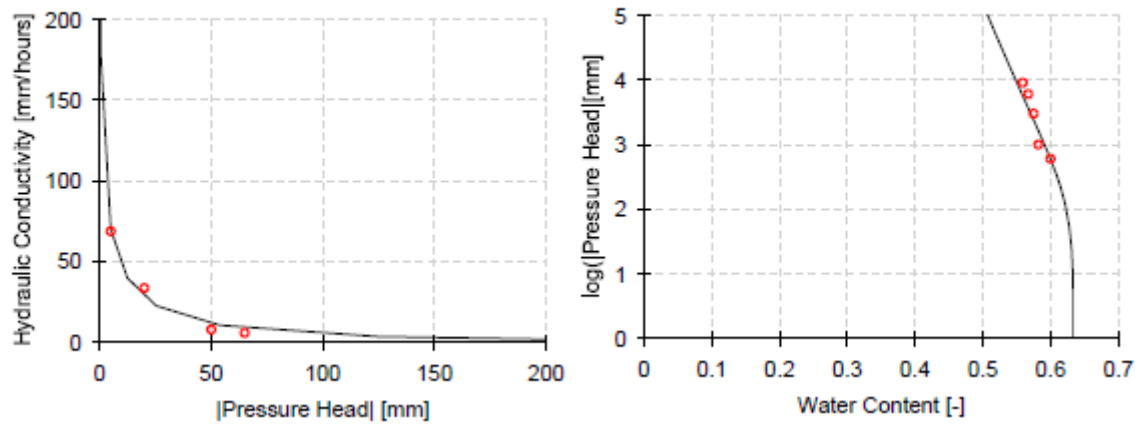
Koko silt loam, Sandy Beach Park, 40 cm depth



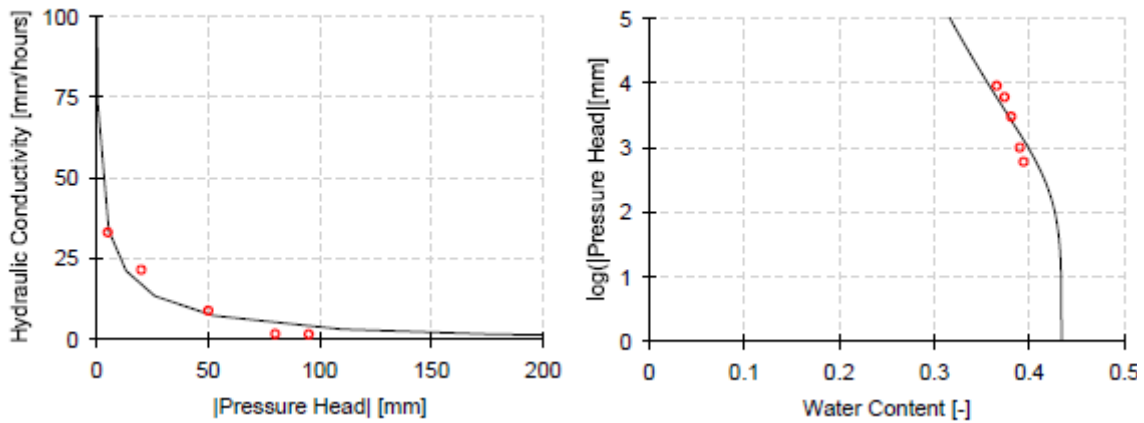
S6, 33 cm, Likelike – H1 IC, Kaena clay



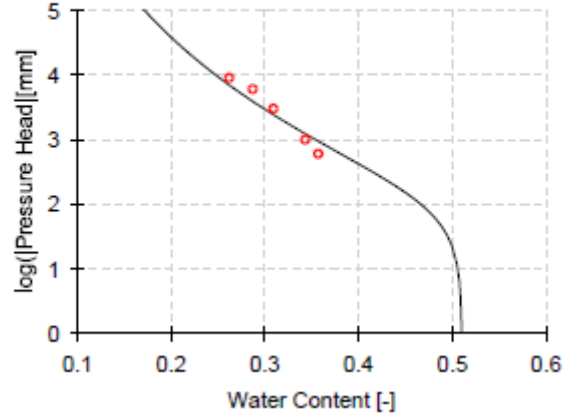
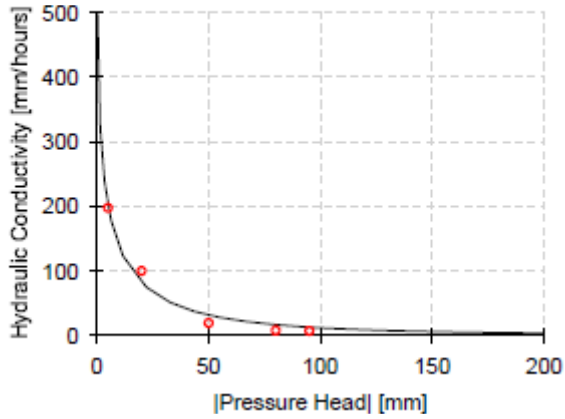
S62 - A, 30 cm, Likelike – Kahekili, Hanalei silty clay



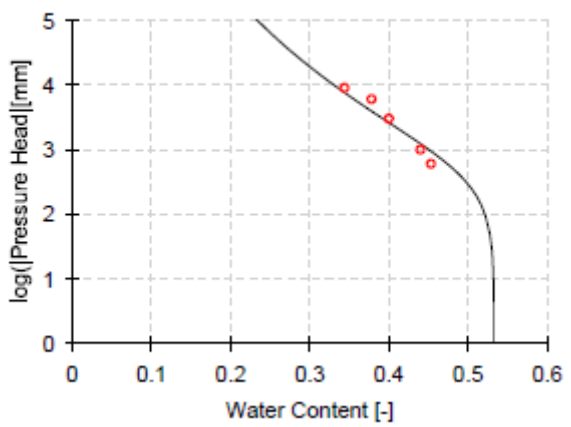
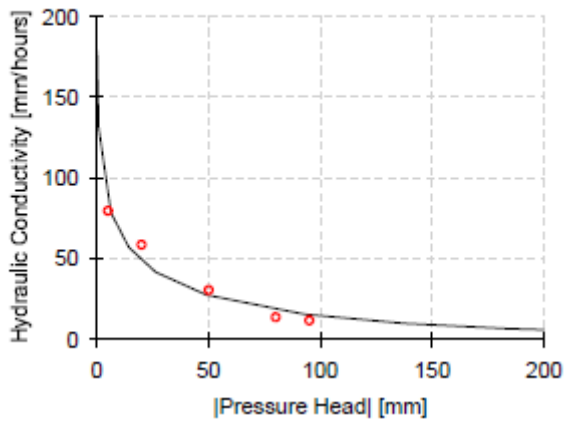
S62 - B, 45 cm, Likelike – Kahekili, Hanalei silty clay



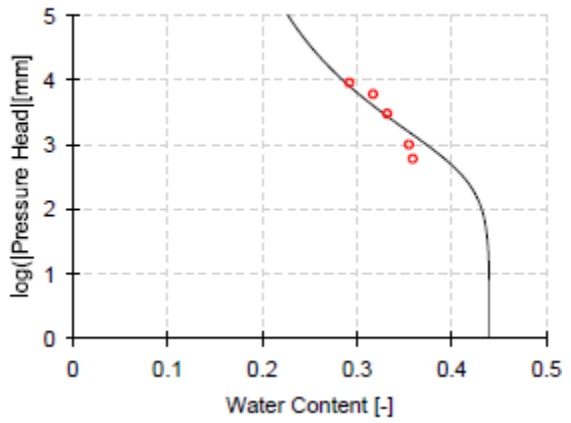
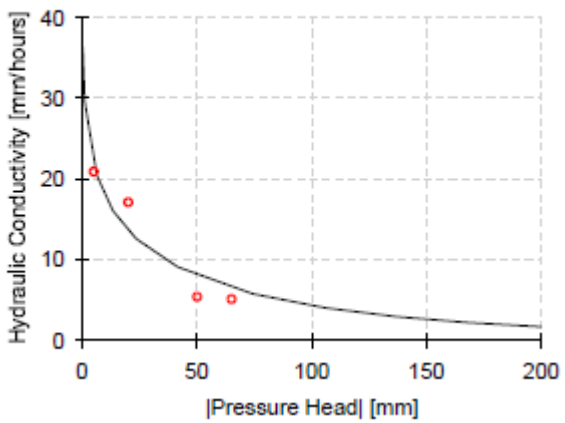
S7, 50 cm



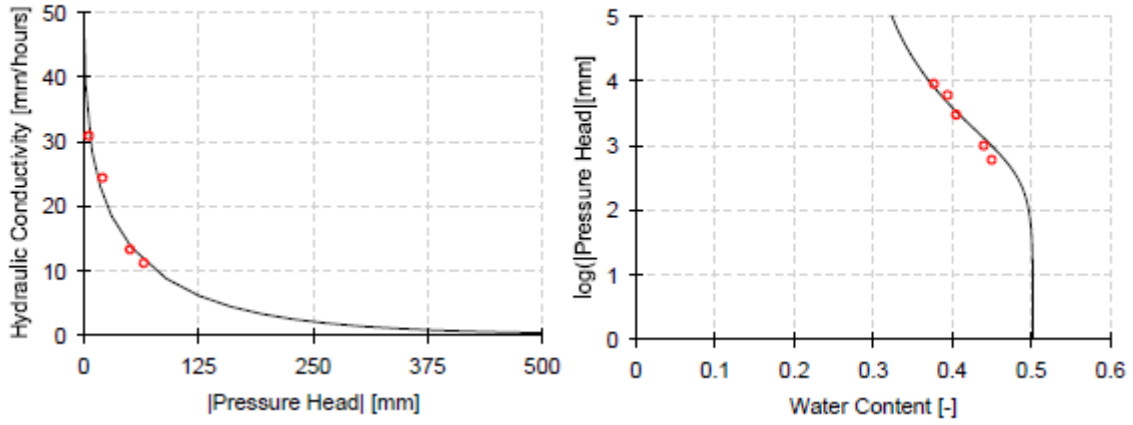
H1 Univ Ave, 65 cm, Makiki clay loam



S9 - 15 cm



S9 – 30 cm



Appendix C. Sampling H3 runoff.



Appendix D. Comparative concentration of heavy metals (dissolved, µg/L) in runoff from H3 during May 2008 and California during 2000 - 2003. H3 runoff was collected at two locations (A & B) at Parsons Brinkerhoff's site on Halawa Valley Street. The California data are from Kayhanian et al. (2007) and show median value and range (shown in brackets).

	Container A	Container B	Average	California 2000-2003
As	6	ND	3	0.7 (0.5-20)
Cd	ND	1	0.5	0.13 (0.2-8.4)
Cr	8	13	10.5	2.2 (1-23)
Cu	ND	ND	ND	10.2 (1.1-130)
Ni	4	11	7.5	3.4 (1.1-40)
Pb	ND	ND	ND	1.2 (1-480)
Zn	6	1	3.5	40.4 (3-1017)
Co	2	1	1.5	no measurements
Se	6	ND	3	no measurements

Appendix E. Summary statistics of the highway runoff quality on Oahu, Hawaii and California.

Constituent		H1 at Kapiolani-King 2006 – 2008			H1 at Punahou 2007 – 2008			H3 at Kapaa 2007 – 2008			H3 – Halawa 2000 - 2008			Kalaniana'ole Hwy. at Waimanalo 2007- 08			H3 1992- 981	California Highways 2000 - 2003			H3 at PB May 2008
Name	Unit	No.	Med	Range	No.	Med	Range	No.	Med	Range	No.	Med	Range	No.	Med	Range	Max ²	No.	Med	Range	
pH	PH unit	20	7.3	6.8 – 8.3							117	7.4	1.5 – 8.4				4.4 - 9.3	633	7	4.5 – 10.1	7.4
TSS	mg/L	8	177	21 – 540	14	72.5	15 - 384	65	65.3	9 – 1280	153	50	5 – 5380	23	63	8 – 775	1030	634	59.1	1 – 2988	3312
TDS	mg/L										154	59.5	15 – 192					635	60.3	3.7 – 1800	464
N total	mg/L	18	2.9	0.73 – 9.3	14	5.62	1.2 - 11.6	65	1.7	0.4 - 13	137	0.6	0.1 – 24	23	2.97	1.1 – 6.1	0.86	626	1.4	0.1 – 17.7	5.91
P total	mg/L	18	0.89	0.11 – 2.2	14	0.6	0.21 – 1.75	65	0.22	0.05 – 2.08	140	0.1	0.02 – 5.45	23	0.53	0.07 – 1.95	0.36	631	0.18	0.03 – 4.69	< 1
P (Dis.)	mg/L	18	0.09	0.05 - 0.15							142	0.02	0.02 - 0.12					630	0.06	0.01 – 2.4	< 1
COD	mg/L										136	20	5 – 410				10	635	13.1	1.2 – 483	51.15
O&G	mg/L	7	9.6	5 – 17							77	4	0.5 – 8				3	39	6	1- 20	8.8
TPH	mg/L	6	5.05	1 – 12							75	1	0.5 - 6					22	1.4	0.12 - 13	8.8
Cd total	µg/L	20	0.87	0.09 – 3.01							151	0.07	0.01 – 0.84					635	0.44	0.2 – 30	13
Cr total	µg/L	20	35	2 – 73							56	6	1 - 289				5	635	5.8	1 – 94	13
Cu total	µg/L	20	187.5	12.1 – 374							158	9.5	1.2 - 168				5	635	21.1	1.2 – 270	0
Pb total	µg/L	20	108	3.84 – 250							134	2.91	0.04 – 25.7				3	635	12.7	1 – 2600	0
Ni total	µg/L	20	36.1	5.4 – 98.2							41	3.68	1.08 – 126				6	635	7.7	1.1 – 130	11
Zn total	µg/L	20	596.5	48 – 1250							158	30	0.5 - 274				30	635	111.2	5.5 – 1680	6

¹The monitoring period varied for different stations and the number of samples was generally less than the number of measurements during 2000 – 2008.

²Instead of maximum value, the range is shown for pH.

³Metal concentrations from H3 at Parsons Brinkerhoff's site May 2008, are dissolved concentrations. Two values (from 2 samples) were obtained of which the larger one is shown here.

Appendix F. Comparison of cations and anions of storm runoff with the tap water.

A comparison of the concentrations of cations and anions in H3 runoff with tap water collected from the University of Hawaii campus shows that concentrations of all elements were lower in the runoff than in the tap water except for fluoride, bromide, nitrate and calcium.

Comparison of results of two different sampling location A (northeast bound lane) with B (southwest bound lane) indicates that the runoff coming from the northeast bound lanes (A) is higher in dissolved organic carbon (DOC), total N, cations and anions in general and nitrate and ammonium in particular. This may be due to the larger number of cars coming from the farm areas in the leeward side of the island in these lanes and more industrial activity in Honolulu area.

Interestingly, copper and zinc were the metals that showed the highest concentrations in the sediments around the H3 drain outlets. This may indicate that copper and zinc are transported mainly bound to particles in the runoff.

Table 1 Minimum, maximum and average concentration of different constituents in runoff from H3 at Parsons Brinkerhoff's portable office building on Halawa Valley Street. Yellow numbers show concentrations that are higher than corresponding constituents in tap water. A total of fourteen samples were collected during eight storm events between February and May 2009.

	Minimum	Maximum	Average	Tap Water
DOC (mg/ L)	7.13	293	50.94	
Total Nitrogen (mg/ L)	0.60	39	6.12	
Fluoride	0.04	0.31	0.12	0.03
Chloride	41.40	214.00	107.53	85.84
Nitrite	<0.2	29.20	14.68	<0.2
Bromide	0.07	0.84	0.31	<0.2
Nitrate	<0.2	7.59	2.35	2.24
Phosphate	<1	32.42	6.76	<1
Sulfate	13.14	323	55.24	14.97
Lithium	<0.02	<0.02	<0.02	<0.02
Sodium	23.60	131.10	57.90	59.75
Ammonium	<0.1	7.63	2.87	<0.1
Potassium	2.02	52.40	7.40	2.64
Magnesium	3.21	28.80	8.79	12.21
Calcium	29.94	185.90	73.08	12.35

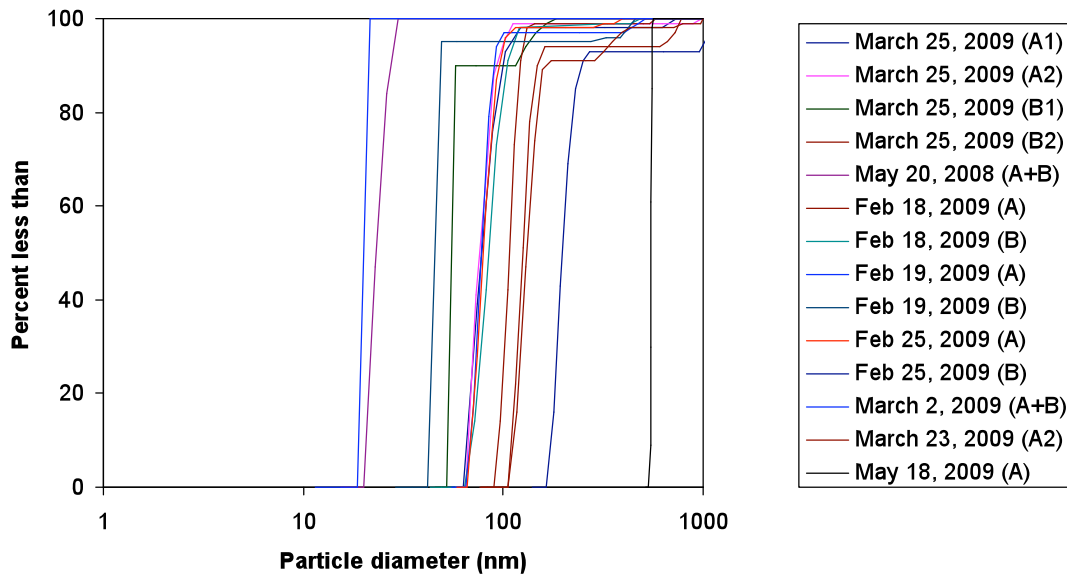
Table 2 Concentrations of different constituents (mg/L) in runoff from H3. The runoff was collected at two locations (A and B) at Parsons Brinkerhoff's portable office building on Halawa Valley Street. Point A represents runoff from Kaneohe heading traffic whereas point B represents runoff from Honolulu heading traffic.

	April 28, 2008 to May 20, 2008	After 8 days of drought 17.8 mm of rain fell in 3 days	Feb 11, 2009 to Feb 15, 2009 (rain=7.9 mm)	It fell 17 mm rain before start of sampling meaning first flush was missed	Feb 18, 2009, 10 am to Feb 19, 2009, 10 am (rain=9.7mm)	72 h of no-rain period prior sampling	Feb 24, 2009, 11:15 pm to Feb 25, 2009, 11 am (rain=2.8mm)	4 days and 18 hours of no-rain period prior the collection	Feb 26, 2009, 10 am to March 2, 2009, 10 am (rain=4.6mm)	Tap Water 10/27/2008 WRRC, UH
Sampling point	A	B	A	B	A	B	A	B	A + B	
DOC (mg/ L)	57.54	44.76	58.83	20.32	10.69	7.13	53.94	27.56	12.52	
Total nitrogen (mg/ L)	7.14	4.67	5.65	4.22	1.11	0.60	3.97	2.02	1.18	
Fluoride	0.14	0.18	0.28	0.04	0.08	0.04	0.12	0.09	0.08	0.03
Chloride	52.82	53.58	113.79	89.40	46.8	50.8	209.2	130.0	51.5	85.84
Nitrite	<0.2	<0.2	<0.2	<0.2	<0.2	<0.2	<0.2	<0.2	<0.2	<0.2
Bromide	0.11	0.12	0.27	0.23	0.08	0.07	0.64	0.36	0.11	<0.2
Nitrate	<0.2	<0.2	<0.2	0.42	<0.2	0.65	7.59	1.54	0.56	2.24
Phosphate	<1	<1	<1	0.52	<1	<1	<1	0.30	<1	<1
Sulfate	26.53	22.77	39.94	28.38	13.1	16.7	74.6	36.8	15.8	14.97
Lithium	<0.02	<0.02	<0.02	<0.02	<0.02	<0.02	<0.02	<0.02	<0.02	<0.02
Sodium	39.71	39.61	60.13	48.11	30.57	33.09	94.41	66.96	33.48	59.75
Ammonium	6.90	4.20	<0.1	0.24	<0.1	<0.1	<0.1	0.16	0.18	<0.1
Potassium	6.02	6.48	3.13	2.81	2.02	2.34	6.08	3.77	2.37	2.64
Magnesium	8.26	8.29	8.21	5.33	5.38	5.15	11.80	5.74	4.29	12.21
Calcium	89.19	82.58	81.03	49.59	44.05	42.65	89.81	45.18	29.94	12.35
pH	7.3	7.4	7.1	7.0	6.4	6.6	6.3	6.2		

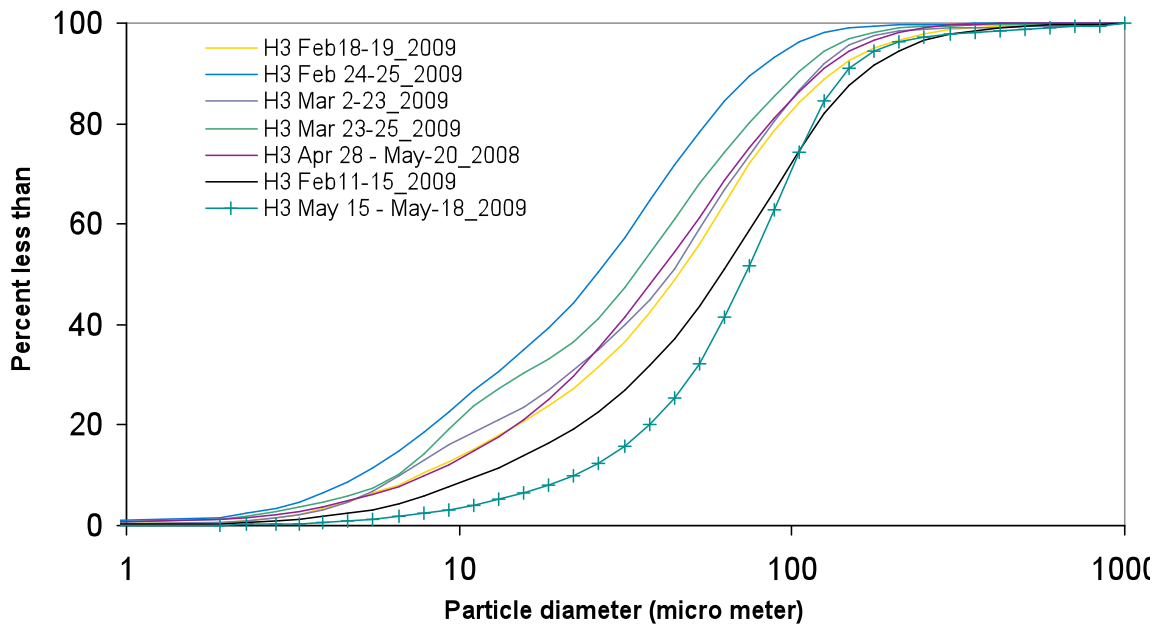
Appendix G. Concentrations of heavy metals (dissolved, µg/l) in runoff from H3. The runoff was collected at two sites (A and B) at Parsons Brinkerhoff's portable office building on Halawa Valley Street. Point A represents runoff from Windward heading traffic whereas point B represents runoff from Honolulu heading traffic.

	Ground water (HDOH)	April 28, 2008 to May 20, 2008	After 8 days of drought 17.8 mm of rain fell in 3 days	Feb 18, 2009, 10 am to Feb 19, 2009, 10 am (rain=9.7 mm)	72 h of no-rain period prior sampling	Feb 24, 2009, 11:15 pm to Feb 25, 2009, 11 am (rain=2.8 mm)	4 days and 18 hours of no-rain period prior the collection	Mar 23, 2009, 10 am to Mar 25, 2009, 10 am (tot rain=mm)	4 days and 18 hours of no-rain period prior the collection
Sampling point		A	B	A	B	A	B	A	B
As	10	6	0	13.5	14.2	11.4	15.5	18.3	12.1
Cd	3	0	1	5.4	6.1	5.9	6.3	5.6	6.1
Co	0.042	2	1	10.0	10.4	10.5	9.8	9.8	11.2
Cr	7.4	8	13	20.3	20.5	40.3	21.5	38.2	29.5
Cu	2.9	0	0	0.0	0.0	0.0	0.0	0.0	0.0
Ni	5	4	11	15.5	14.0	18.5	16.1	17.1	14.5
Pb	5.6	0	0	45.4	42.7	39.5	412.0	40.5	47.7
Se	5	6	0	44.5	58.8	59.8	59.9	60.9	59.2
Zn	22	6	1	0.0	0.0	0.0	0.0	0.0	0.0

Appendix H. Cumulative particle size distribution for particles ranging from 1 to 1000 nm (colloidal) in fourteen samples collected during eight storm events in H3 runoff.



Appendix I. Cumulative particle size distribution for particles ranging from 1 to 1000 μm (non-colloidal) in H3 runoff during seven storm events.



Appendix J. Detailed description of a suitability index map development.

Selected thematic layers as input data

Among the various criteria for site siting of infiltration trenches recommended by several states and EPA in the US, seven (GIS) data layers were initially compiled and then used for subsequent (spatial) overlay analyses (see Appendix J Tables 1 and 2. In Appendix J Table 2, the road layer was additionally included as the main thematic layers for assessing site feasibility because infiltration trenches should be implemented (or are as being more suitable) along the highway, where possible.

Before the main overlay analyses, the coordinate system for the thematic layers were transformed to NAD83 (datum) / UTM zone 4N (projection) which are commonly used in Hawaii (i.e., the state plane coordinate system). All vector files, made up of (digital) lines, curves and shapes, were also converted to raster files, which use a grid made up of pixels, for the main overlay analyses.

Comparison of traditional overlay analyses

Two popular overlay approaches - Analytic Hierarchy Process (AHP) and Rank Order Centroid (ROC), which are commonly employed in site suitability or vulnerability determination, were compared in regard to how they would affect the site selection for infiltration trenches.

AHP derives the weights of (individual) thematic layers from pair-wise comparisons between the two thematic layers based on their relative (or conditional) importance, i.e. by deciding one thematic layer (or criteria) is more important than another (Saaty, 1980; Sener et al., 2010). For example, analyst compares the relative importance of slope (computed as percentage from DEM) and proximity to water bodies (estimated using the euclidean distance tool from digital line graph of hydrography - streams) for assessing the site suitability of infiltration trenches.

As in all previous studies (Saaty, 1980; Sener et al., 2010), a seventeen-point grading scale from nine (extremely important) through one (equally important) to 1/9 (extremely less important) is added to a pair-wise comparison matrix (see Appendix J Table 4), a square matrix that arranges the relative importance of the thematic layers (or criteria) into rows and columns in the same order. The weight of a particular layer is then calculated from normalizing the Eigenvector that corresponds to the highest Eigen value of the matrix (see Appendix J Tables 5 and 6). Eigen value and Eigenvector are technical terms widely used in both pure and advanced mathematics (e.g., matrix factorization) and are employed to describe the fundamental properties of a given matrix (i.e., characteristic values and characteristic vectors, respectively). In mathematics, scalars λ and vectors x (consisting of $n \times 1$) which satisfy $Ax = \lambda x$ are defined as Eigenvalues and Eigenvectors for a square matrix A (consisting of $n \times n$), respectively. The sum of weights assigned for all thematic layers should be thus a unity.

Once the matrix and the weights of individual thematic layers are determined, the Consistency Ration CR (Saaty, 1980) is finally examined to verify whether the original matrix determined by the relative ranking from pair-wise comparisons of the thematic layers (or criteria) needs to be better adjusted. This can be due to a lack of consistency in a series of analyst's judgments - the conditional importance are maintained among thematic layers. The CR is given by (Saaty, 1980):

Table 1 Site suitability criteria (i.e., macroscopic criteria) suggested by EPA and several states in the US (including the criteria selected for (spatial) overlay analysis in this study¹).

Categories	Subcategories	Units	US EPA	MN	GA	CA	HI	TN (NE)	IA	NY	This study
Runoff Quality	Pollutant types ²	-	S/HC	SS	SS/TM/P	C/HM	-	SS/TM/P	C/HM	-	-
Soil quality	Permeability (hydraulic conductivity)	hr	-	≤ 72	≤ 48	-	≤ 48	≤ 48	≤ 72	-	-
	Infiltration rate	inches/hr	≥ 0.5	-	≥ 0.5	≥ 0.5	-	≥ 0.5	≥ 0.5	≥ 0.5	-
	Drainage area	acres	≤ 5	≤ 2	≤ 5	-	≤ 5	≤ 5	≤ 5	-	-
	Soil type ³	HSG	A/B	NS	A/B	A/B	-	A/B	A/B	-	A/B/C
	Land use ⁴	Not suitable (R/C/I)	-	-	C/I	I	-	I	C/I	I	OW/WW/EHW
	Slope	%	≤ 5	-	≤ 6	≤ 15	-	≤ 6	≤ 6	≤ 15	≤ 45
	Geologic sensitivity ⁵	Not suitable (C/SS/K)	-	C/SS	K	-	-	-	K	-	-
Minimum setbacks	Depth to water table and bedrock	ft	≥ 4	≥ 3	≥ 4	≥ 10	≥ 4	≥ 4	≥ 4	≥ 3	≥ 4
	Property lines	ft	-	-	≥ 10	-	-	-	≥ 10	-	-
	Building foundation	ft	≥ 100	≥ 10 or 100	≥ 25	≥ 20	≥ 25	≥ 25	≥ 25	≥ 25	-
	Private wells	ft	≥ 100	-	≥ 100	-	-	≥ 100	≥ 100	-	-
	Public water supply wells	ft	≥ 100	≥ 150	≥ 1200	≥ 100	≥ 100	≥ 1200	≥ 1000	≥ 100	≥ 100
	Septic system tank/leach field	ft	-	-	≥ 100	-	-	≥ 100	≥ 100	≥ 25	-
	Surface waters	ft	-	-	≥ 100	-	-	≥ 100	≥ 100	-	≥ 100
	Surface drinking water sources	ft	-	-	≥ 400	-	-	≥ 400	-	-	-
Climate conditions	Yes or No	Yes	Yes	-	-	-	-	Yes	-	-	

¹ References: 1) US EPA, 1999, 2) MN, 2001, 3) ARC, 2001, 4) CASQA, 2003, 5) DOH, 2007, 6) TN- TN- AMEC Earth & Environmental, Inc. 2008, 7) IT, 2009, 8) CWP, 2010.

² C/HC/P/TM/HM/S/SS: chemicals, hydrocarbons, pesticides, trace metals, hazardous materials, sediments, or soluble substances.

³ HSG: hydrologic soil group (A, B, C, or D) determined by Natural Resources Conservation Service (NRCS), US Department of Agriculture (USDA).

⁴ R/C/I: residential, commercial services, or industrial area. OW/WW/EHW: open water/woody wetlands/emergent herbaceous wetlands in National Land Cover Database (NLCD) 2001 Land Cover Class Definitions (released by United States Geological Survey, USGS). In this study, land cover classes of “developed, medium intensity” and “developed, high intensity” in NLCD 2001 received the lowest rating scores to indicate unsuitable areas instead of R/C/I (see Table 6).

⁵ C/SS/K: carbonate, surficial sand, or karst aquifers.

$$CR = \frac{\lambda_{max} - n}{(n - 1) \cdot RI} \quad (1)$$

where n indicates the number of thematic layers (or criteria), λ_{max} represents the principal Eigen value, and RI is the mean random consistency index determined by n (here $RI = 1.32$ when $n = 7$). In our study, the CR value is 0.082 (< 0.1) which indicates that the matrix has acceptable consistency (Chen et al., 2010).

The other weighting method used in our overlay analysis is the ROC which simply provides the weight of each thematic layer according to their importance (Noh and Lee, 2003). For example, analyst simply arranges thematic layers in order of importance for assessing the site suitability of infiltration trenches (see Appendix J Table 6), and derives their weights based on the following formula:

$$W_i = (1/n) \cdot \sum_{x=i}^n \frac{1}{x} \quad (2)$$

where n indicates the number of thematic layers (or criteria) and W_i presents the weight of each layer. When there are seven thematic layers as shown in this study, the weight ranked first can be computed as $(1/7) \times (1 + 1/2 + 1/3 + 1/4 + 1/5 + 1/6 + 1/7) = 0.3704$, and the second will be weighted as $(1/7) \times (1/2 + 1/3 + 1/4 + 1/5 + 1/6 + 1/7) = 0.2276$, and the last $(1/7) \times (1/7) = 0.0204$. A detailed description of each approach is also available in literature (Noh and Lee, 2003; Chen et al., 2010).

Table 2 Thematic layers used for site suitability analysis in siting infiltration trenches.

	Layer names	Layer information	Data types	Publication date	Sources	Remark ¹
1	Extract_lulc (LULC)	Land use and land cover	Raster	2001	National land cover database, USGS ²	30m resolution, WGS 1984
2	Extract_ned (DEM)	National elevation dataset	Raster	2000-Present	USGS	30m resolution, NAD 1983
3	hyd_revised (SW)	Hydrography, digital line graph	Shape	2005	USGS	1:24000 scale, NAD 1983
4	oahu_dtw (DGT)	Depth to water table	Raster	2008	SWAP in Hawaii ³	100m resolution, NAD 1983
5	Oahu_PWS_Wells (Wells)	Public water supply	Shape	2008	SWAP in Hawaii	-
6	road_major (Roads)	Roads, digital line graph	Shape	2005	USGS	1:24000 scale, NAD 1983
7	soilmu_a_hi990 (HSG)	Soil survey geographic database	Shape	2006	NRCS SSURGO, USDA ⁴	1:24000 scale, NAD 1983

¹ WGS- World Geodetic System; NAD- North American Datum.

² USGS- United States Geological Survey.

³ Source Water Assessment Program (SWAP) in Hawaii, References- Rotzoll, K. and A. I. El-Kadi (2008). "Estimating hydraulic conductivity from specific capacity for Hawaii aquifers, USA" Hydrogeology Journal 16(5): 969-979.

⁴ NRCS- the Natural Resources Conservation Service; SSURGO- Soil Survey Geographic database; USDA- United States Department of Agriculture.

Table 3. The relative (or conditional) importance of two thematic layers (Hossain and Das, 2010).

1/9	1/8	1/7	1/6	1/5	1/4	1/3	1/2	1	2	3	4	5	6	7	8	9
Extremely		Very strongly		Strongly		Moderately		Equal		Moderately		Strongly		Very strongly		Extremely
← Less important								More important →								

Table 4. A pair-wise comparison matrix for siting infiltration trenches using Analytic Hierarchy Process (AHP) which focuses on performance of infiltration trenches (by giving more weight to the layers that are likely to affect system performance than environmental management aspects)¹.

	DEM	LULC	SW	Wells	Roads	HSG	DGT	Weights
DEM	1	1/3	5	4	1/4	1/5	3	0.0939
LULC	3	1	6	5	1/3	1/4	4	0.1523
SW	1/5	1/6	1	1/3	1/7	1/8	1/4	0.0233
Wells	1/4	1/5	3	1	1/6	1/7	1/3	0.0361
Roads	4	3	7	6	1	1/3	5	0.2454
HSG	5	4	8	7	3	1	6	0.3912
DGT	1/3	1/4	4	3	1/5	1/6	1	0.0579

¹ Definitions of abbreviations of individual layers are indicated in Table 2.

Table 5. A pair-wise comparison matrix for siting infiltration trenches using Analytic Hierarchy Process (AHP) which highlighting aspect of environmental protection (by giving more weight to the layers that seem to play an important role in environmental management than system performance)¹.

	DEM	LULC	SW	Wells	Roads	HSG	DGT	Weights
DEM	1	1/3	1/6	1/7	1/4	1/5	1/8	0.0233
LULC	3	1	1/5	1/6	1/3	1/4	1/7	0.0361
SW	6	5	1	1/3	4	3	1/4	0.1523
Wells	7	6	3	1	5	4	1/3	0.2454
Roads	4	3	1/4	1/5	1	1/3	1/6	0.0579
HSG	5	4	1/3	1/4	3	1	1/5	0.0939
DGT	8	7	4	3	6	5	1	0.3912

¹ Definitions of abbreviations of individual layers are indicated in Table 2.

Table 6. Weights of individual thematic layers estimated from Rank Order Centroid. The layers are arranged in order of importance (which are likely to affect system performance) from the top of the table.

Thematic layers	Weights
HSG	0.3704
Roads	0.2276
LULC	0.1561
DEM	0.1085
DGT	0.0728
Wells	0.0442
SW	0.0204

Comparison of traditional and recent overlay approaches

Once different weights were assigned to individual thematic layers either from AHP or ROC, all layers were merged into a single suitability map by means of a weighted sum (or overlay) technique. The weighted sum (or overlay) technique provided by Spatial Analyst toolbox in ArcGIS combines weights (assigned for individual thematic layers) and ratings (assigned for object classes or cell values in a given layer) to compute a numerical value (or index) which visualizes area of interest in terms of suitability potential. The “weighted overlay” and the “weighted sum” tools provide the same functionality in terms of the superposition of thematic layers, but they differ in that the weighted overlay only allows for integer raster as inputs whereas the other tool can accept both integer and floating-point number. A similar rule also applies to weights of input rasters - the weighted overlay tool accepts weights of input rasters as a relative percentage (i.e., percent influence), whereas decimal weights are required for the weighted sum tool. In combining multiple raster inputs, we employed the weighted sum tool so that the output raster from the weighted sum could be compared to that of fuzzy logic which ranged between 0 and 1 (see Appendix J Figure 2).

In a weighted sum analysis, all objects in a given layer (or cell values of input raster) were also classified into several classes (which are grouped into ranges) using a “reclassify” tool in ArcGIS (see Appendix J Figure 2). The reclassify tool assigns a single value of each range in terms of a priority level of a class (e.g., low, medium or high importance). When grouping the values of continuous rasters into several ranges, slope and euclidean distance tools in Spatial Analyst toolbox at ArcGIS were used to compute the steepness of the ground (as percentage) and the proximity to water bodies (streams and wells) or major roads/highways. Note that some classes in a given layers (or input raster) were also excluded from the classification using the conditional operator “Set Null” in ArcGIS due largely to their physical constraints as locations to implement infiltration trenches (see Appendix J Table 1). Appendix J Tables 4, 5, 6, and Table 3 show the weights of individual thematic layers determined from AHP or ROC and ratings of object classes or cell values in a given layer classified from the reclassify tool, respectively. Finally, a numerical value which visualizes area of interest in terms of suitability potential is computed from these weights and ratings (i.e., multiplying them for each cell, summing them up, and then dividing it by 10 again).

As an alternative to traditional overlay analyses (i.e., AHP and ROC), a fuzzy logic tool provided with the new release of ArcGIS 10 through Spatial Analyst was employed to assess the site suitability for placing infiltration trenches. The fuzzy logic employs fuzzy membership and fuzzy overlay to perform the site suitability analysis, both of which reclassifies ratings of a given layer and combines a series of fuzzy membership results, respectively. In particular, the fuzzy membership tool classifies the input values of a layer between 0 (as being the least suitable, no membership) and 1 (as being the most suitable, full membership), rather than discrete classes (i.e., ratings) scaled in traditional overlay analyses, as the possibility of being a member based on a specified fuzzy function (i.e., fuzzification algorithm). For example, the fuzzy Gaussian, one of fuzzy membership functions (e.g., fuzzy large and fuzzy linear), reclassifies original values in a given layer into normal distribution. Also, the fuzzy overlay merges multiple fuzzy membership results to generate site suitability raster dataset ranging from 0 to 1 using fuzzy operators or overlay types (e.g., fuzzy and, fuzzy sum, fuzzy product, and fuzzy gamma). Fuzzy product and fuzzy sum return the membership of each cell (i.e., degree of membership belonging to all fuzzy

data sets) by multiplying and adding the fuzzy values obtained from fuzzy membership results of individual layers, respectively, for instance. In this study, we used fuzzy linear (reclassifying rasters on a continuous scale between the minimum and maximum values) and fuzzy gamma (an algebraic product of fuzzy product and fuzzy sum) as fuzzy membership and fuzzy overlay tools. The fuzzy gamma can be expressed using the power of gamma as follows:

$$\mu(x) = (f_{\text{fuzzy sum}})^{\gamma} \times (f_{\text{fuzzy product}})^{-\gamma} \quad (5)$$

Note that special care must be taken with use of fuzzy operators because the site suitability maps created significantly vary depending on these overlay types. Also, individual thematic layers, in contrast to those in AHP and ROC, are not weighted differently in the fuzzy logic assuming that all layers are equally important. A full description of each overlay analysis including fuzzy functions and operators in fuzzy logic can be accessed through the (online) ArcGIS Desktop Help.

Results

Appendix J Tables 4 through 6 show weights of the seven thematic layers used in our site suitability analysis. As shown in Tables, weights of individual layers slightly differed between the two weighting approaches (AHP vs ROC), but large differences were observed between the weights assigned by analyst's preferences. Appendix J Table 7 also presents ratings for different object classes in individual thematic layers classified from the "reclassify" tool for both AHP and ROC overlay analyses. Based on these results, it could be expected that applying different weights in (traditional) overlay analysis probably produced different suitability maps, where the difference is larger between different analyst's preferences than that of weighting approaches.

Appendix J Figure 1 illustrates a schematic diagram that shows the major steps to develop site suitability (index) maps using these weights and ratings derived for AHP and ROC overlay analyses. Appendix J Figures 1a and 1b represent two different aspects of "flow diagram" - Model Builder view (i.e., how a series of tools in ArcGIS are employed in site suitability analysis) and Image Browser view (i.e., how thematic layers are processed during the analysis), respectively. Numbers in both figures indicate the corresponding steps used in our site suitability analysis (see also the top panel of the figure). In the Model Builder of the fuzzy logic analysis, the fuzzy (linear) membership and the fuzzy (gamma) overlay tools were used instead of (traditional) reclassify and weighted sum tools. Example of site suitability analysis in Model Builder view using AHP is provided in Appendix J Figure 2. In ROC, only weights in the weighted sum tool should be changed according to Appendix J Table 6.

Appendix J Figure 4 shows the site suitability (index) maps for sitting infiltration trenches developed from the four different overlay approaches - two types of AHP (a and b), ROC (c), and fuzzy logic (d). In the figure, color bars, recorded as high (i.e., dark blue) and low scores (i.e., dark brown), indicate suitable and less suitable areas for placing infiltration trenches, respectively. The white-colored areas inside the island boundary also indicate regions excluded from the analysis due to their physical constraints as sites for implementing infiltration trenches (e.g., a low water table depth less than 4 ft and hydrologic soil group D, see Appendix J Tables 1 and 7). From the figure, it was shown that some areas seemed to be more suitable for siting infiltration trenches than the other areas on Oahu (see dark blue areas with black arrows in

Appendix J Figure 4). Those areas were mainly located in the middle of the island (regardless of methodology) and additional sites might be considered for potential locations of infiltration trenches depending on both types of overlay analyses (Appendix J Figures 4a or 4c vs Appendix Figure 4d) and analyst's preferences (Appendix J Figures 4a or 4c vs J Figure 4d).

Very little difference was, however, observed when evaluating potential sites between the two traditional overlay analyses - AHP vs ROC. Since this little difference could not easily be detected in site suitability maps, we redrew them as percentage of count (%) that fall within ranges of suitability scores (see Appendix J Figure 6). As shown in the figure, the major difference between the two analyses mainly occurred in the middle range of suitability scores (compare frequency distribution ranging from 0.50 to 0.69 in Appendix J Figures 6a and 6c), which is attributed to a small difference in the weights assigned for individual thematic layers (see Appendix J Tables 4 and 6). The ranges of scores recorded in four site suitability maps (from the highest to lowest scores) are 0.92 and 0.31, 0.87 and 0.18, 0.91 and 0.32, and 0.74 and 0 for Appendix J Figures 4a, 4b, 4c, and 4d, respectively.

From these results, we can conclude that applying various overlay approaches including analyst's preferences will result in significantly different site suitability maps. Thus, particular care needs to be taken in selecting types of overlay analyses in addition to determining which layers (e.g., rainfall in the area, pollutant attenuation capacity of soils, etc) should be considered for site suitability analysis. Among the suitability maps created, we finally determined the site suitability map based on the result of one AHP (in Appendix J Figure 4a) was the best with respect to suitability scores and clear evidence of additional site selections.

Table 7. Ratings for object classes in individual thematic layers classified from the reclassify tool for AHP and ROC overlay analyses¹.

LULC ²		Slope (from DEM)		SW		DGT		Wells		Roads		HSG ³	
Old values	New values	Old values	New values	Old values	New values	Old values	New values	Old values	New values	Old values	New values	Old values	New values
[-]		[%]		[m]		[m]		[m]		[m]		[-]	
11	0	0 - 0.83	10	30 - 81.26	1	1.22 - 22.62	1	30 - 942.61	1	0 - 800	10	1	6
21	5	0.83 - 1.94	9	81.26 - 113.63	2	22.62 - 51.49	2	942.61 - 1704.96	2	800 - 1600	9	2	10
22	4	1.94 - 3.44	8	113.63 - 164.89	3	51.49 - 90.46	3	1704.96 - 2341.81	3	1600 - 2400	8	4	3
23	3	3.44 - 5.48	7	164.89 - 246.06	4	90.46 - 143.06	4	2341.81 - 3104.17	4	2400 - 3200	7	NoData	NoData
24	2	5.48 - 8.22	6	246.06 - 374.61	5	143.06 - 214.04	5	3104.17 - 4016.77	5	3200 - 4000	6		
31	10	8.22 - 11.91	5	374.61 - 578.19	6	214.04 - 309.84	6	4016.77 - 5109.24	6	4000 - 4800	5		
42	7	11.91 - 16.90	4	578.19 - 900.57	7	309.84 - 439.14	7	5109.24 - 6417.02	7	4800 - 5600	4		
52	6	16.90 - 23.64	3	900.57 - 1411.12	8	439.14 - 613.63	8	6417.02 - 7982.53	8	5600 - 6400	3		
71	8	23.64 - 32.73	2	1411.12 - 2219.62	9	613.63 - 849.13	9	7982.53 - 9856.59	9	6400 - 7200	2		
82	9	32.73 - 45	1	2219.62 - 3500	10	849.13 - 1166.97	10	9856.59 - 12100	10	7200 - 8000	1		
90	0	NoData	NoData	NoData	NoData	NoData	NoData	NoData	NoData	NoData	NoData	NoData	NoData
95	0												

¹ Individual object classes in most continuous rasters (such as slope, SW, DGT, Wells) are categorized based on the geometrical interval classification (GI, recommended to visualize spatial databases which do not show a normal data distribution), equal interval scheme was used for Roads raster. Another reason to implement GI method was that we had to assess the site suitability in a limited land area. However, all these rasters were transformed on a continuous scale between 0 and 1 using a fuzzy linear membership tool in a fuzzy logic analysis, rather than discrete classes scaled in traditional overlay analyses, as shown above. For example, new values in the slope raster increased linearly with increase of slope percentage (thus, old values of 0 and 45 were transformed to new values of 0 and 1, respectively).

² Old values from 11 to 95 represent Open Water, Developed, Open Space, Developed, Low Intensity, Developed, Medium Intensity, Developed, High Intensity, Barren Land, Evergreen Forest, Shrub/Scrub, Herbaceous, Cultivated Crops, Woody Wetlands, Emergent Herbaceous Wetlands, respectively.

³ Old values of 1, 2, 3, and 4 represent hydrologic soil groups B, A, D, C, respectively. Here, hydrologic soil group D was excluded from the analysis.

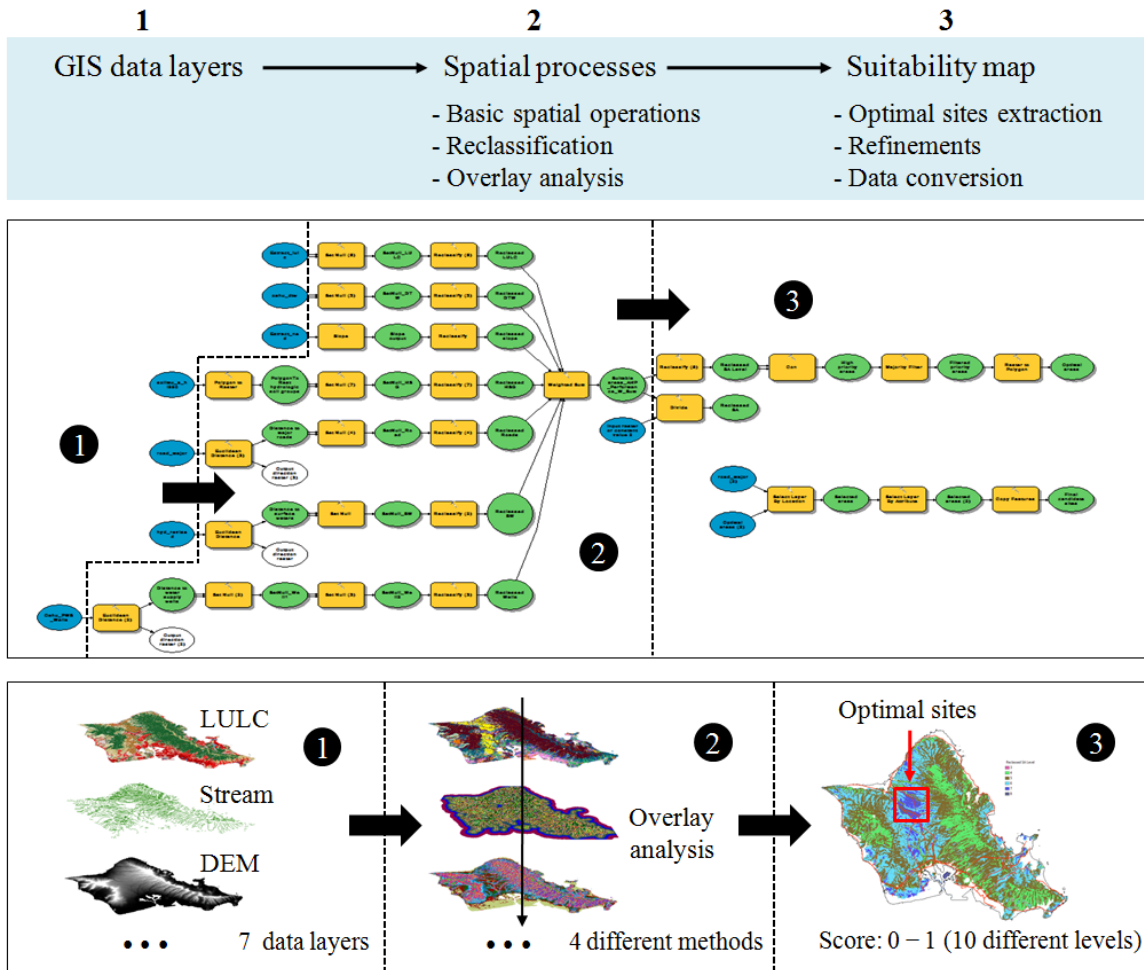


Figure 1 Schematic illustration of a suitability map determination in siting infiltration trenches: (a) Model Builder view (for more information, please refer to Figure 9) and (b) GIS data layer view.

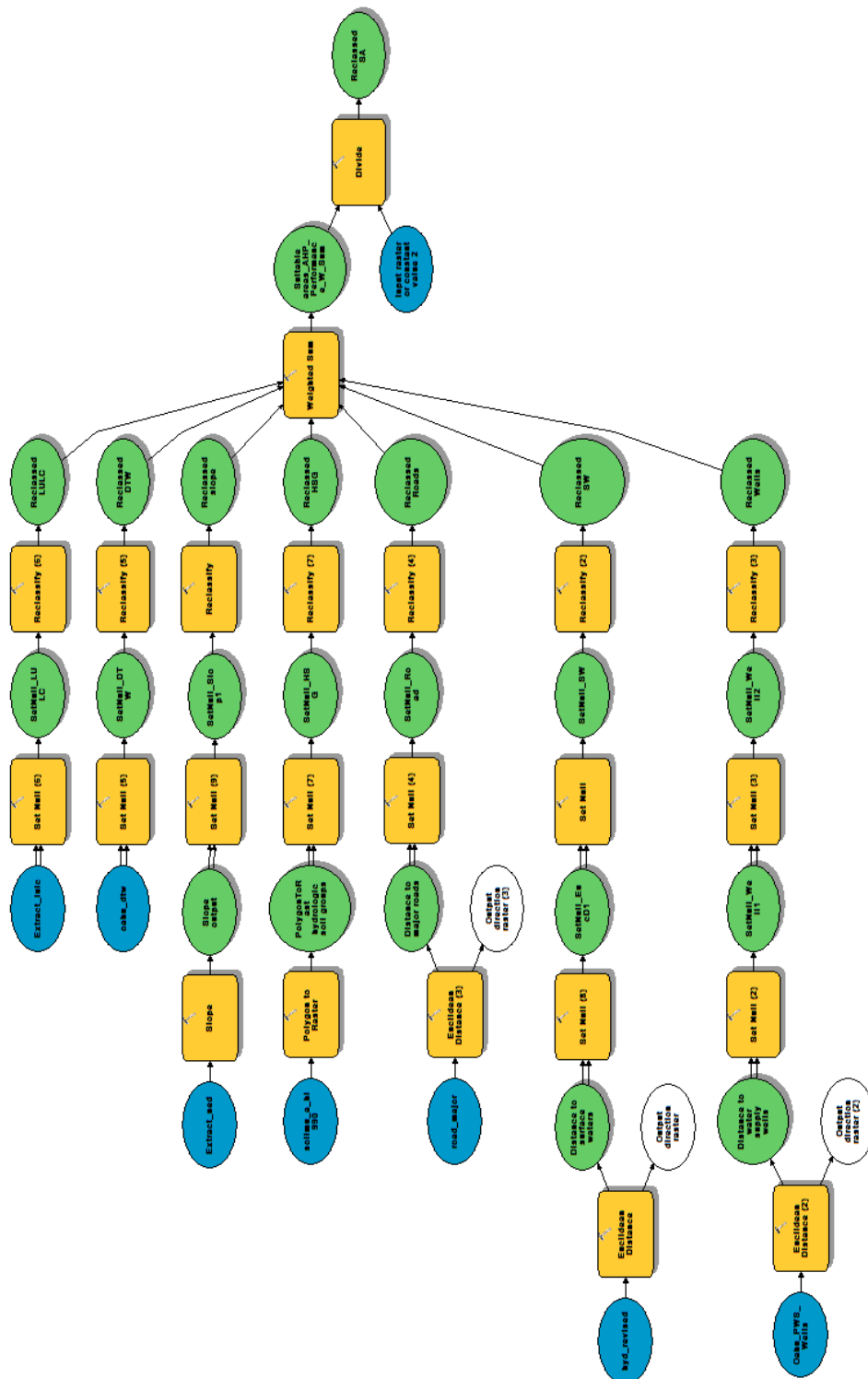
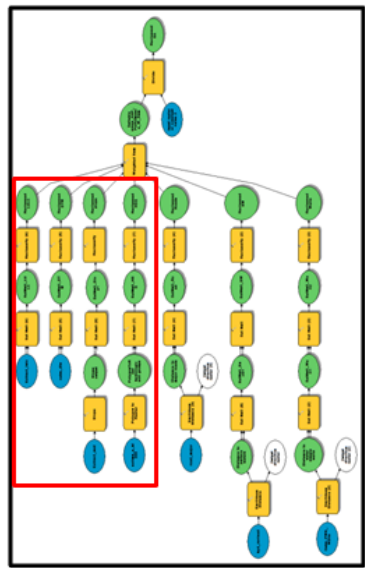


Figure 1a Schematic illustration of a suitability map determination for siting infiltration trenches in Model Builder view (see Appendix J Figure 1). Here, miscellaneous tools to finally refine the suitability maps were eliminated to briefly show important processes employed in ArcGIS. Shown below is an example of Model Builder view to develop final suitability maps using Analytic Hierarchy Process (AHP) in Appendix J Figure 4a.

Site suitability analysis in Model Builder View



Parts A

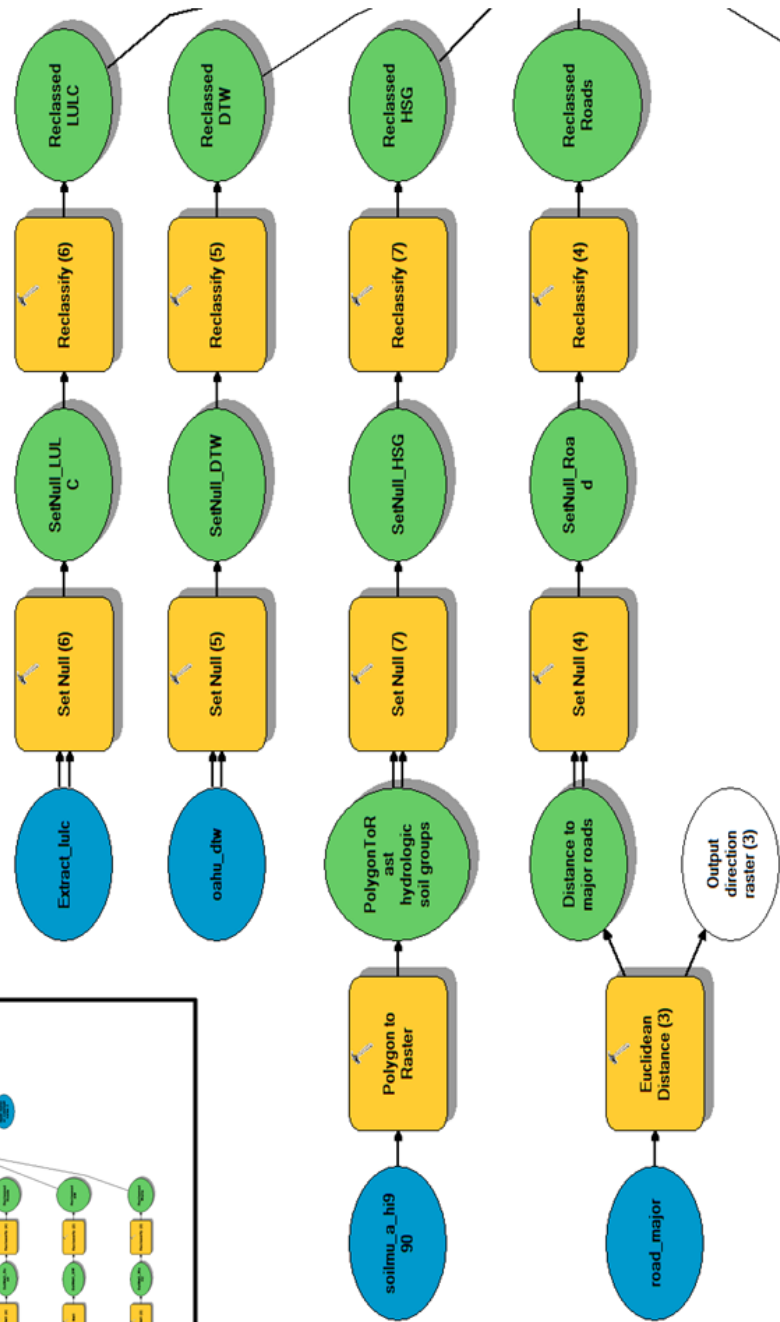
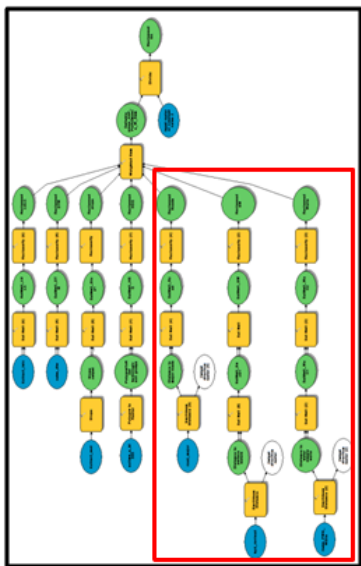


Figure 1b Parts A from Appendix J Figure 2.

Site suitability analysis in Model Builder View



Parts B

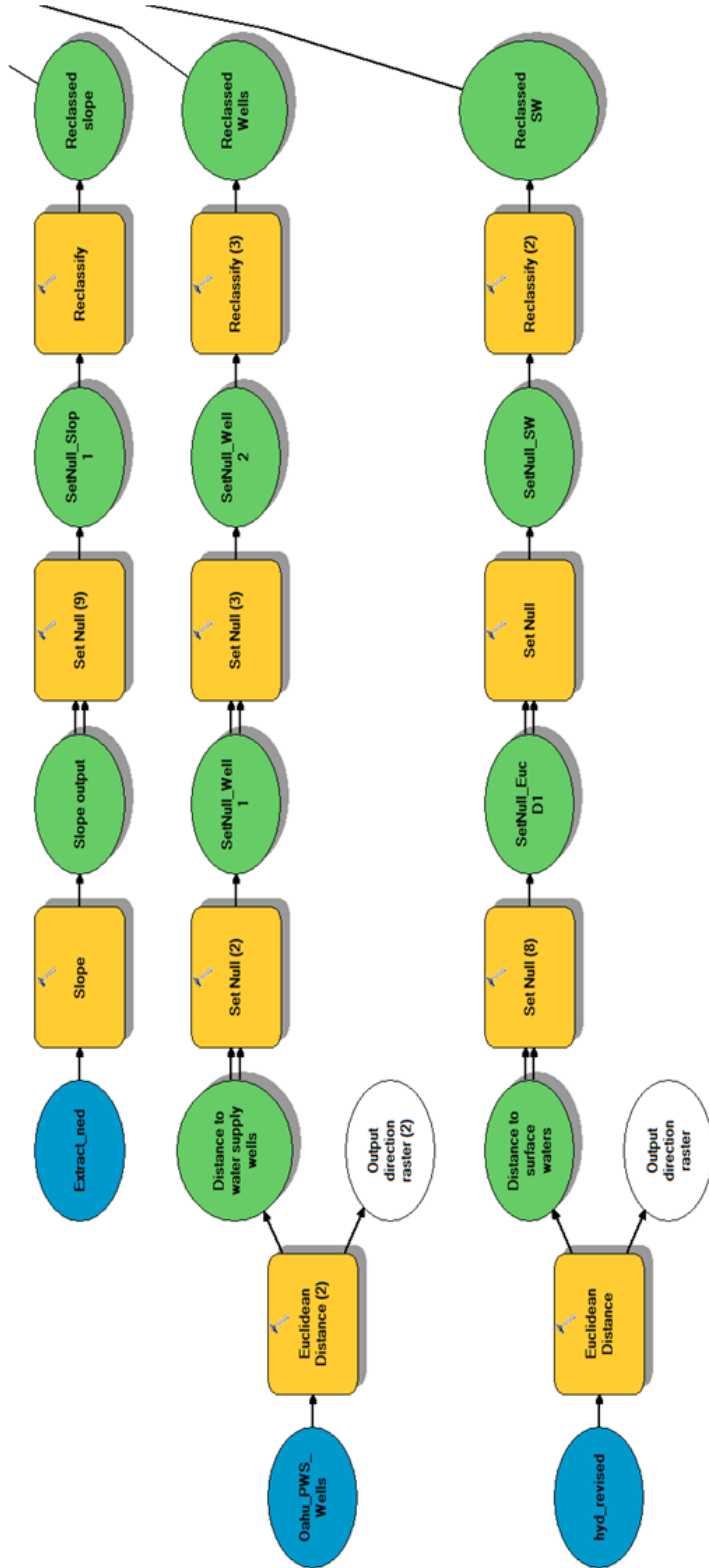
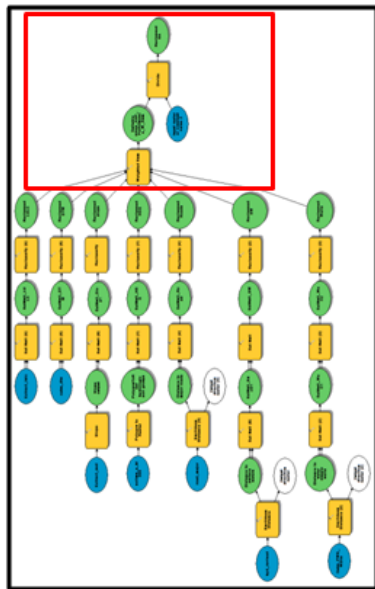


Figure 1c Parts B from Appendix J Figure 2.

Site suitability analysis in Model Builder View



Parts C

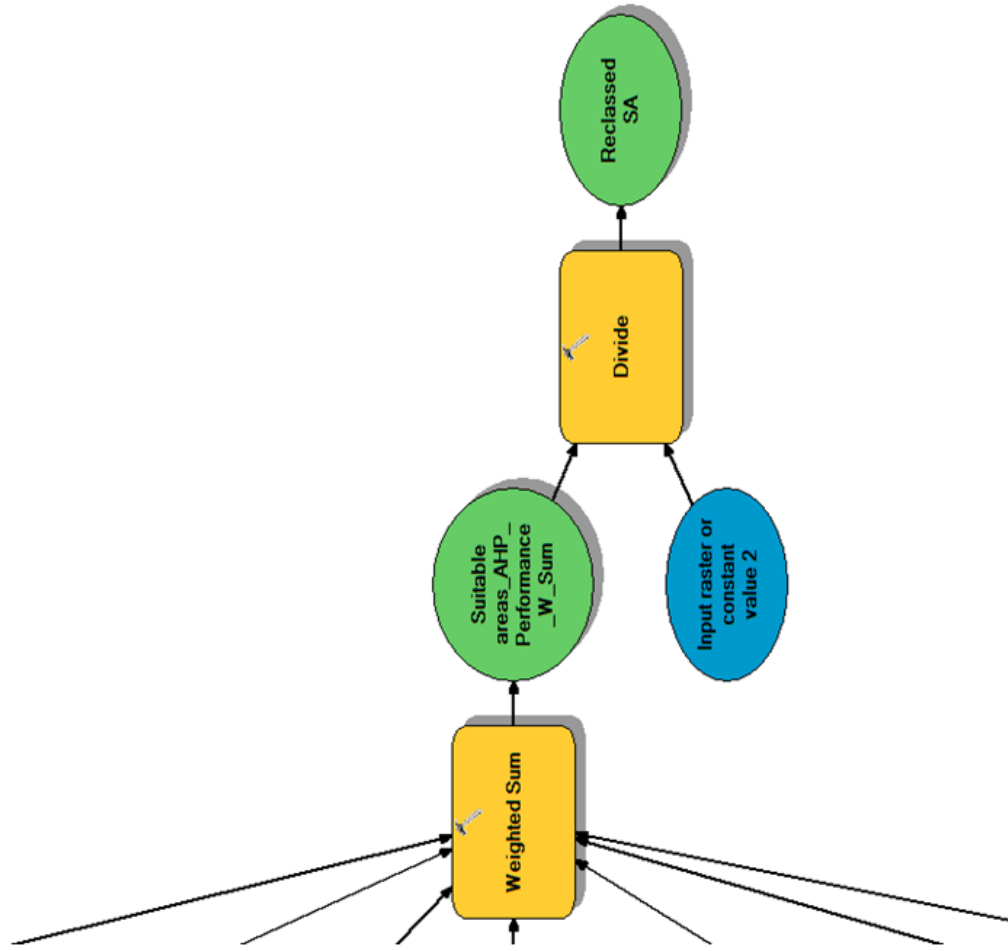


Figure 1d Parts C from Appendix J Figure 2.

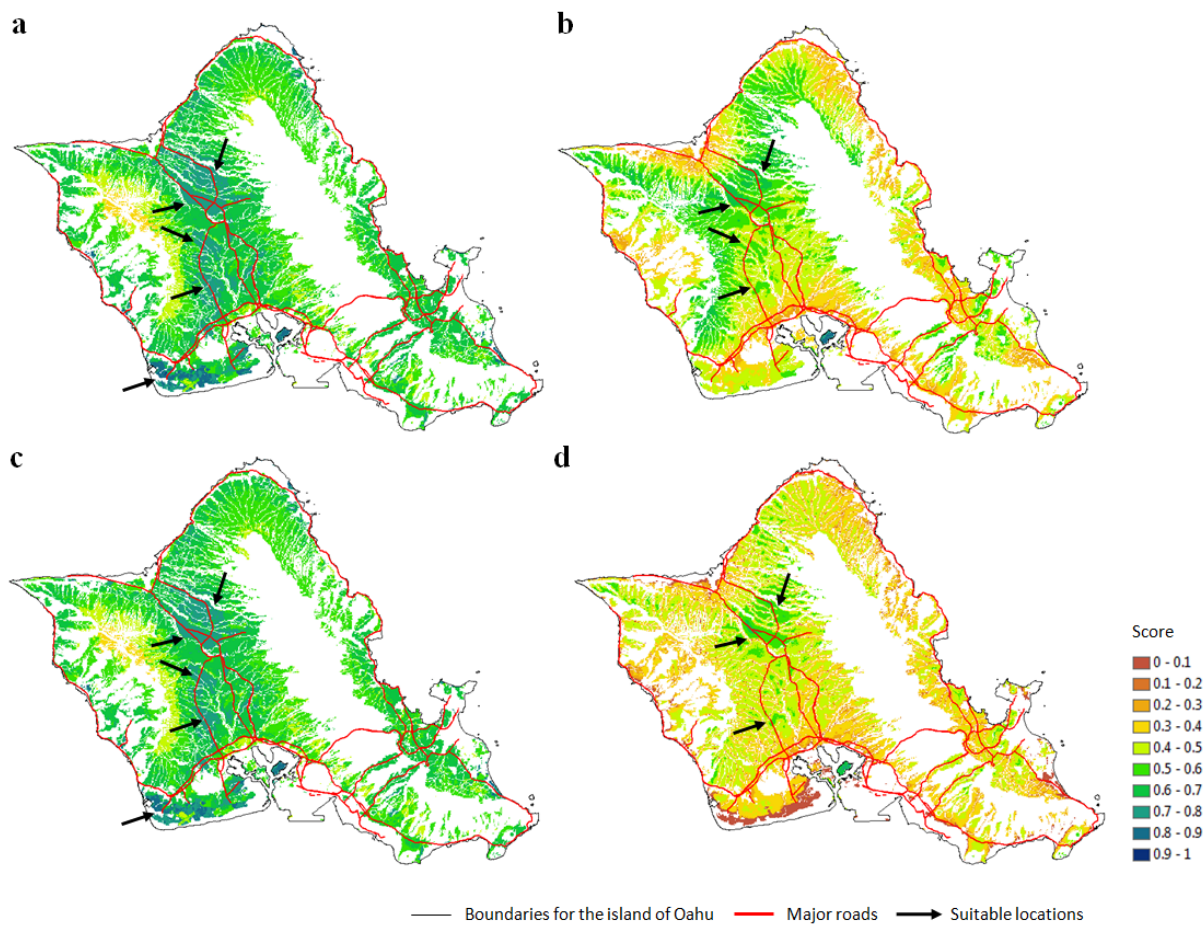


Figure 4 Site suitability maps (1:300,000 scale) drawn from different overlay analysis techniques and analyst's preferences: (a) Analytic Hierarchy Process (AHP) focusing on performance of infiltration trenches (by giving more weight to the layers that are likely to affect system performance than environmental management aspects), (b) AHP highlighting aspect of environmental protection (by giving more weight to the layers that seem to play an important role in environmental management than system performance), (c) Rank Order Centroid stressing system performance rather than protection, and (d) fuzzy logic overlay analysis (when Gamma, an optional overlay type of fuzzy logic, is 0.9). In the figure, suitability scores 0 and 1 indicate less suitable and highly suitable areas for placing infiltration trenches, respectively.

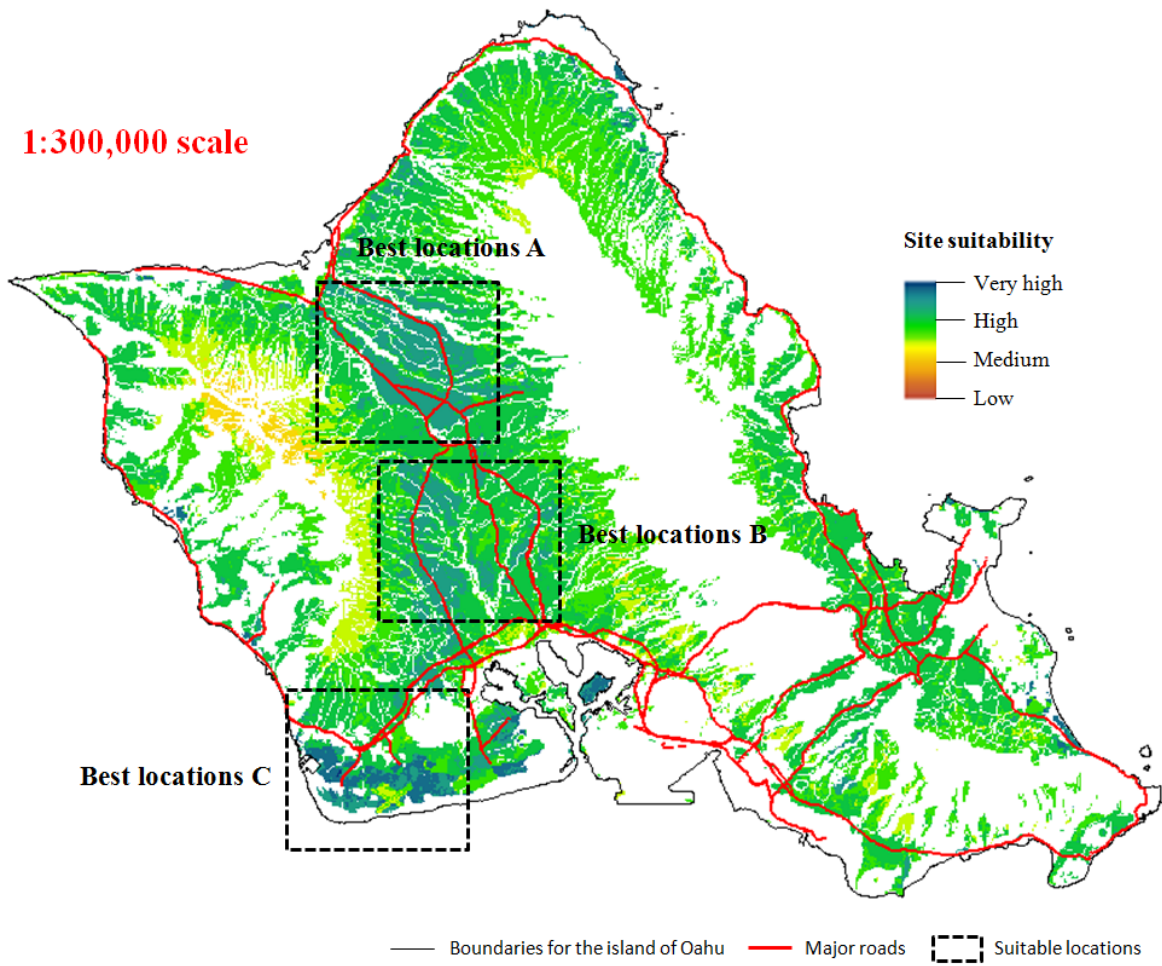
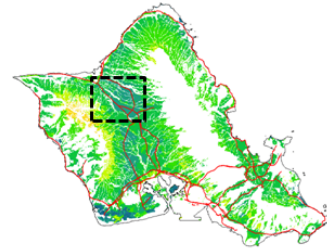
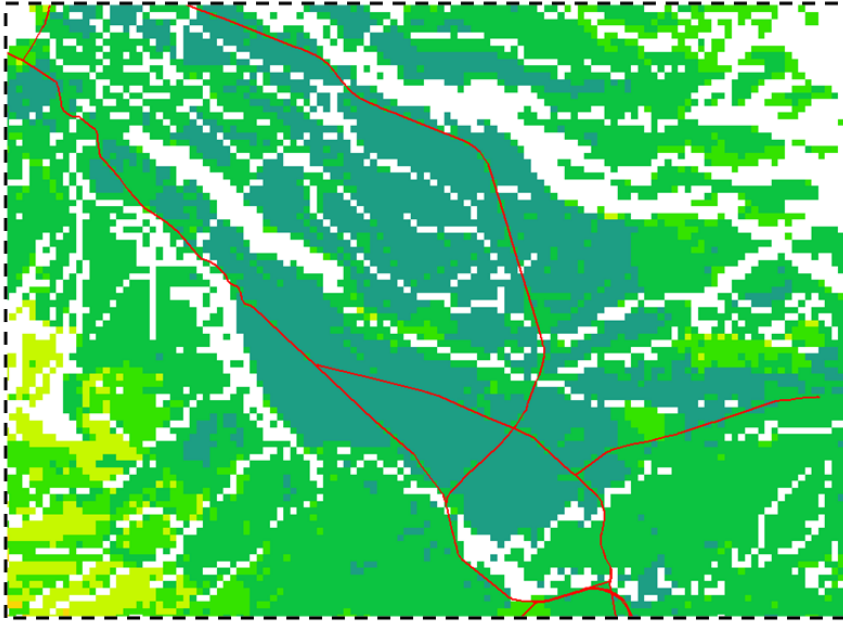
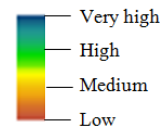


Figure 4a Site suitability maps (1:300,000 scale) developed by Analytic Hierarchy Process (AHP) which focuses system performance rather than environmental protection. The resolution of raster is 100×100 meters.

1:50,000 scale



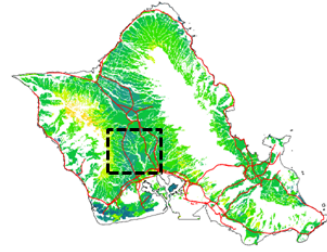
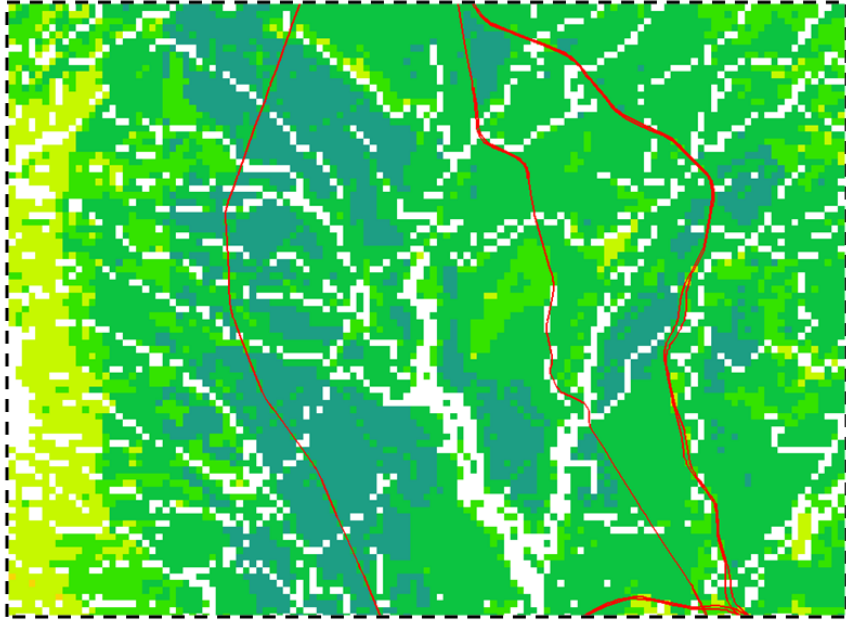
Site suitability



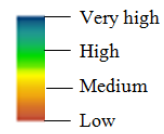
— Boundaries for the island of Oahu — Major roads — Suitable locations

Figure 4b Best locations A (1:50,000 scale) from Appendix J Figure 4a.

1:50,000 scale



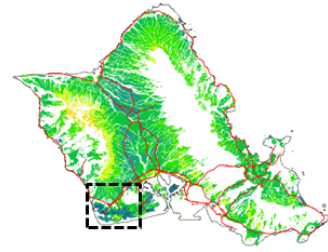
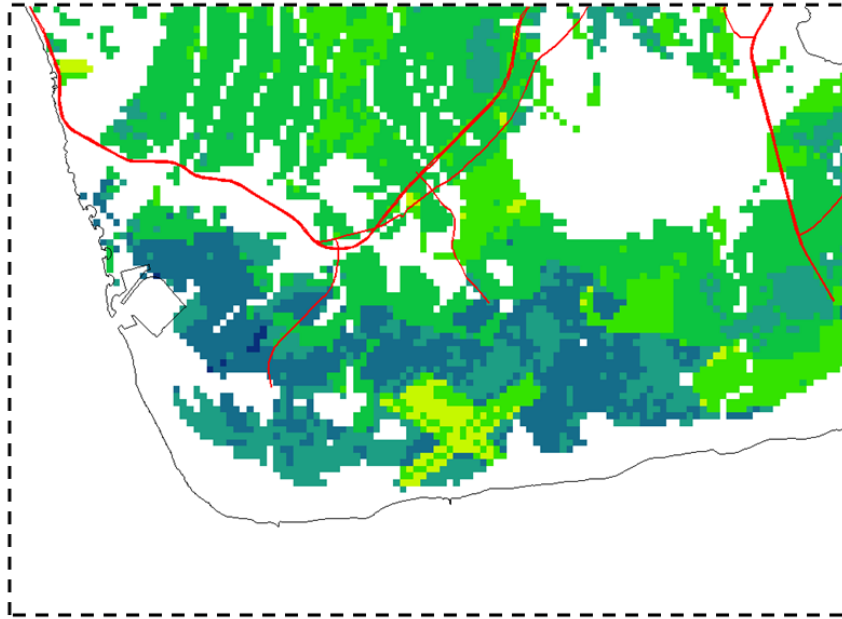
Site suitability



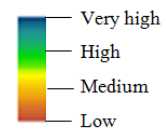
— Boundaries for the island of Oahu — Major roads - - - - Suitable locations

Figure 4c Best locations B (1:50,000 scale) from Appendix J Figure 4a.

1:50,000 scale



Site suitability



— Boundaries for the island of Oahu — Major roads — Suitable locations

Figure 4d Best locations C (1:50,000 scale) from Appendix J Figure 4a.

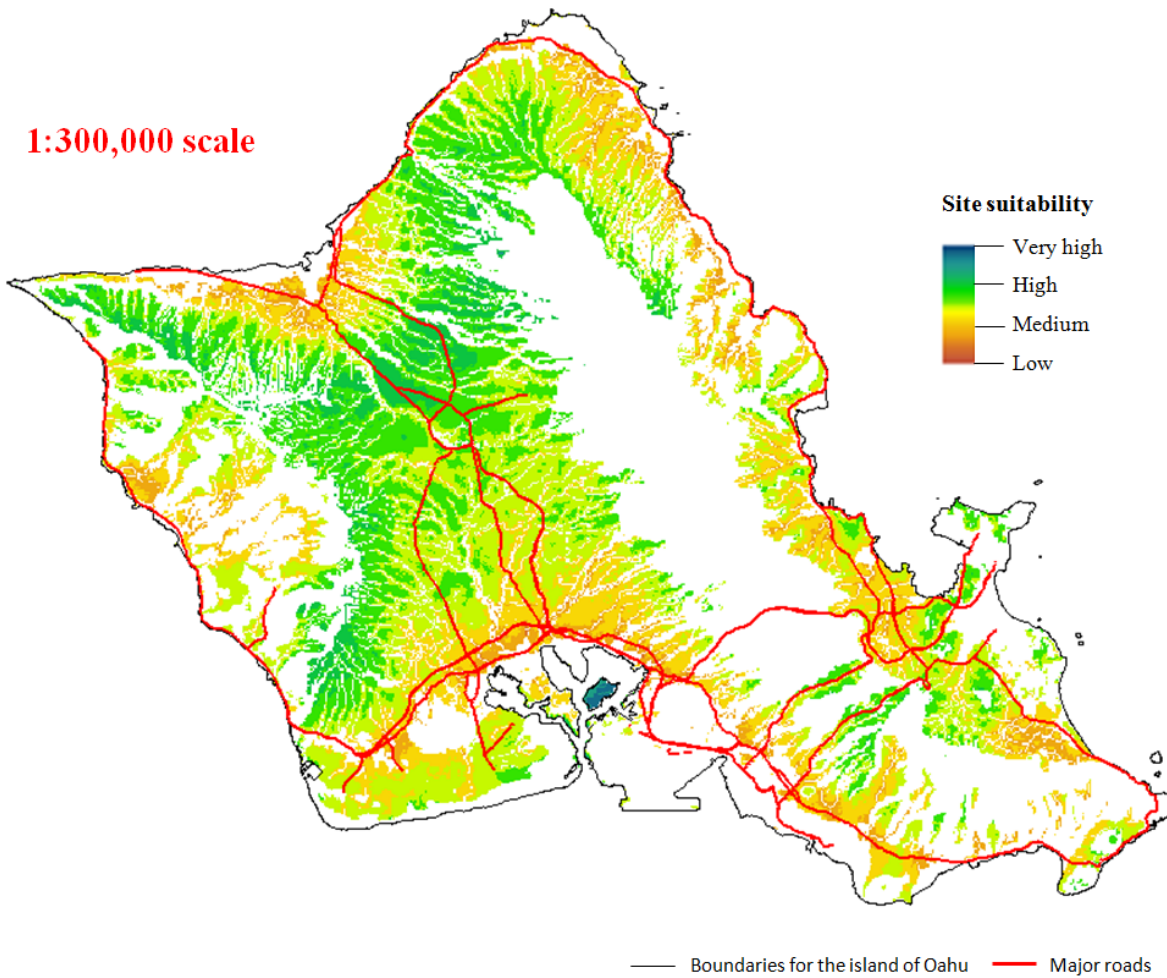


Figure 5 Site suitability maps (1:300,000 scale) developed by Analytic Hierarchy Process (AHP) which focuses environmental protection rather than system performance. The resolution of raster is 100×100 meters.

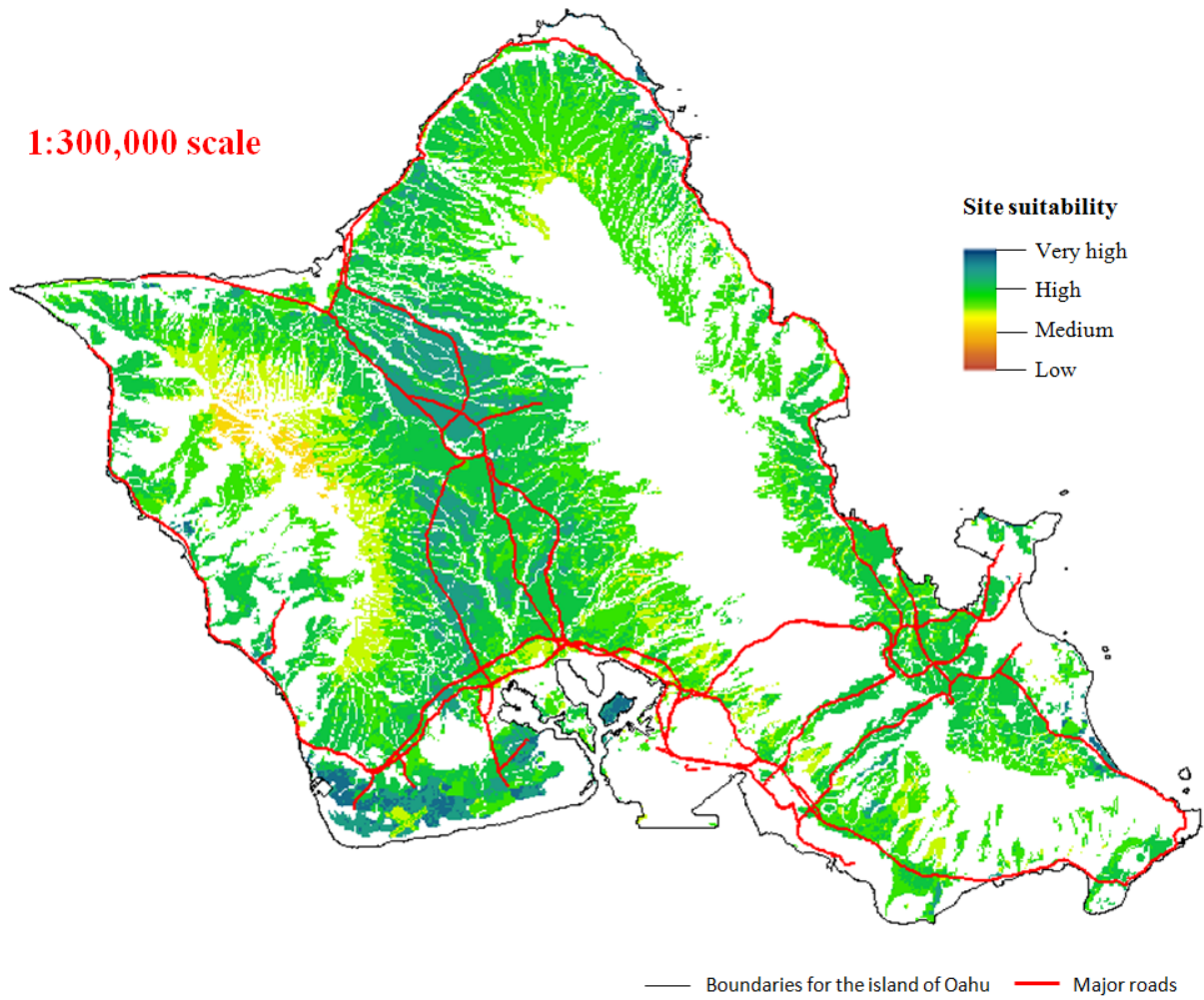


Figure 6 Site suitability maps (1:300,000 scale) developed by Rank Order Centroid (ROC) which focuses system performance rather than environmental protection. The resolution of raster is 100×100 meters.

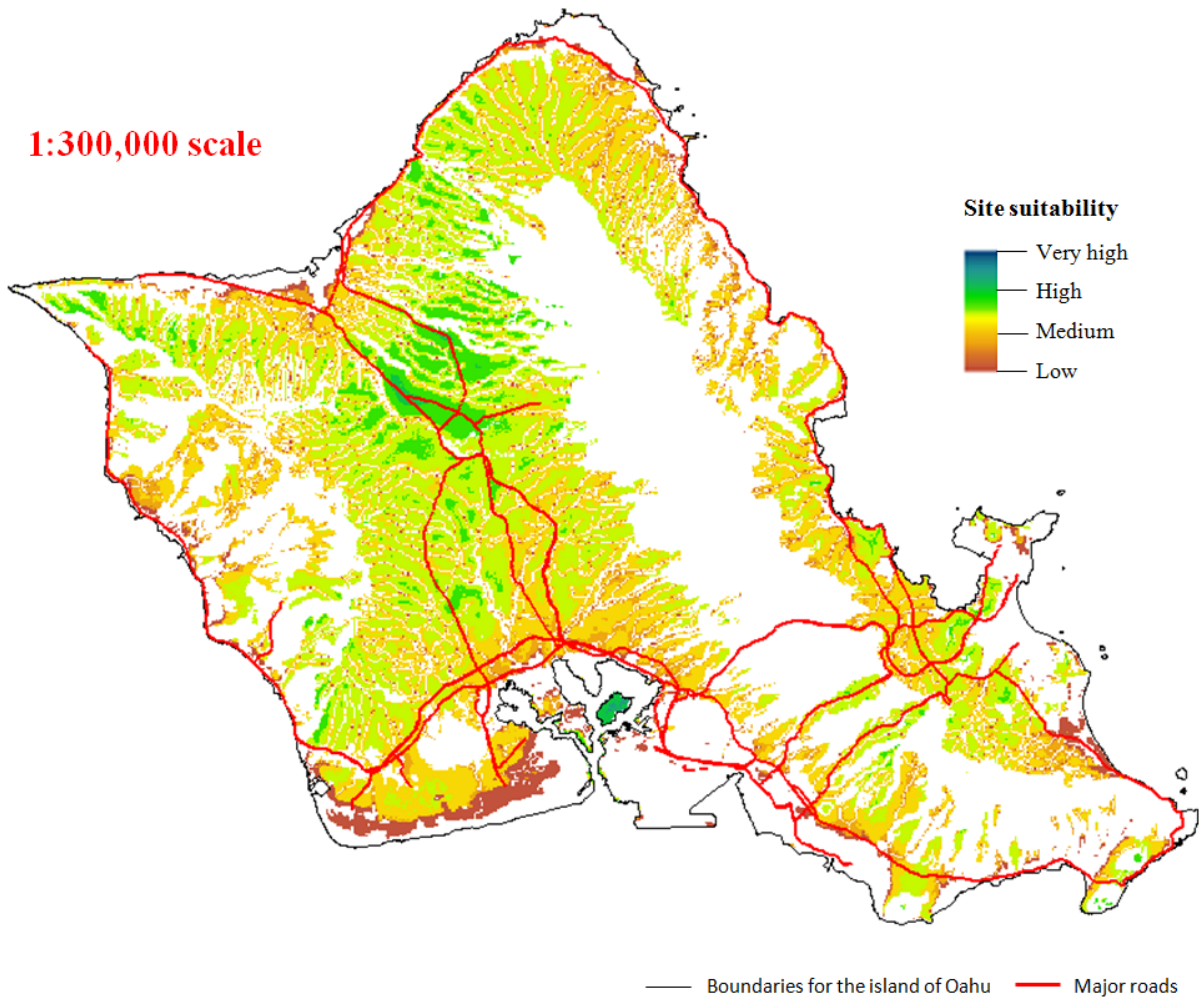
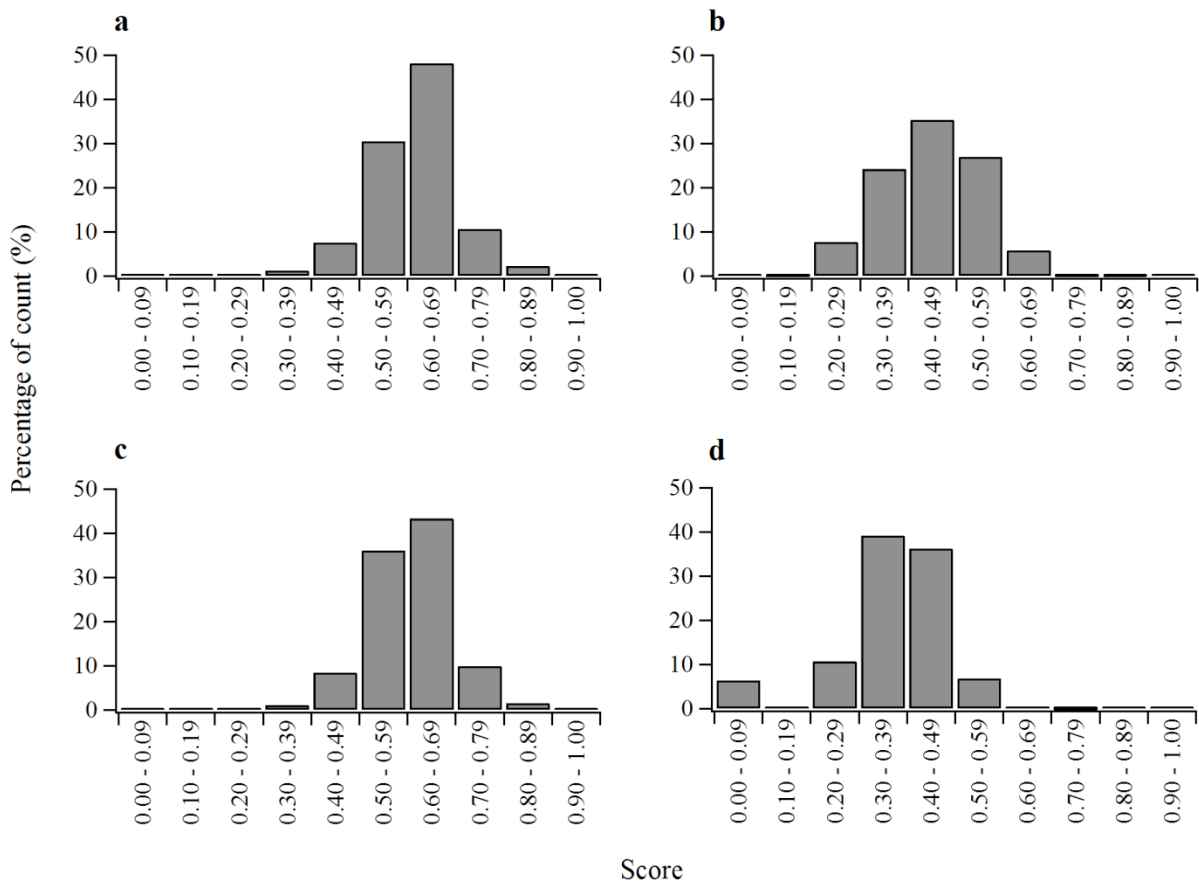


Figure 7 Site suitability maps (1:300,000 scale) developed by fuzzy logic overlay analysis (when Gamma, an optional overlay type of fuzzy logic, is 0.9). The resolution of raster is 100 × 100 meters.

Figure 8 Percentage of count (%) that fall within ranges of suitability scores: (a) Analytic Hierarchy Process (AHP) which focuses system performance rather than environmental protection (see Appendix J Figure 4a), (b) Analytic Hierarchy Process (AHP) which focuses environmental protection rather than system performance (see Appendix J Figure 4d), (c) Rank Order Centroid (ROC) which focuses system performance rather than environmental protection (see Appendix J Figure 4c), and (d) fuzzy logic overlay analysis (when Gamma, an optional overlay type of fuzzy logic, is 0.9, see Appendix J Figure 4d). Percentage of count (%) is calculated by dividing the frequency of scores for each interval by the total number of cells in the final (output) raster layer, 73,457.



Appendix K. Review of literature.

Chemical clogging can be due to the formation of insoluble precipitates and the production of byproducts during infiltration (e.g. Mays and Hunt, 2005; Pfeiffer et al., 2000). To form precipitates, the concentration of the relevant ion has to exceed the equilibrium concentration at a particular pH. Most commonly, calcium carbonate is formed as a precipitate, however, manganese carbonate and insoluble forms of sulfides and silicates have also been found to cause clogging (Pfeiffer et al., 2000). The byproducts of chemical reactions include gases, e.g. methane, carbon dioxide and nitrogen which may become trapped within the media bed and reduce permeability (Oberdorfer and Peterson, 1985).

Biological clogging will occur when the growth of organisms or byproducts fills the media pores. Here, clogging depends on available nutrients and environmental conditions. Biological clogging can be caused by both aerobic and anaerobic growth processes depending on prevalent conditions. Faster clogging has been shown to take place where aerobic microbes occur due to their higher metabolic rates. Baveye et al. (1998) showed that three dimensional microbial aggregates are formed within the media, instead of forming a biological mat. These aggregates occupy open pore spaces and become entrapped when they detached and migrate with the fluid. Furthermore, this study showed that instead of uniformly distributed aggregates, the colonization of the filter grains appeared sparse and irregular. According to Cook et al. (1994) due to their encapsulation as solids bacteria that changed from an active to a quiescent form after a long lapse of nutrient supply, are able to cause greater reductions in permeability than the active form. This is pertinent for non-continuously fed systems, as bacterial die-off and a recovery of permeability would be expected after a certain drying period.

Clogging caused by limitations of particulate transport is attributed to straining and non-straining phenomena. Permeability reduction by straining occurs when particles and particle aggregates are the same size or larger than the filter media and get entrapped in the pore spaces. Whereas the smaller particles are able to penetrate the media but finally get trapped in narrower pore spaces, larger particles and particle aggregates will form a cake layer on the surface of the media. In both cases the substantial particle accumulation near the surface will lead to a decrease of pore openings and thus successively smaller particles will be retained (McDowell-Boyer et al., 1986). Non-straining mechanisms occur in cases where very small particles in comparison with the media grain size are removed. The non-straining phenomena can be divided into three processes; interception, sedimentation and Brownian motion, which are caused by physical and chemical forces between particles and the media. Interception takes place by collision of the suspended particles with the filter grain, while sedimentation refers to deviation from streamlines and settling on the filter grain due to different densities of particle and fluid. Attachment of particles and filter media by Brownian motion results from diffusivity and is characterized as a stochastic process (Reddi, 1997).

Literature review showed that a one-dimensional column experiment to simulate the physical clogging process for stormwater was carried out by Siriwardene et al. (2007). This study mainly focused on the processes of sediment accumulation and clogging layer formation in the filter media for laterally flowing levels. A filter consisting of 90 cm of gravel was built on top of a layer of very fine sand with a hydraulic conductivity ranging 2×10^{-5} to 8×10^{-5} m/s. The experiment was carried out with constant and variable water levels and different sediment inflow concentrations. For the clogging experiments, semi-artificial stormwater was prepared by collecting sediment from a stormwater retention basin and mixing with tap water after passing through 300 μ m sieve. The inflow was maintained by a computer-controlled rotating sprinkler according to the desired water level in the column and thus not constant during the duration of the experiment. The initial outflow varied between 0.7 and 4 cm^3/s (42 – 240 ml/min). Experiments were run until the outflow rate approximated asymptote conditions ranging between 10 % and 25 % referring to

the initial outflow. In the gravel filter the hydraulic heads did not change during experiment period whereas the hydraulic heads in the soil underneath decreased gradually to zero. Experiments with a constant water level formed a plug around the water level whereas experiments with variable water levels tended to form a clogging layer at the filter/soil interface. It was determined that sediment particles with less than 6 μm diameter were mainly responsible for development of clogging at the filter soil interface.

Likewise Hatt et al. (2008) focused on performance of stormwater filtration systems comprised of gravel and sand or soil. They conducted laboratory-scale experiments to model long-term hydraulic pollutant removal performance. They found that mechanical straining was the primary mechanism for sediment removal. Moreover they found that adequate contaminant and sediment removal was achieved by gravel filters with a depth of 0.5 m based on the fact that physical clogging is likely to occur prior to chemical breakthrough. They observed little effect on hydraulic conductivity and contaminant removal during wet/dry cycles.

To simulate particle capture in infiltration trench, Li and Davis (2008a) conducted column experiments with 5 cm diameter Plexiglas columns under constant and variable flow conditions. A 0.5 cm bottom sand layer was covered with 5 to 10 cm of soil from two different sites and a ponding water level was maintained. Synthetic stormwater for the column experiments was prepared from 10^{-3} M CaCl_2 solution and kaolin. This solution was introduced into the columns at rates of 5, 10, and 20 cm/h. Input, output, TSS, water head, effluent volume and surface filter cake thickness were recorded. Obvious cake layer formation occurred in most experiments. The hydraulic conductivity for both sandy loams was initially 54 cm/h and 72 cm/h and was reduced to 3 cm/h and 11 cm/h respectively when clogging occurred. With this set of experiments Li and Davis (2008a) came to the conclusion that incoming suspended solids cannot significantly penetrate more than the upper 5 - 20 cm of the soil. Furthermore they found that it was mainly clay-sized particles that contributed to clogging layer formation, while coarse suspended particles had little impact on effluent quality and hydraulic conductivity reduction. Li and Davis (2008a) looked at long-term performance of trenches for removing different sized particles in inflow water and examined various factors responsible for clogging. They hypothesized that larger particles cause less clogging compared to smaller particles. Large particles tended to be removed at the surface of the filter, while smaller particles were able to penetrate the surface and resulted in stratified clogging throughout the filter media. Furthermore they concluded, based on their experimental data, that a cake layer on the surface formed when the ratio of equivalent hydraulic conductivity of the media in the column K_e and the initial hydraulic conductivity K_o decreased to a value of 0.3 to 0.4 (Li and Davis, 2008b). This assumption is based on a three-layer model for particulate capture including both mechanisms of depth filtration and cake filtration. Bioretention in soil was modeled as three distinct layers: bottom (pristine soil), middle (working accumulation zone) and top cake layer. Particulate penetration depth was expressed as a first-order relationship. A differential mass balance was used to describe the partitioning of deposited solids among the layers. They found that cake layer formation was predicted by a decrease in permeability and it became the dominant filtration mechanism once a critical value of cake thickness was attained.

Clark and Pitt (2009) tested stormwater pollutant retention under aerobic and anaerobic conditions. They found that although stormwater entering infiltration trenches is usually aerobic, anaerobic conditions on a macro- or micro scale can develop when pore water stagnation occurs. To determine the possibility of contaminant release under changing redox conditions, Clark and Pitt used different filter media (municipal leaf compost, fine-grade sand, peat moss and granular activated carbon) in sorption experiments focusing on nutrients and heavy metals. Their results indicated that permanent retention of nutrients may not occur under anaerobic conditions especially in organic media, but heavy metals are very likely permanently trapped in a low oxygen environment.

Pavelic and Dillon (2011) assessed the influence of soil-type, level of pre-treatment, ponding depth, temperature and sunlight on clogging. Their experiments demonstrated that clogging takes place more in

permeable sand than in loam; nevertheless sand still retained an order of magnitude higher absolute permeability. Furthermore it was shown that improved influent water quality resulted in significantly higher infiltration, that higher ponding depth resulted in higher infiltration rates, and that physical clogging was the dominant clogging process. Microbial clogging became more important as particulate levels in the source water were reduced.

There are several options for setting up column clogging experiments, depending on the focus of the study. For example, Zhao et al. (2009) maintained constant head conditions with an overflow port located near the top of the column which maintained constantly saturated conditions. Closed columns with constant flow conditions were used by Mays and Hunt (2007) and closed columns with variable flow conditions by Bright et al. (2010). The influence of different water levels on clogging phenomena was studied by Siriwardene et al. (2007). Columns driven under constant flux will respond with increasing pressure when clogging occurs, whereas experiments conducted with a constant head will display a decreasing rate of flow. Though the permeability reduction under both conditions is similar, experimental tests as well as physical clogging models suggest that clogging under constant head conditions occurs after many fewer pore volumes than it does under constant flow rates. Furthermore, several studies used sediment packed columns (Bright et al., 2010; Siriwardene et al., 2007; Nogaro et al., 2006). Li and Davis (2008a) found that suspended solids are not able to penetrate soil significantly below 5 – 10 cm in column tests and approximately 20 cm in the field.

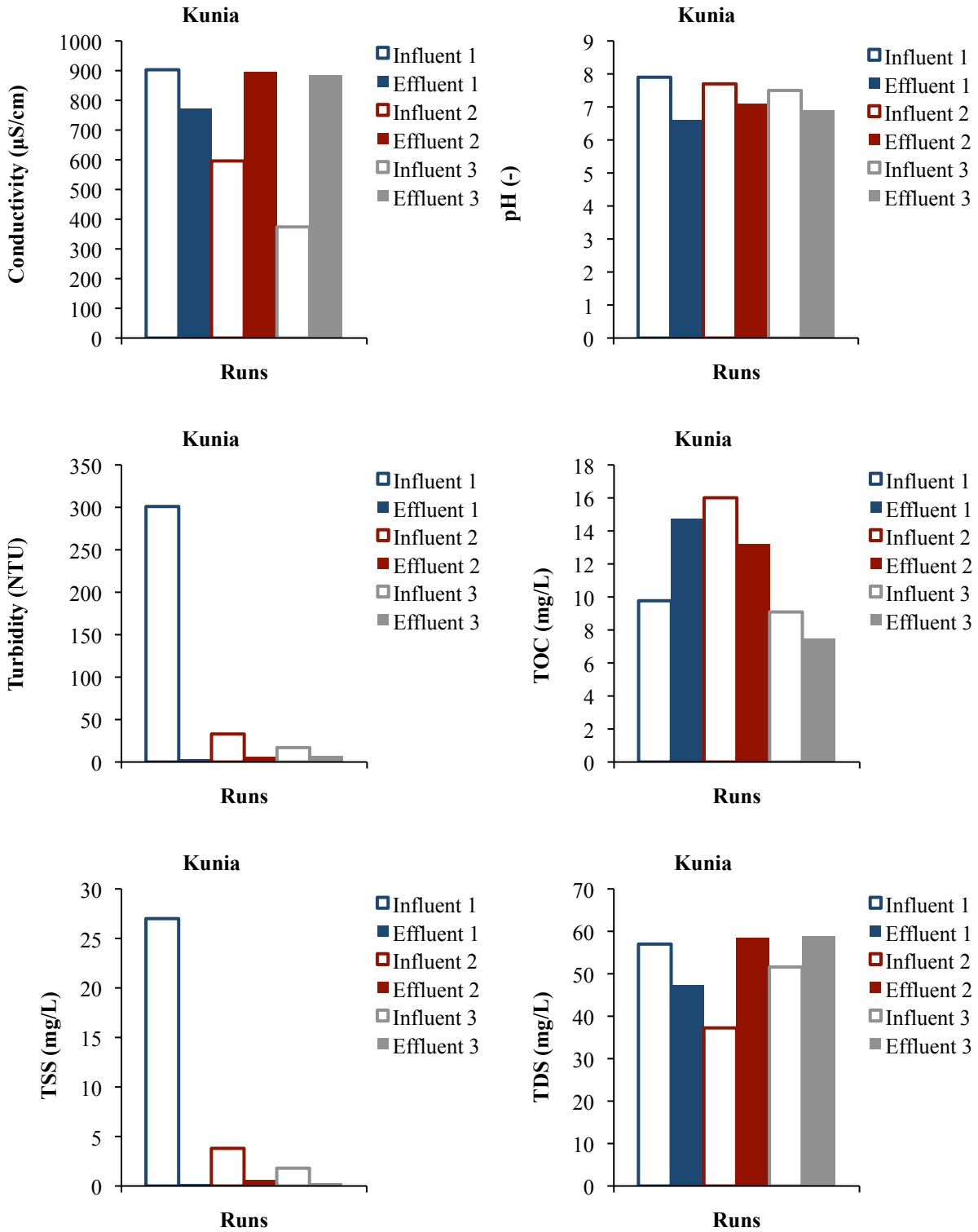
The transport of particles in soil and filter media has been analyzed in reference to various activities and applications such as wastewater infiltration, clogging of soil and geotextile filters, erosion and piping in earth dams and facilitated transport of contaminants. Some studies focused on transport and entrapment, while particle release was of primary importance for others (Reddi, 1997).

The potential clogging of pervious concrete by clay under extreme conditions is described by Haselbach (2010). His studies focused on examining the effect of events that lead to a series of clogging situations caused by clay-laden runoff, followed by simple remediation and regular precipitation. The experiments were performed with soil cores 72 and 92 mm in diameter, taken from beneath three different field placements of pervious concrete. Suspensions of natural red clay from Greenville, S.C., and two commercial clays, kaolin and bentonite, were used as clogging material. Bentonite was the most cohesive of the three clays used. After each clogging cycle extreme conditions were modeled. These cycles were repeated four to ten times until the sample was clogged and thereafter each sample underwent a maintenance procedure of sweeping the excess clay off the top. The samples were then subjected to rinsing cycles, designed to mimic subsequent rainfall, using water instead of clay suspensions and applying the drying procedure described above. It was seen during the clogging cycles that clay rapidly accumulated on the surface and cracks would form in this top layer during the drying cycles, thus allowing additional infiltration during the next clogging cycle until the accumulation became a nearly impenetrable barrier to the suspension. Results showed that higher clay loading rates increased the rate. After the rinsing cycles considerable increases in infiltration rates were seen for kaolinite and the natural clay, whereas samples treated with bentonite suspensions showed less improvement. The overall conclusion was that extreme storm events cause a substantial reduction in infiltration capacity due to deposition of large quantities of suspended particles that might temporarily clog an area. Nevertheless, most of the material would be loosely trapped on the surface of the pavement and could be removed with simple maintenance procedures such as sweeping.

Reddi et al. (2005) looked at the reduction in permeability of a sandy soil due to physical clogging using experimental and theoretical methods. The experiments involved a packed soil column that was fed with a suspension of two different particulates that differed in their specific gravity and their size distributions. One suspension contained smaller kaolinite particles (up to 12 μm) whereas the second suspension was prepared with polystyrene microspheres consisting of larger particles up to 35 μm . The soil filter sample

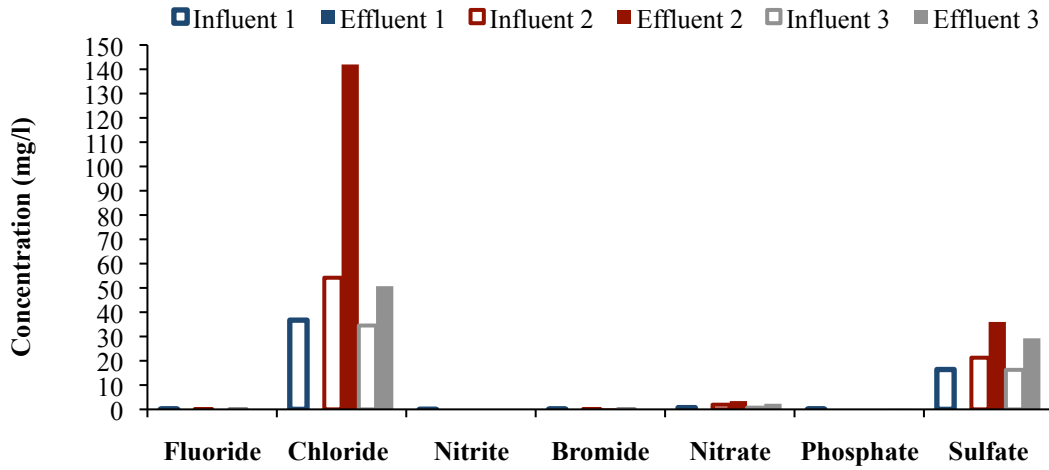
was 64 mm in length and 76 mm in diameter. Moreover results showed that increasing particle concentration in the suspensions led to faster reduction of permeability, while the ultimate reduction remained nearly the same. The reduction in permeability was comparable for both suspension types even though the polystyrene spheres were considerably larger. The authors attribute this to flocculation. For the inert polystyrene spheres flocculation was not a factor.

Appendix L. Chemical analysis of pH, conductivity, turbidity and dissolved organic carbon, total organic carbon, TSS and TDS during intermittent flow experiment of Kunia column.

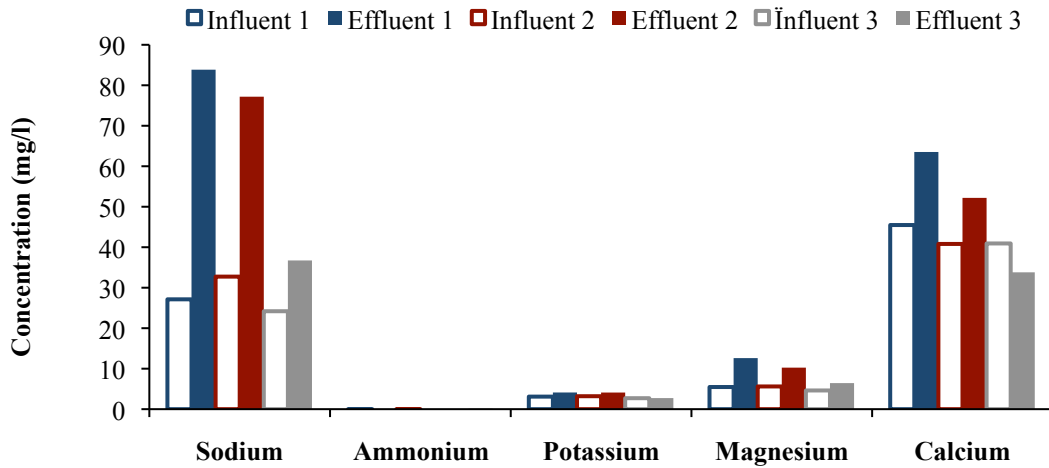


Appendix M. Chemical analysis of a) anions and b) cations during intermittent flow experiment of Kunia column.

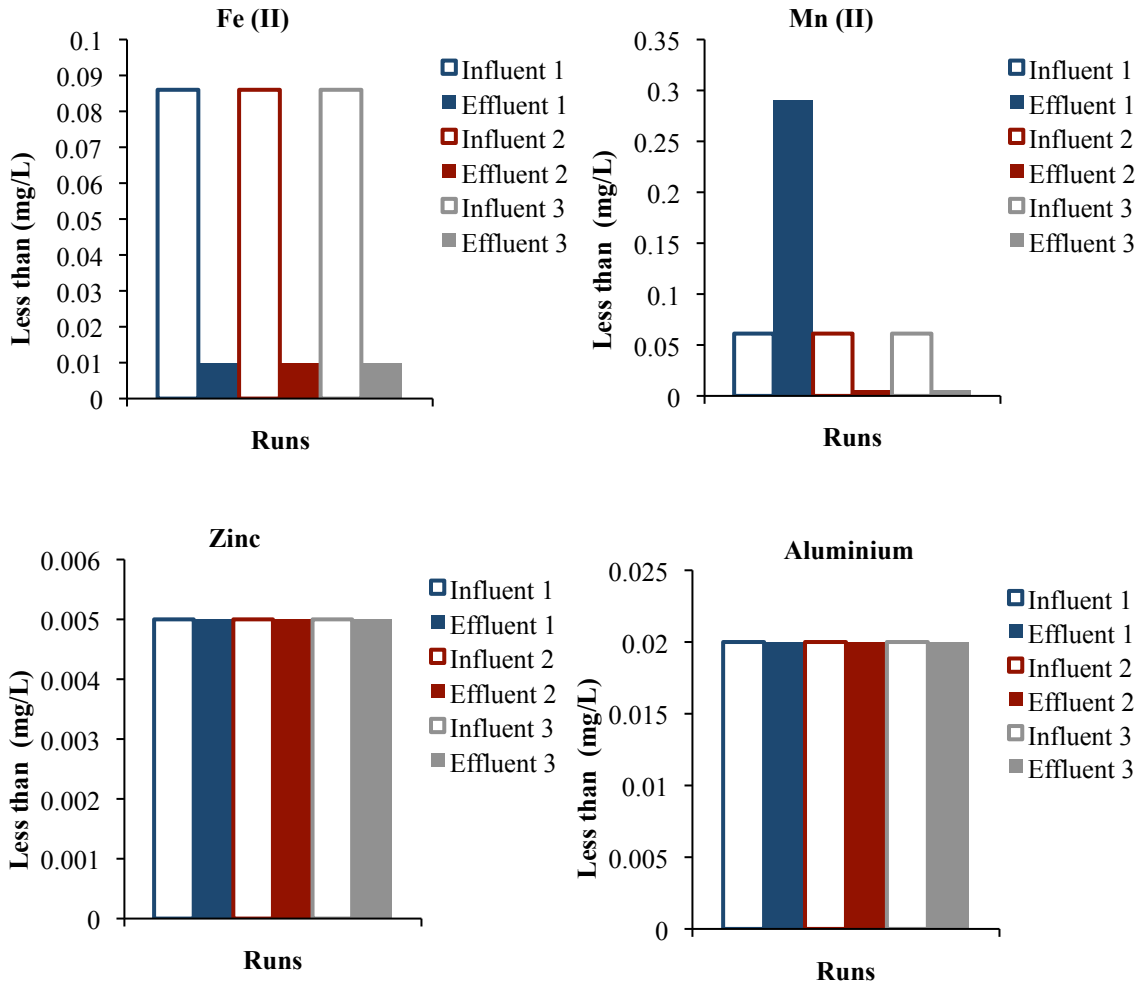
a)



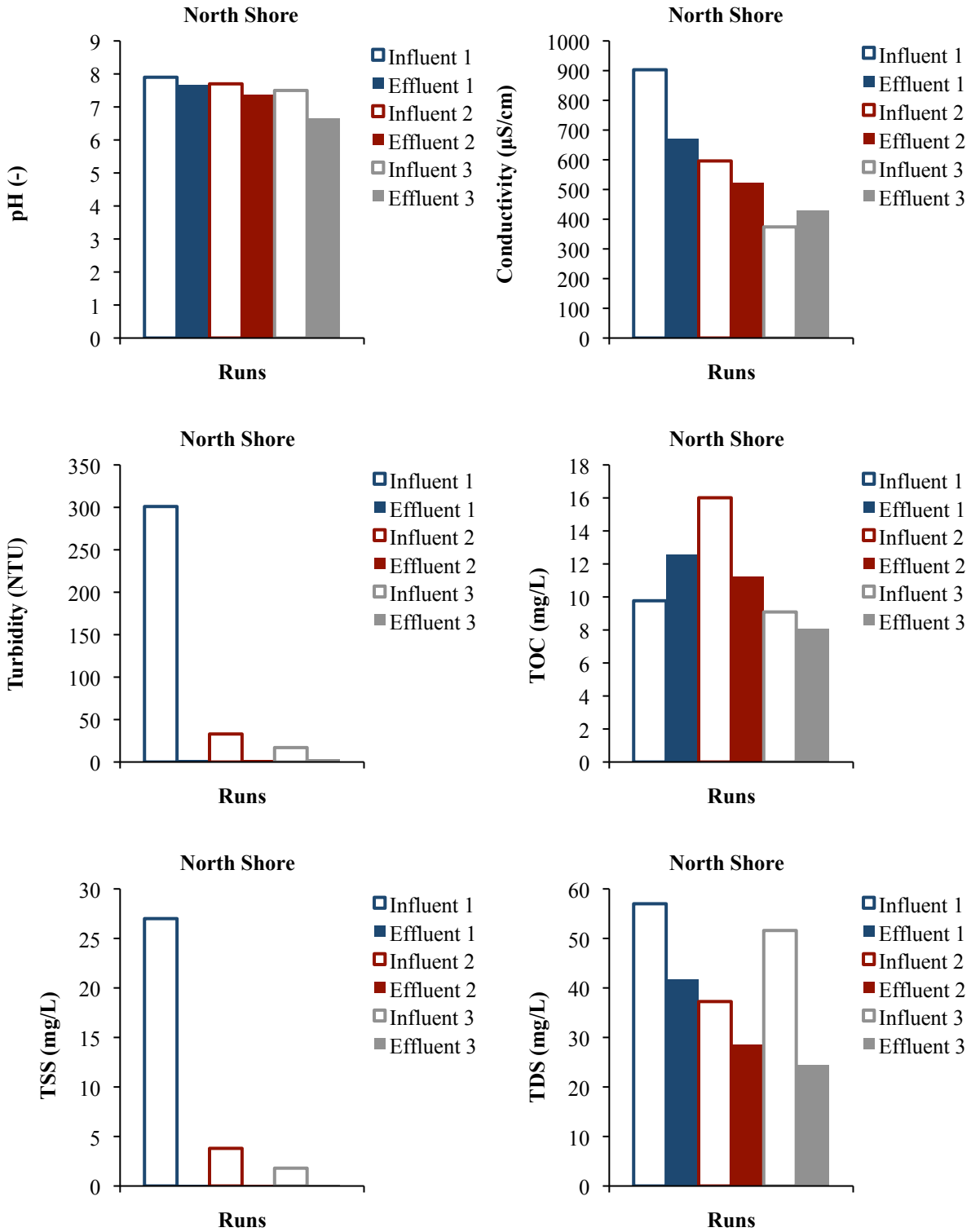
b)



Appendix N. Chemical analysis of heavy metals during intermittent flow experiment of Kunia column.

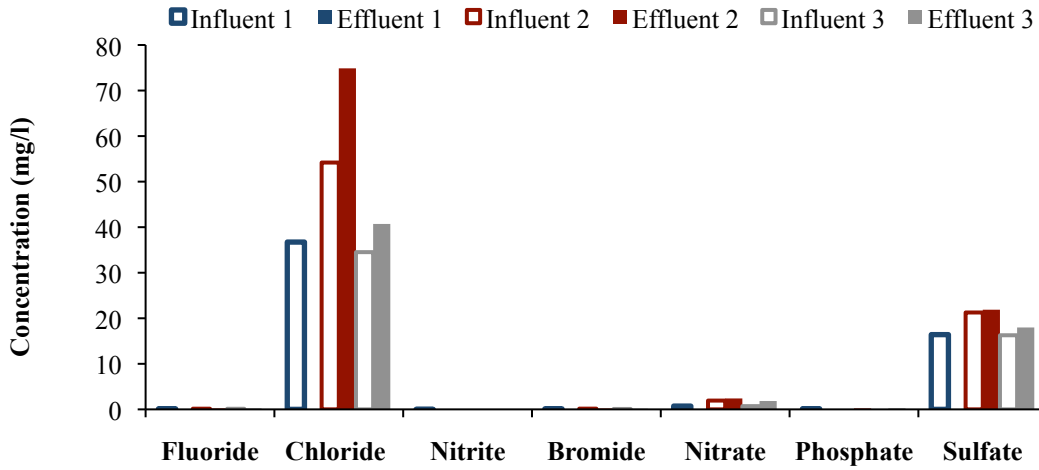


Appendix O. Chemical analysis of pH, conductivity, turbidity and dissolved organic carbon, total organic carbon, TSS and TDS during intermittent flow experiment of the North Shore column.

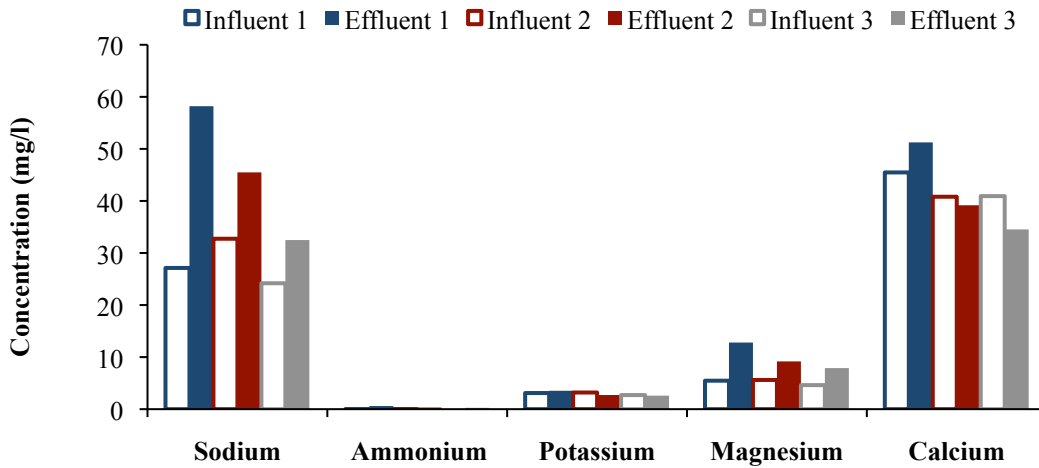


Appendix P. Chemical analysis of a) anions and b) cations during intermittent flow experiment of the North Shore column.

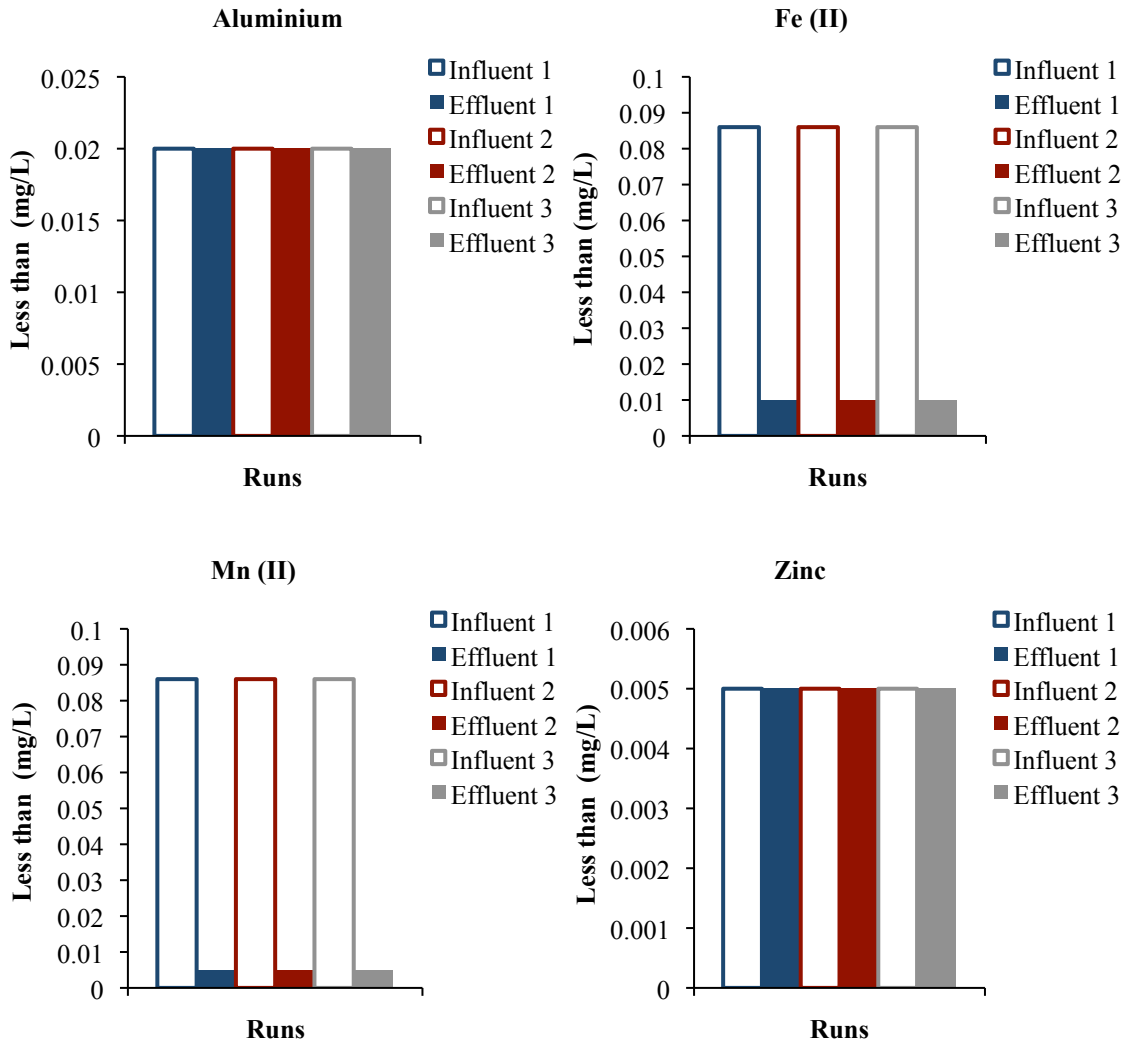
a)



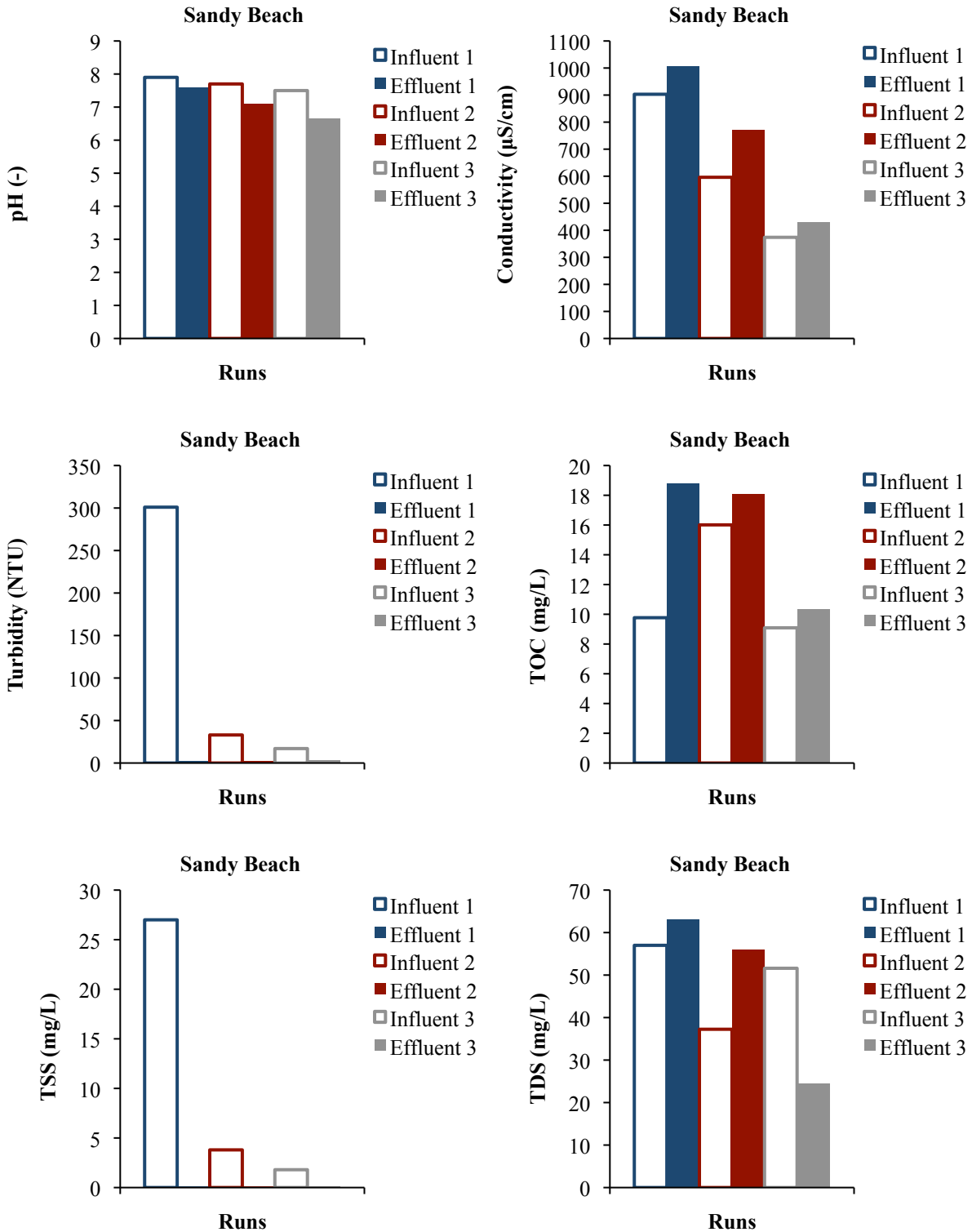
b)



Appendix Q. Chemical analysis of heavy metals during intermittent flow experiment of the North Shore column.

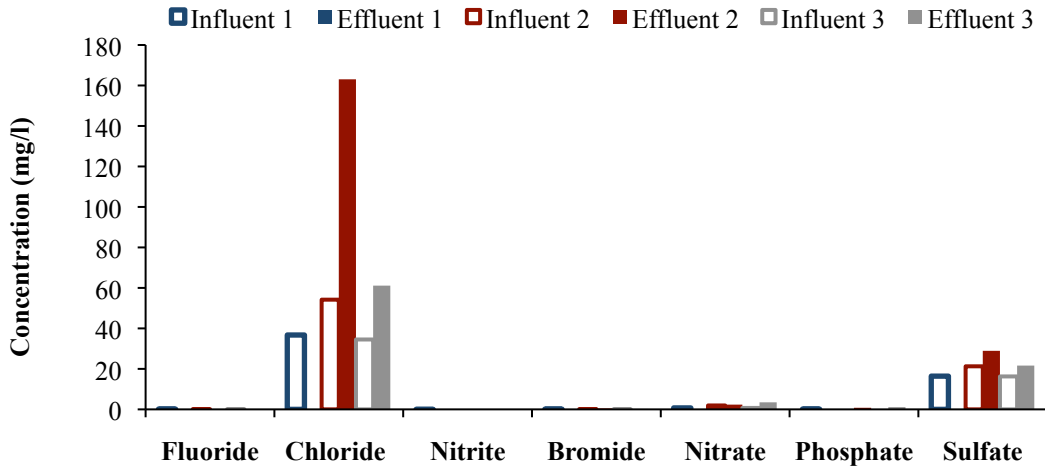


Appendix R. Chemical analysis of pH, conductivity, turbidity and dissolved organic carbon, total organic carbon, TSS and TDS during intermittent flow experiment of the Sandy Beach column.

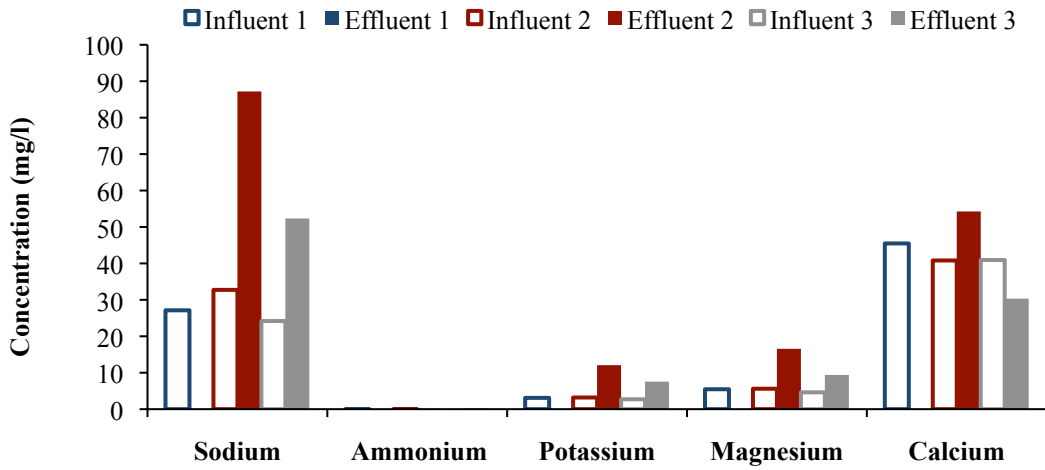


Appendix S. Chemical analysis of a) anions and b) cations during intermittent flow experiment of the Sandy Beach column.

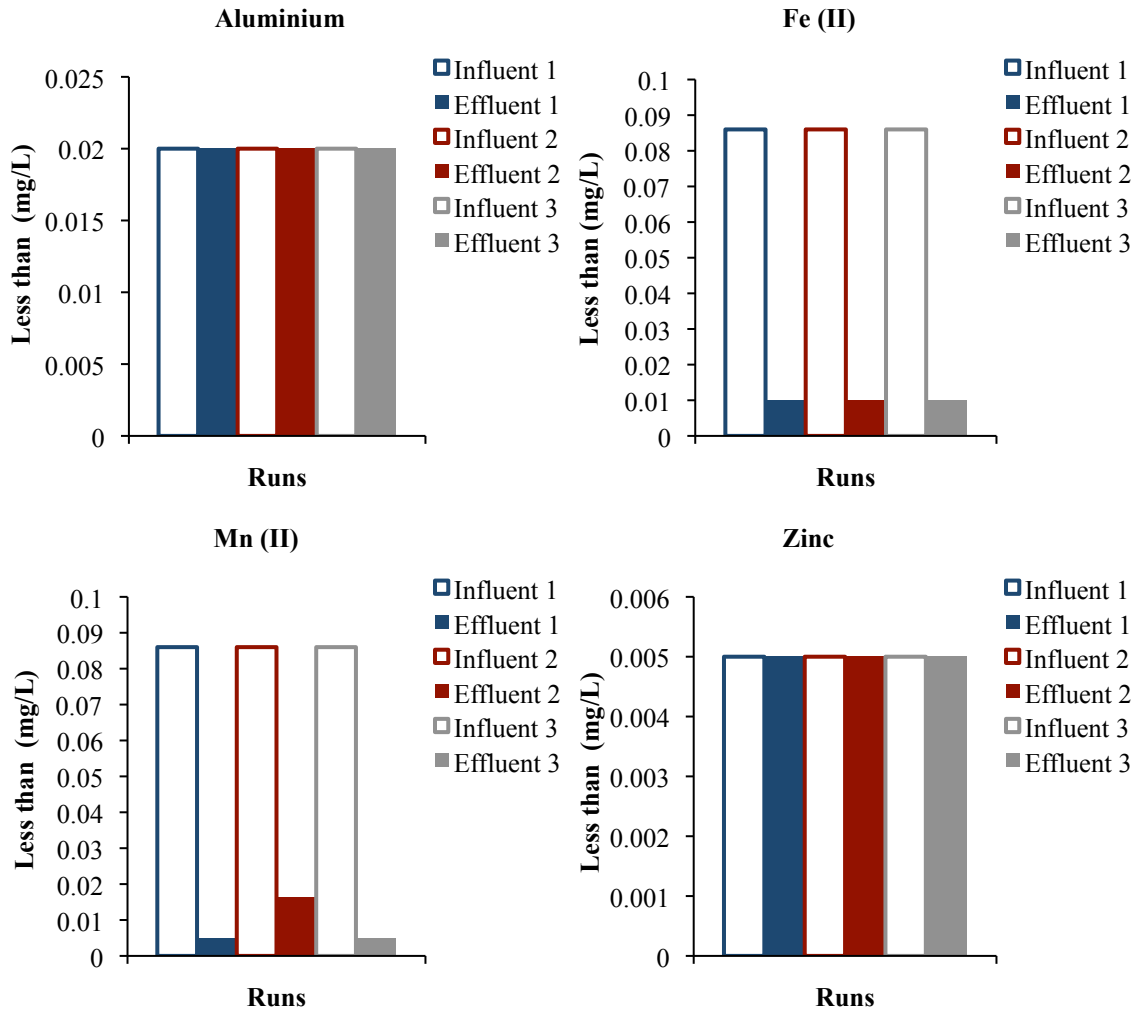
a)



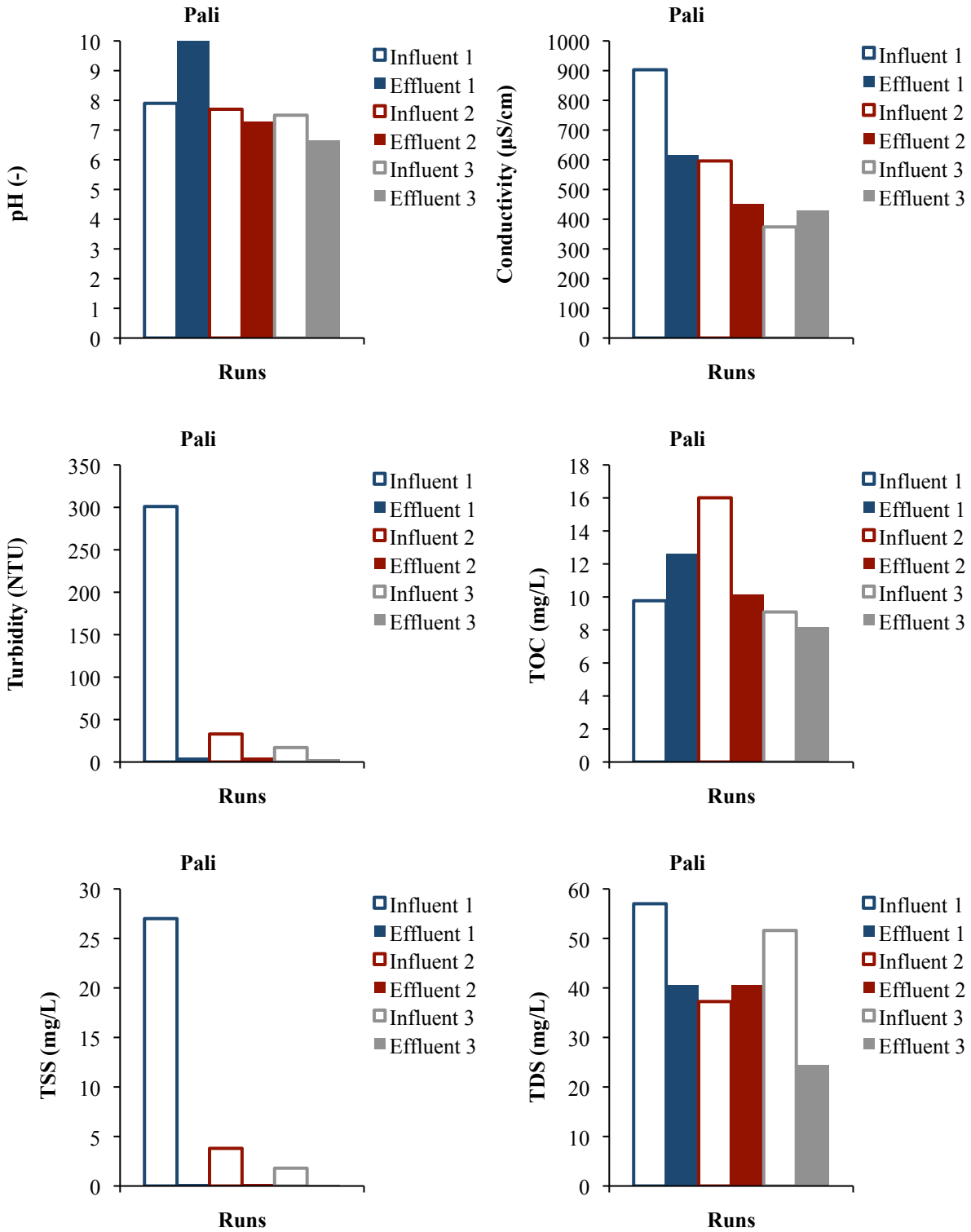
b)



Appendix T. Chemical analysis of heavy metals during intermittent flow experiment of Sandy Beach column.

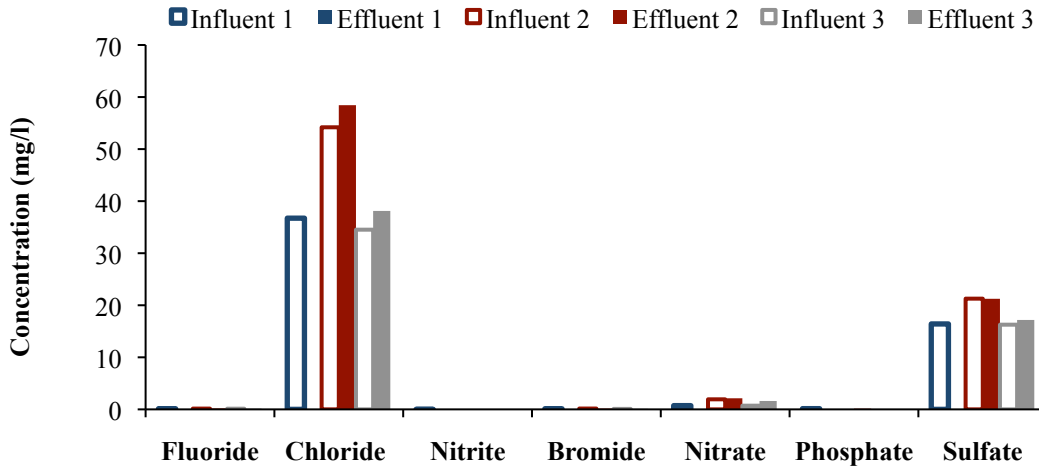


Appendix U. Chemical analysis of pH, conductivity, turbidity and dissolved organic carbon, total organic carbon, TSS and TDS during intermittent flow experiment of Pali column.

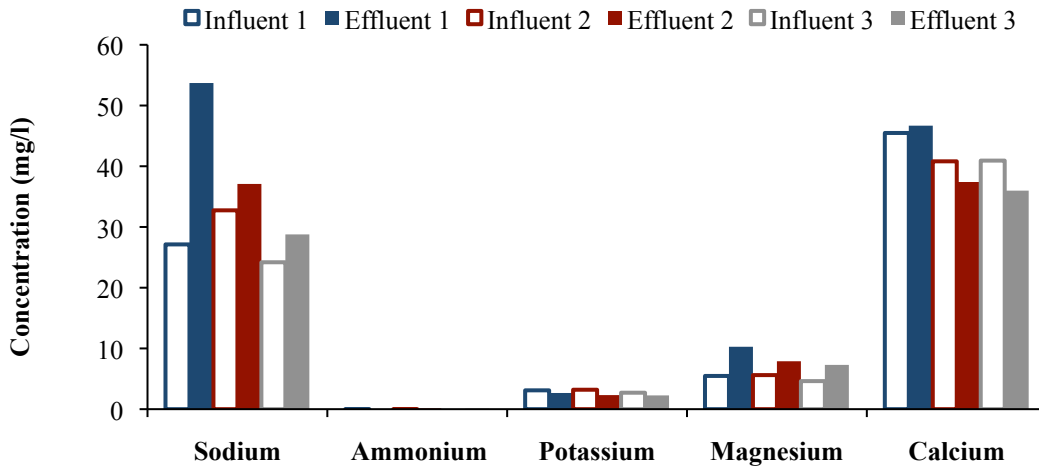


Appendix V. Chemical analysis of a) anions and b) cations during intermittent flow experiment of Pali column.

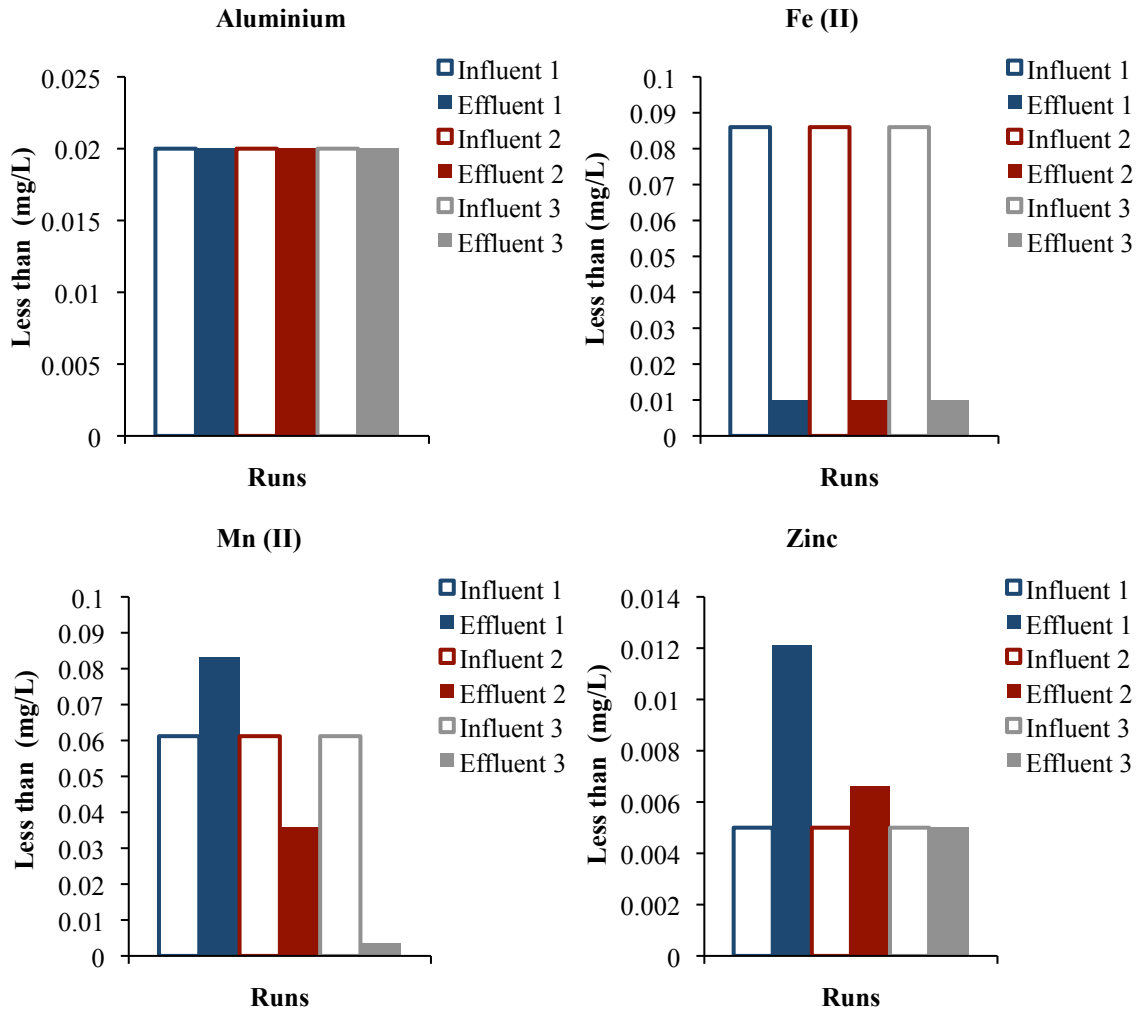
a)



b)

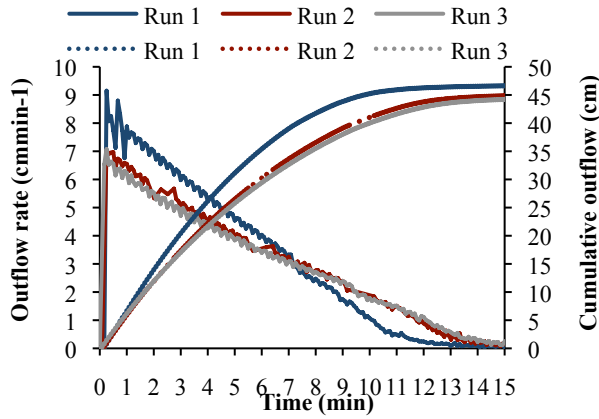


Appendix W. Chemical analysis of heavy metals during intermittent flow experiment of Pali column.

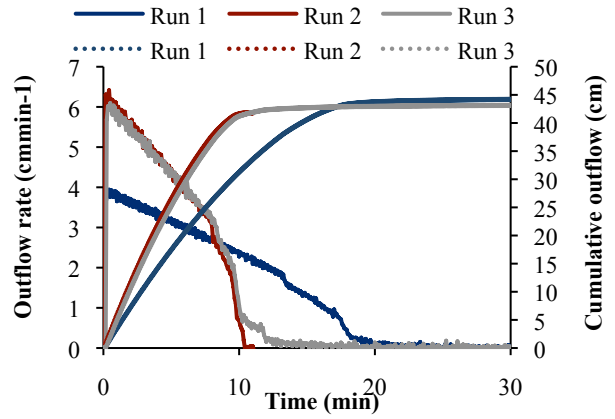


Appendix X. Outflow rate and cumulative outflow calculated from balance data for run 1 (dark blue dots), run 2 (dark red dots) and run 3 (gray dots) for a) the North Shore, b) Kunia, c) Sandy Beach and d) Pali column.

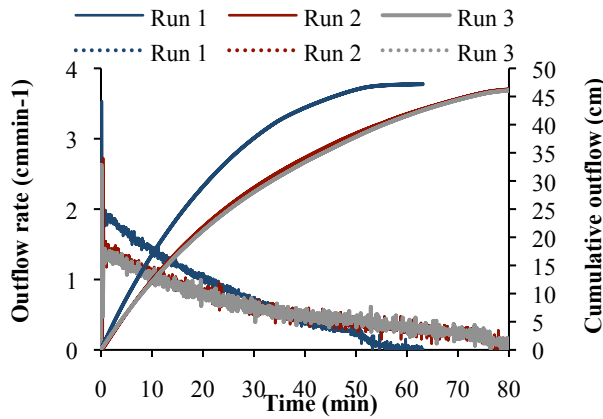
a)



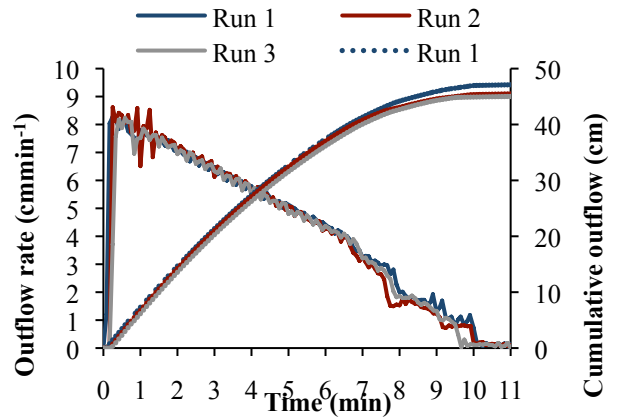
b)



c)

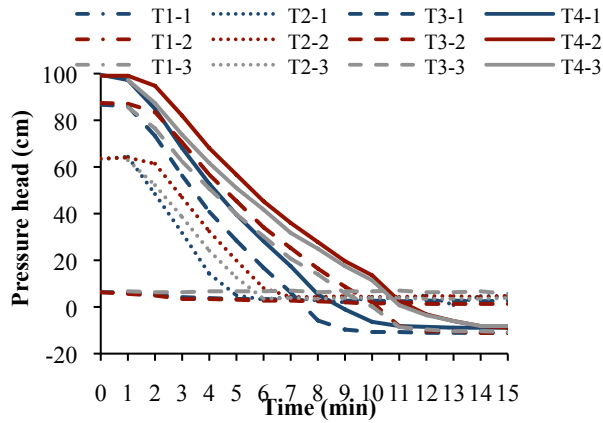


d)

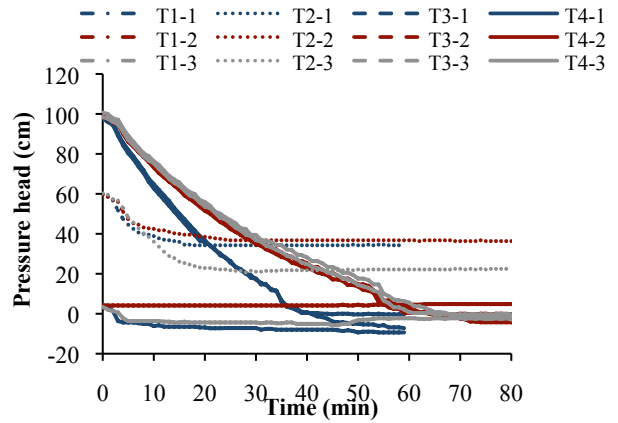


Appendix Y. Pressure heads in four depths for a) North Shore column, b) Kunia, c) Sandy Beach and d) Pali.

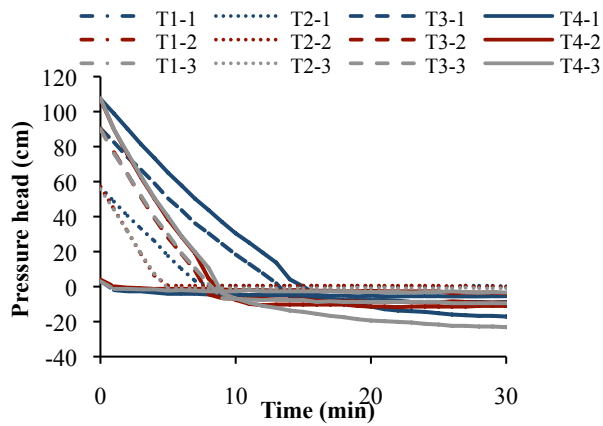
a)



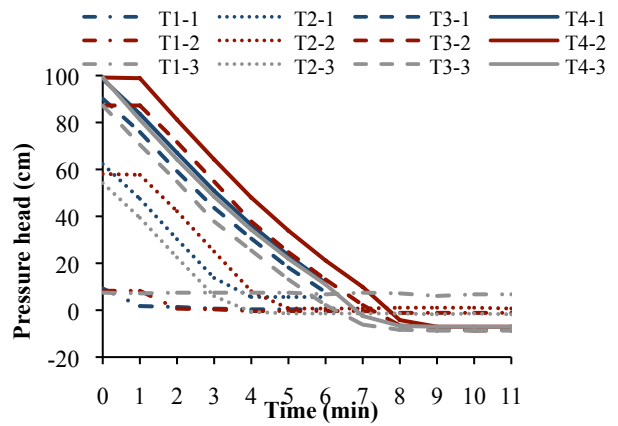
b)



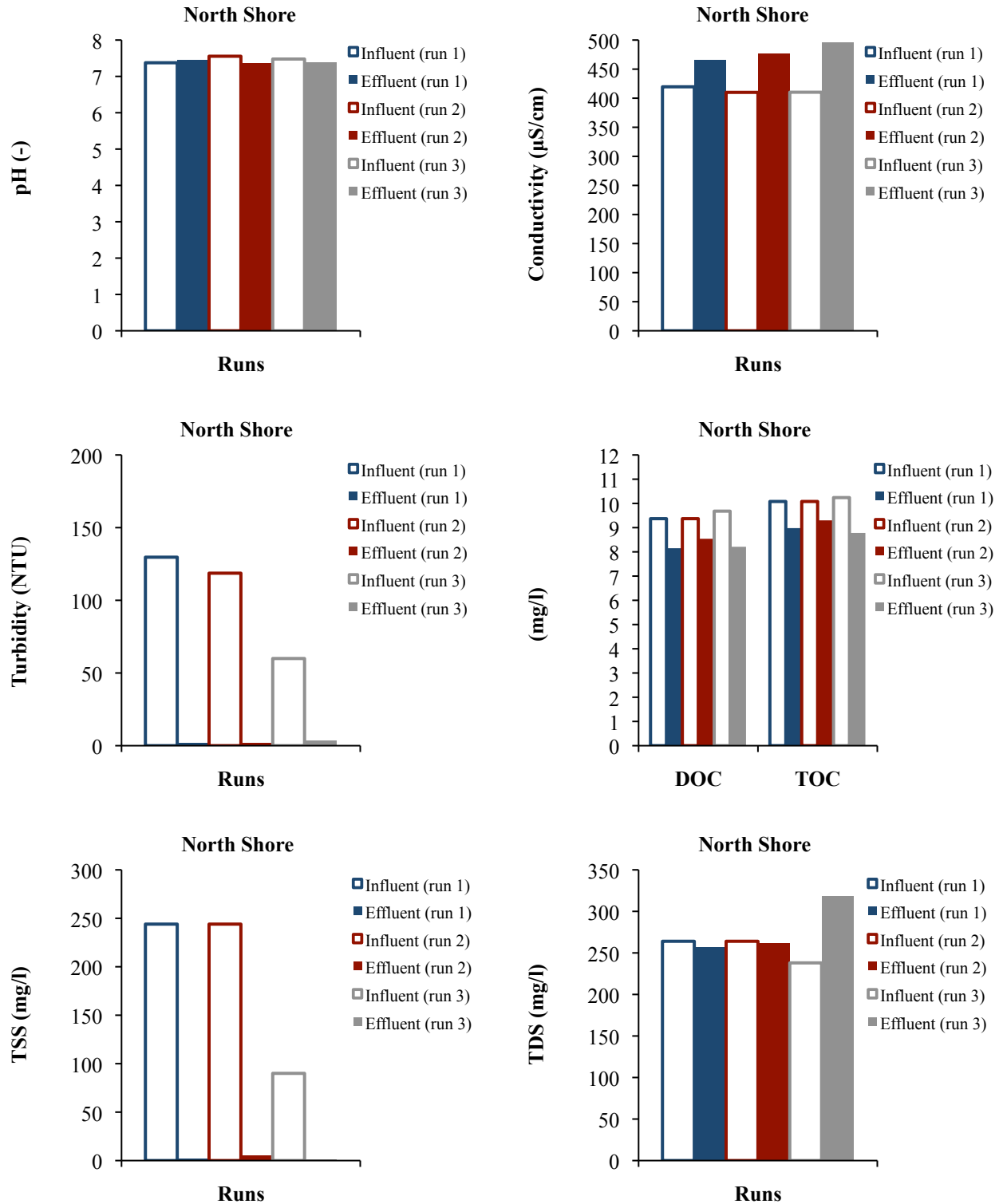
c)



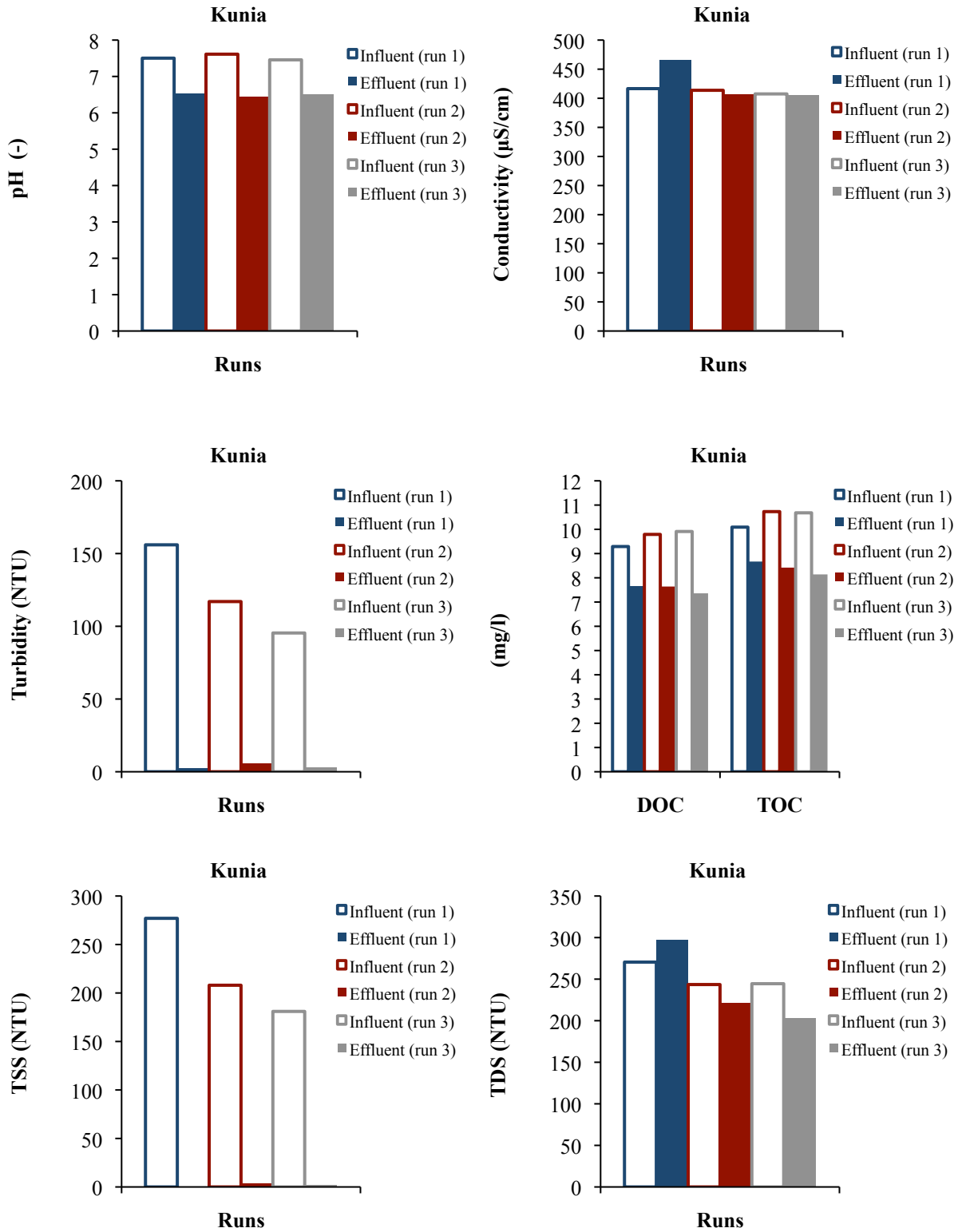
d)



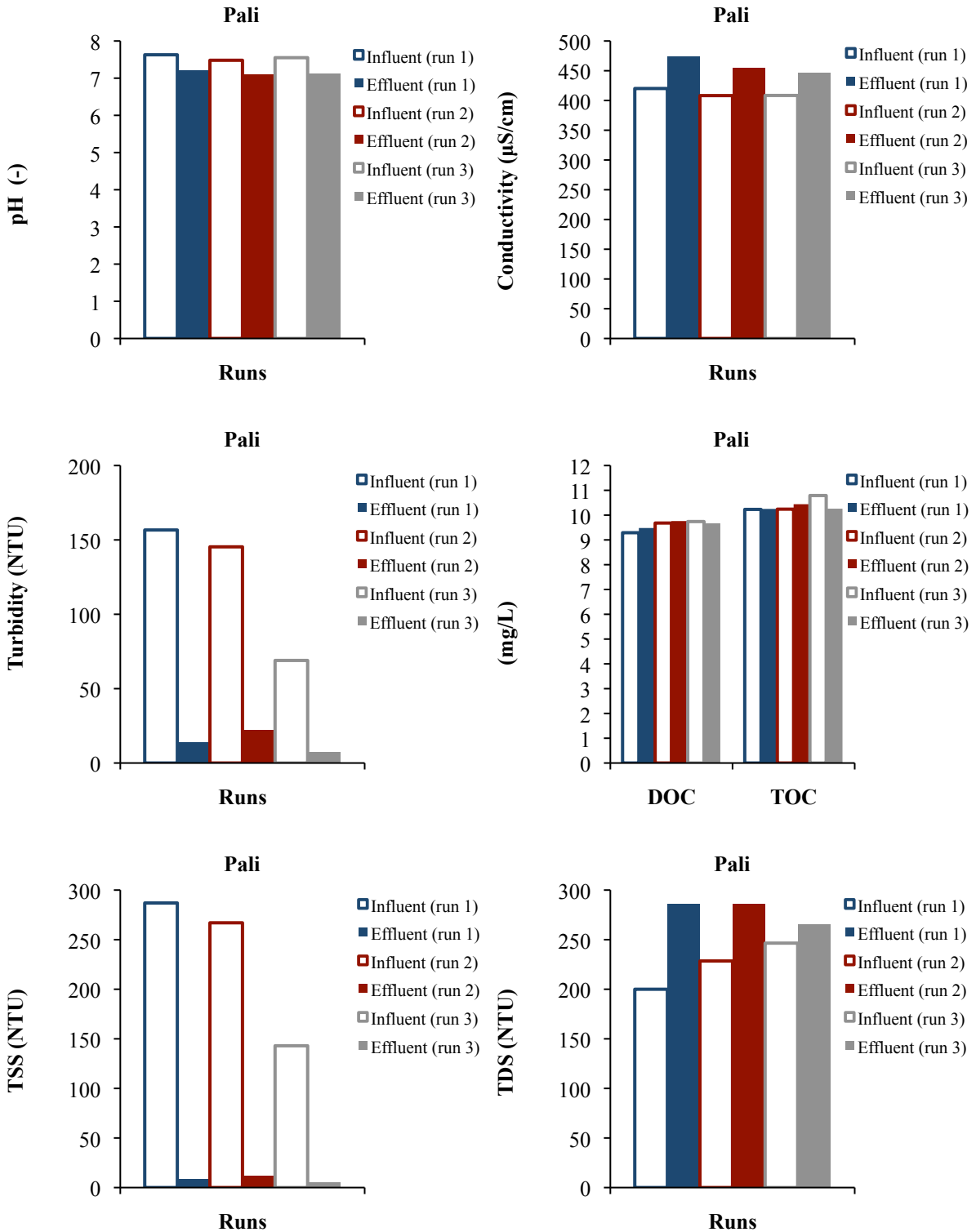
Appendix Z. Chemical analysis of pH, conductivity, turbidity and dissolved organic carbon, total organic carbon, TSS and TDS during wet/dry cycling experiment of the North Shore column.



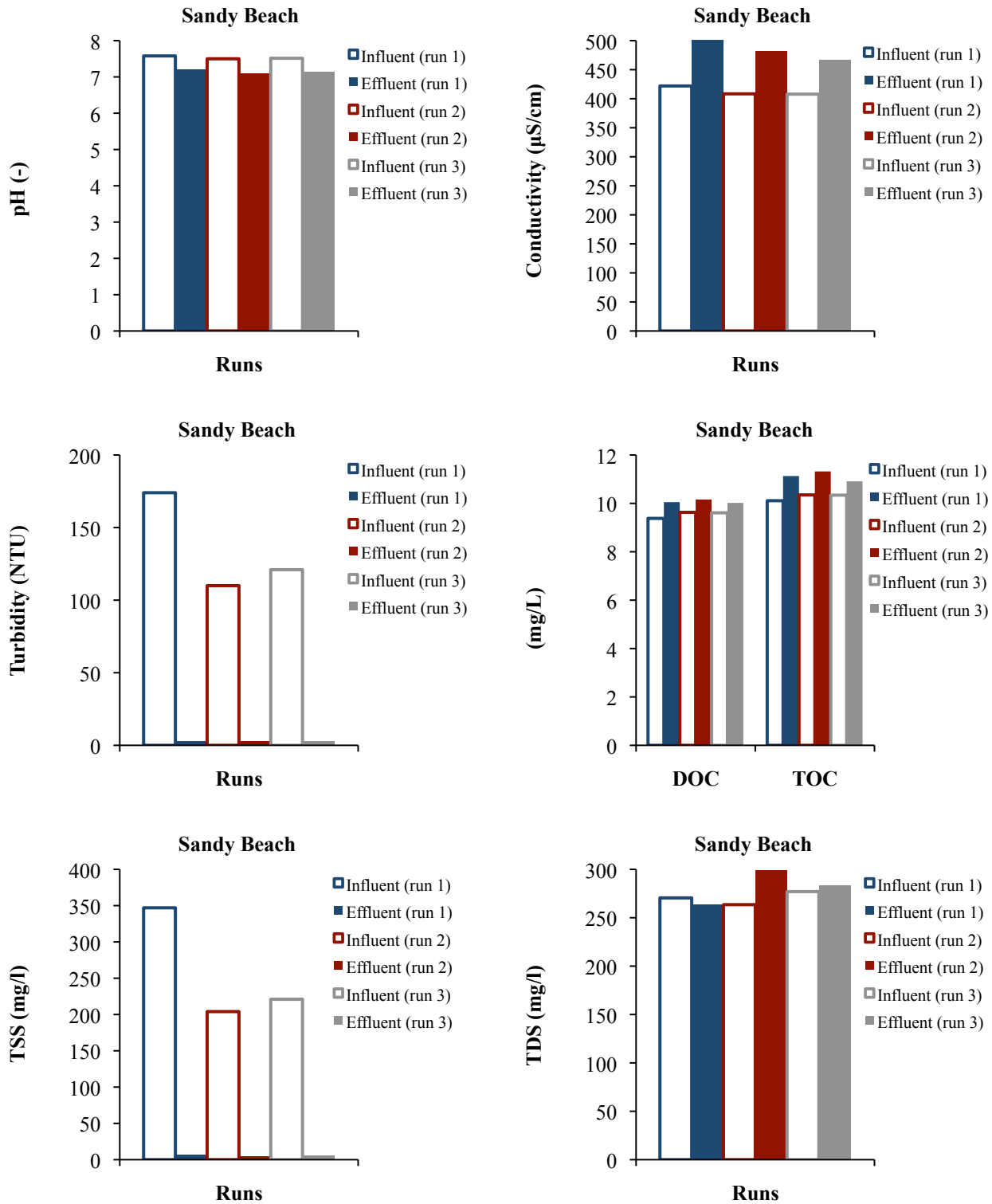
Appendix AA. Chemical analysis of pH, conductivity, turbidity and dissolved organic carbon, total organic carbon, TSS and TDS during wet/dry cycling experiment of Kunia column.



Appendix BB. Chemical analysis of pH, conductivity, turbidity and dissolved organic carbon, total organic carbon, TSS and TDS during wet/dry cycling experiment of Pali column.

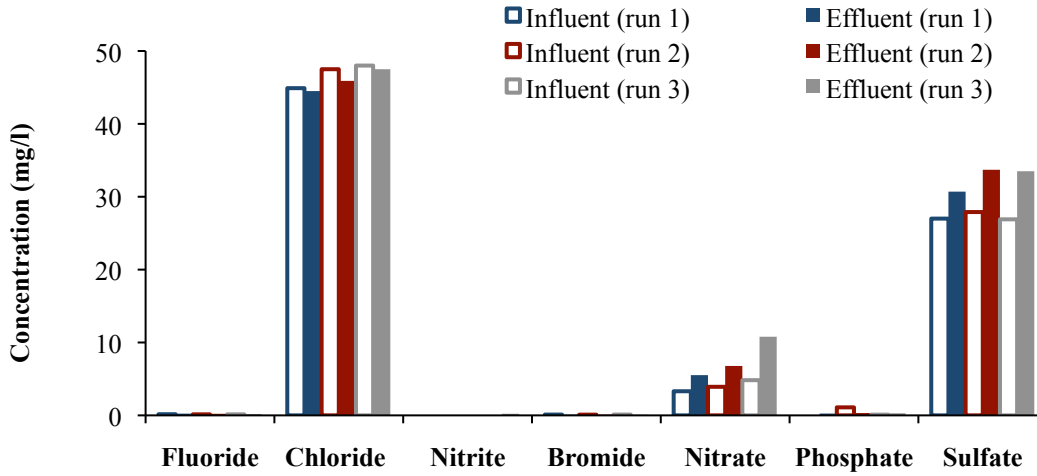


Appendix CC. Chemical analysis of pH, conductivity, turbidity and dissolved organic carbon, total organic carbon, TSS and TDS during wet/dry cycling experiment of the Sandy Beach column.

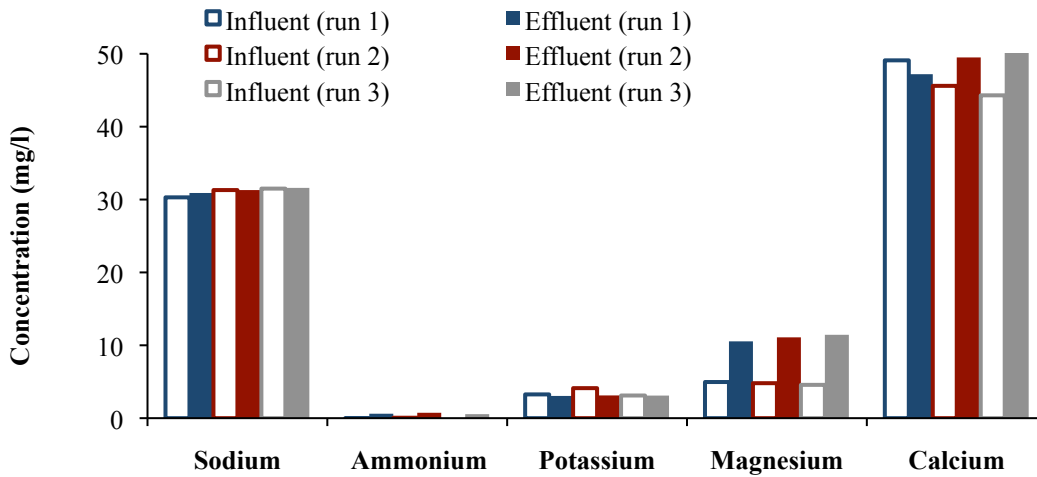


Appendix DD. Chemical analysis of a) anions and b) cations during one step outflow experiment of the North Shore column.

a)

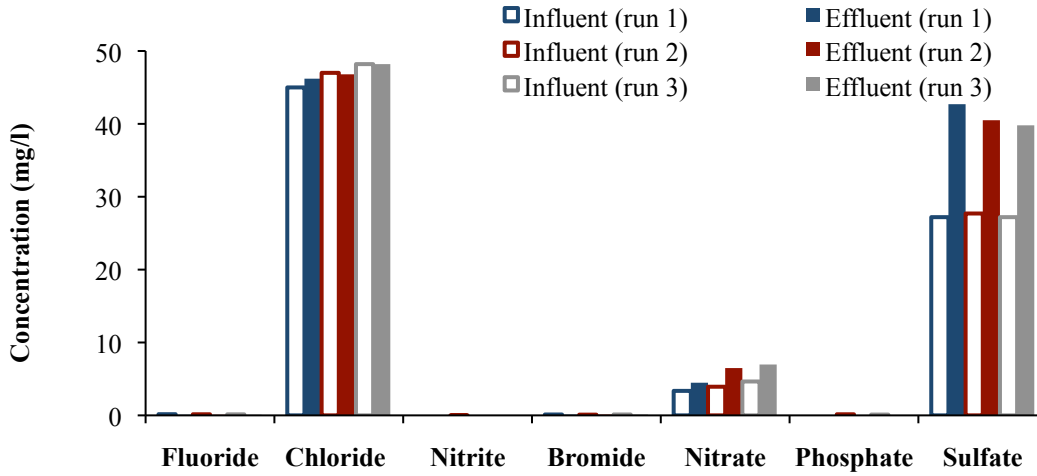


b)

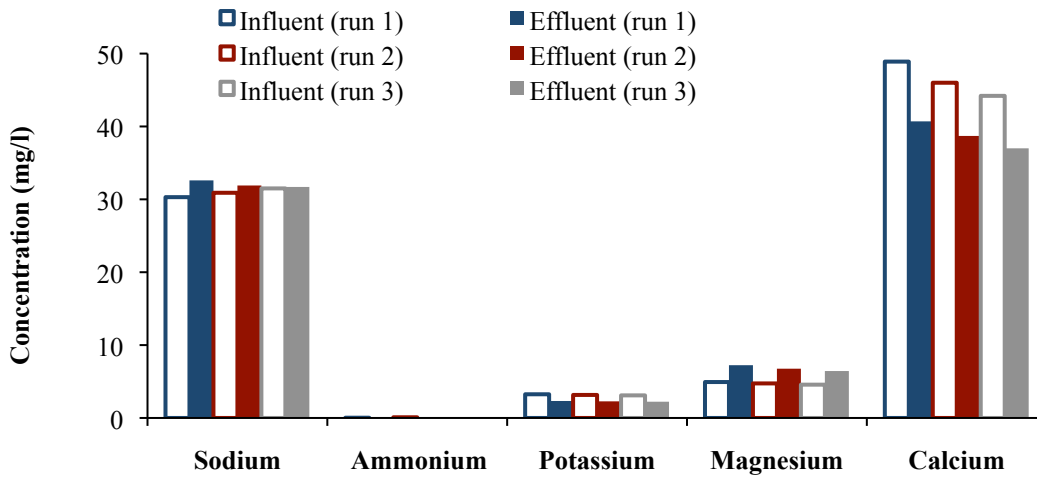


Appendix EE. Chemical analysis of a) anions and b) cations during one step outflow experiment of Kunia column.

a)

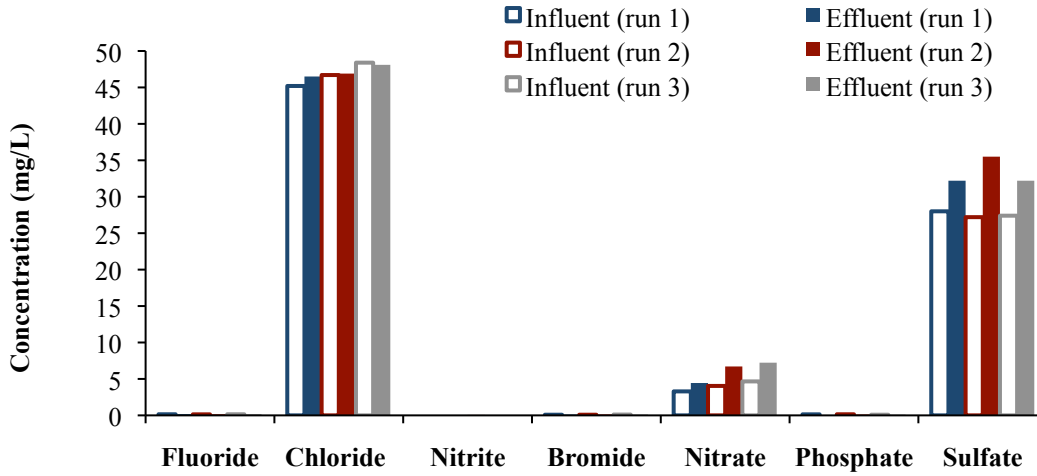


b)

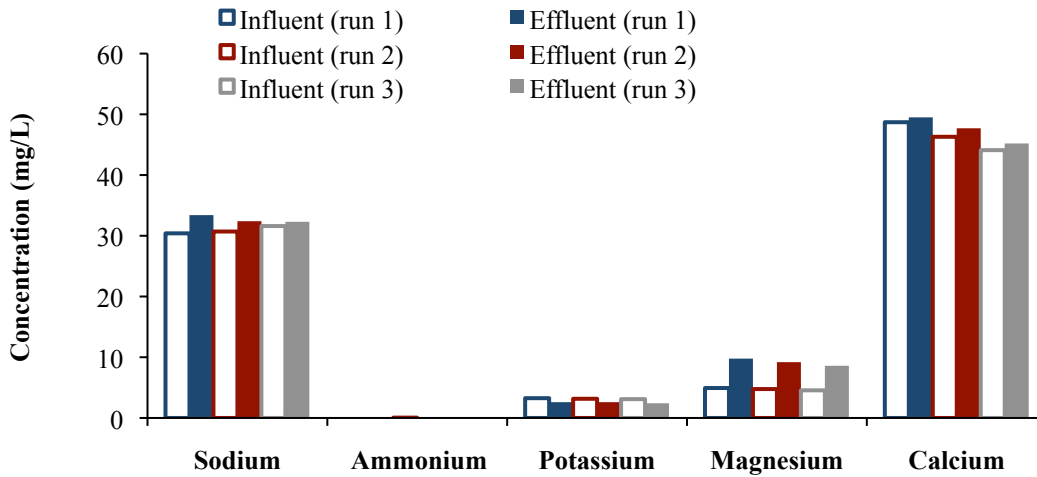


Appendix FF. Chemical analysis of a) anions and b) cations during one step outflow experiment of Pali column.

a)

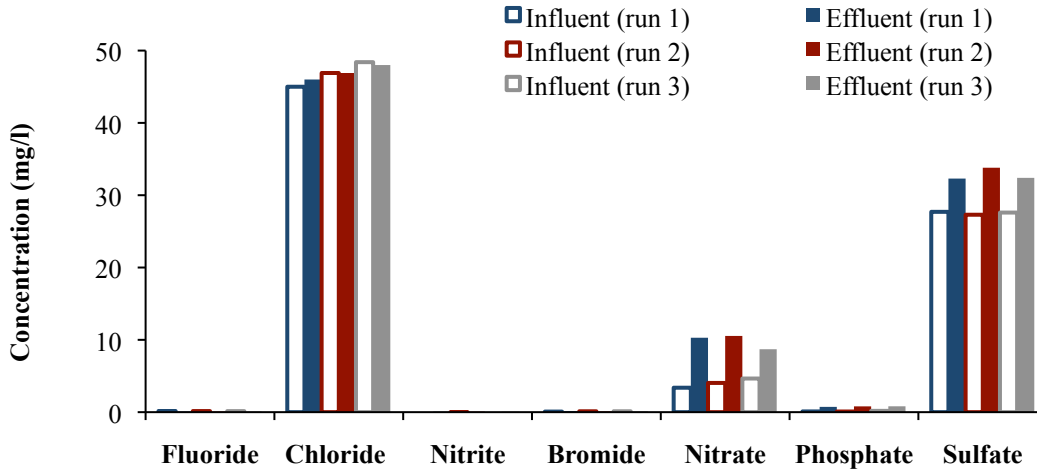


b)

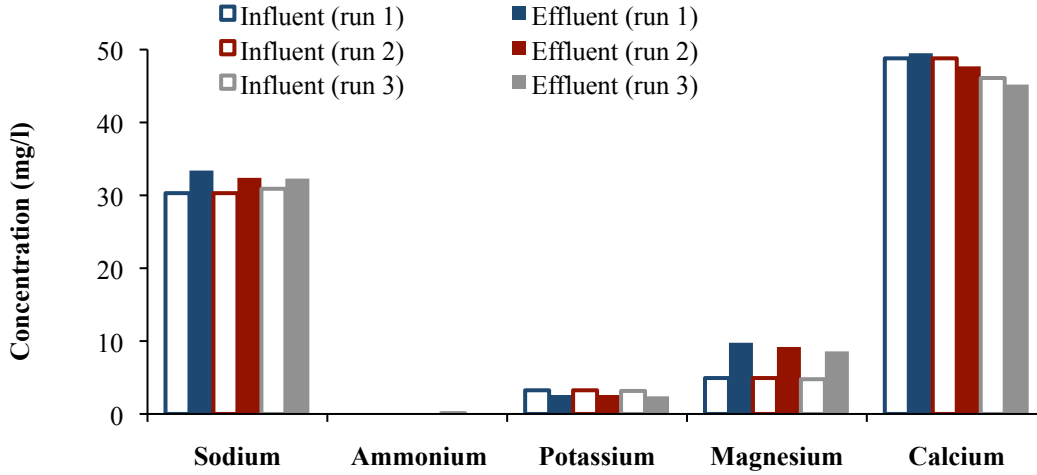


Appendix GG. Chemical analysis of a) anions and b) cations during one step outflow experiment of the Sandy Beach column.

a)



b)



Appendix HH. Summary of chemical analysis done on the North Shore and Kunia sample.

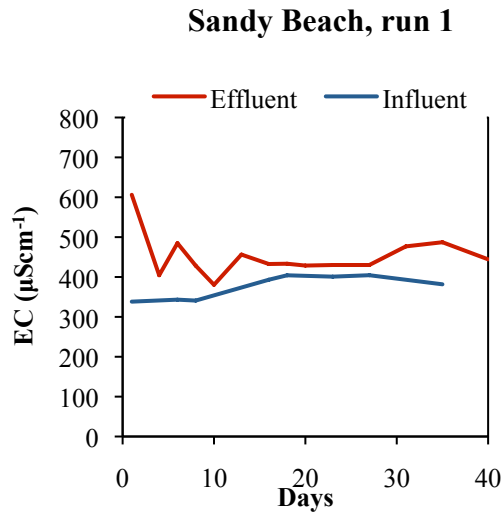
		North Shore						Kunia					
		Influent	Influent	Influent	Effluent	Effluent	Effluent	Influent	Influent	Influent	Effluent	Effluent	Effluent
		1	2	3	1	2	3	1	2	3	1	2	3
pH	-	7.38	7.56	7.48	7.46	7.37	7.39	7.50	7.61	7.46	6.54	6.43	6.51
EC	µS/cm	419.6	410.0	410.3	466.3	476.2	496.0	416.6	413.7	407.5	431.3	407.4	405.8
Turbidity	NTU	129.7	118.7	60.0	2.0	1.7	3.5	156.0	117.0	95.4	2.4	5.9	3.3
TOC	mg/l	10.08	n.a.	10.24	8.98	9.30	8.78	10.09	10.73	10.68	8.67	8.42	8.14
DOC	mg/l	9.37	n.a.	9.68	8.15	8.54	8.21	9.29	9.79	9.91	7.66	7.64	7.36
TSS	mg/l	244.0	n.a.	90.0	1.7	5.7	1.2	277.0	208.0	181.0	0.8	3.4	2.4
TDS	mg/l	264.0	-	238.0	257.0	261.5	318.0	270.5	243.5	244.5	297.4	221.4	203.6
Zeta potential		-13.29		-12.14	-9.35	-8.39	-6.88	-11.24	-11.99	-10.77	-11.70	-11.70	-11.66
Anions													
Fluoride	mg/l	0.16	0.14	0.14	0.24	0.22	0.18	0.16	0.15	0.14	0.09	0.09	0.09
Chloride	mg/l	44.90	47.50	48.00	44.50	45.90	47.50	45.00	47.00	48.20	46.20	46.80	48.20
Nitrite	mg/l	n.a.	n.a.	n.a.	0.02	0.04	0.22	n.a.	0.01	n.a.	0.03	0.01	0.01
Bromide	mg/l	0.11	0.10	0.11	0.10	0.11	0.09	0.12	0.10	0.12	0.11	0.12	0.11
Nitrate	mg/l	3.31	3.92	4.83	5.52	6.78	10.79	3.36	3.93	4.65	4.48	6.49	6.98
Phosphate	mg/l	n.a.	1.10	0.10	0.25	0.32	0.29	n.a.	0.15	0.11	n.a.	n.a.	n.a.
Sulfate	mg/l	27.00	27.90	26.90	30.70	33.70	33.50	27.20	27.70	27.20	42.70	40.50	39.80
Cations													
Lithium	mg/l	0.01	0.01	0.01	n.a.	n.a.	n.a.	0.01	0.01	0.01	0.00	0.00	0.00
Sodium	mg/l	30.30	31.30	31.50	30.90	31.30	31.60	30.30	30.90	31.50	32.60	31.90	31.70
Ammonium	mg/l	0.02	0.06	n.a.	0.61	0.74	0.55	0.03	0.09	n.a.	n.a.	n.a.	n.a.
Potassium	mg/l	3.26	4.12	3.11	3.05	3.12	3.10	3.25	3.16	3.10	2.33	2.28	2.23
Magnesium	mg/l	4.96	4.80	4.57	10.54	11.09	11.44	4.93	4.74	4.57	7.24	6.76	6.44
Calcium	mg/l	49.10	45.60	44.30	47.20	49.50	51.50	48.90	46.00	44.20	40.70	38.70	37.00

Appendix II. Summary of chemical analysis done on Pali and the Sandy Beach sample.

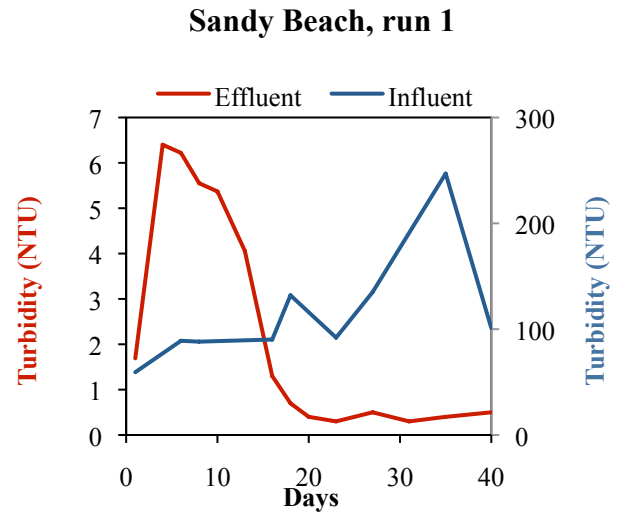
		Pali						Sandy Beach					
		Influent	Influent	Influent	Effluent	Effluent	Effluent	Influent	Influent	Influent	Effluent	Effluent	Effluent
		1	2	3	1	2	3	1	2	3	1	2	3
pH	-	7.63	7.48	7.55	7.21	7.10	7.12	7.58	7.50	7.51	7.22	7.09	7.15
EC	µS/cm	420.1	408.2	408.4	474.7	454.4	447.1	421.9	408.4	407.9	506.1	481.6	467.4
Turbidity	NTU	156.7	145.3	69.0	14.2	22.0	7.2	174.0	110.0	121.0	2.9	3.1	2.6
TOC	mg/l	10.23	10.24	10.79	10.25	10.44	10.26	10.11	10.35	10.34	11.13	11.32	10.91
DOC	mg/l	9.29	9.68	9.74	9.48	9.76	9.67	9.38	9.63	9.61	10.05	10.16	10.02
TSS	mg/l	287.0	267.0	143.0	9.0	12.3	5.6	306.0	263.5	277.0	306.0	299.2	238.0
TDS	mg/l	200.0	228.5	246.5	286.3	286.3	265.5	270.5	263.5	277.0	306.0	299.2	283.2
Zeta potential		-10.28	-9.52	-11.49	-13.23	-9.59	-9.26	-9.80	-9.92	-12.22	-14.26	-9.66	-12.28
Anions													
Fluoride	mg/l	0.15	0.14	0.15	0.18	0.16	0.16	0.16	0.15	0.14	0.09	0.09	0.08
Chloride	mg/l	45.20	46.70	48.40	46.50	46.90	48.10	45.00	46.90	48.40	46.00	46.90	48.00
Nitrite	mg/l	n.a.	n.a.	n.a.	0.01	0.06	0.03	n.a.	0.01	n.a.	0.06	0.07	0.05
Bromide	mg/l	0.09	0.09	0.11	0.13	0.14	0.11	0.08	0.12	0.12	0.16	0.11	0.11
Nitrate	mg/l	3.29	4.04	4.66	4.44	6.71	7.23	3.38	4.04	4.65	10.29	10.54	8.70
Phosphate	mg/l	0.14	0.15	0.09	n.a.	0.13	0.10	0.10	0.09	0.18	0.73	0.80	0.81
Sulfate	mg/l	28.00	27.20	27.40	32.20	35.50	32.20	27.70	27.30	27.60	32.30	33.80	32.40
Cations													
Lithium	mg/l	0.01	0.01	0.00	0.00	0.00	0.00	0.01	0.01	0.00	n.a.	n.a.	n.a.
Sodium	mg/l	30.40	30.70	31.60	33.40	32.40	32.30	30.30	30.90	31.70	39.80	38.10	35.60
Ammonium	mg/l	0.00	0.05	n.a.	n.a.	0.07	n.a.	0.00	0.11	n.a.	0.17	0.28	0.26
Potassium	mg/l	3.26	3.16	3.10	2.60	2.60	2.42	3.25	3.16	3.11	8.18	8.05	7.85
Magnesium	mg/l	4.93	4.76	4.55	9.77	9.19	8.59	4.93	4.77	4.61	12.81	12.18	11.56
Calcium	mg/l	48.70	46.30	44.10	49.50	47.70	45.20	48.80	46.10	43.90	42.30	39.70	37.60

Appendix JJ. Electrical conductivity, turbidity, total suspended solids and total dissolved solids during the first long term column experiment on Sandy Beach.

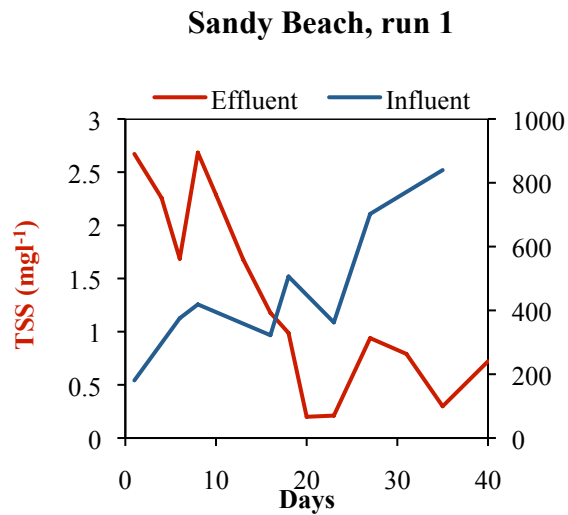
a)



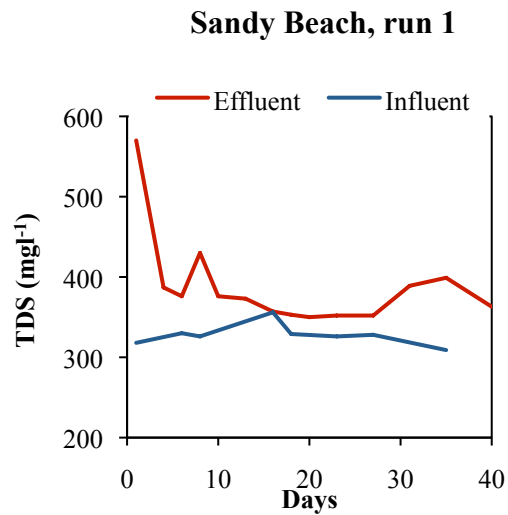
b)



c)

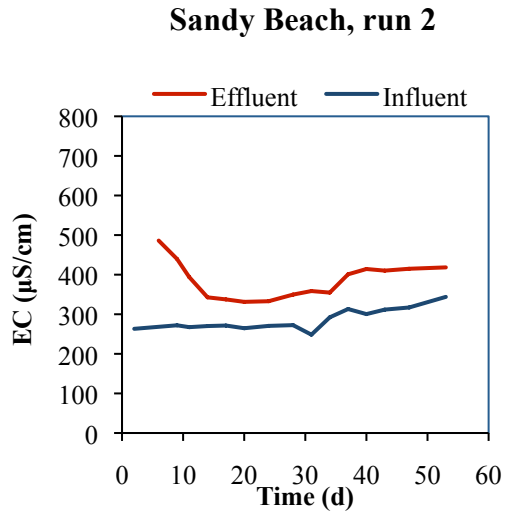


d)

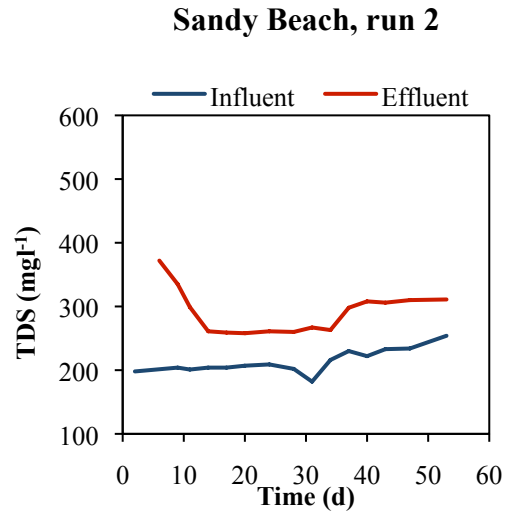


Appendix KK. Influent and effluent of a) electrical conductivity, b) turbidity, c) total suspended solids and d) total dissolved solids during the second long term column experiment on Sandy Beach.

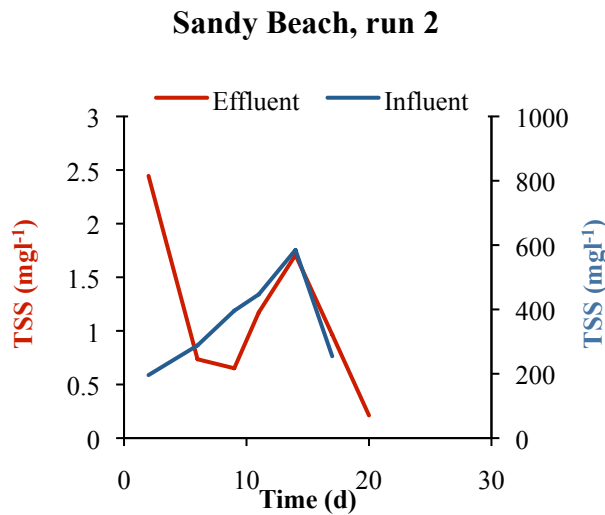
a)



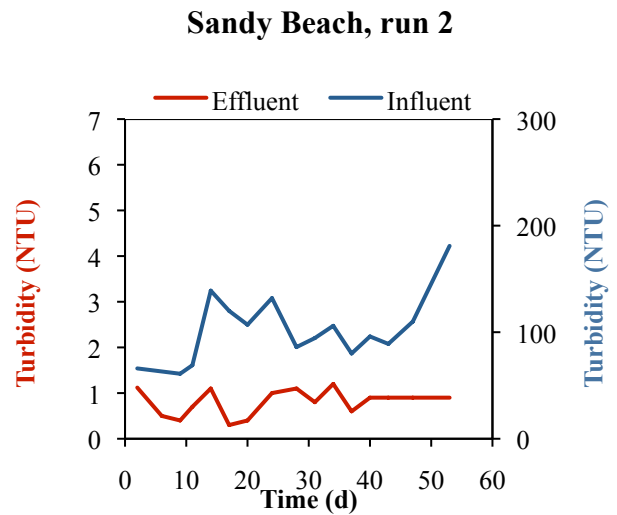
b)



c)

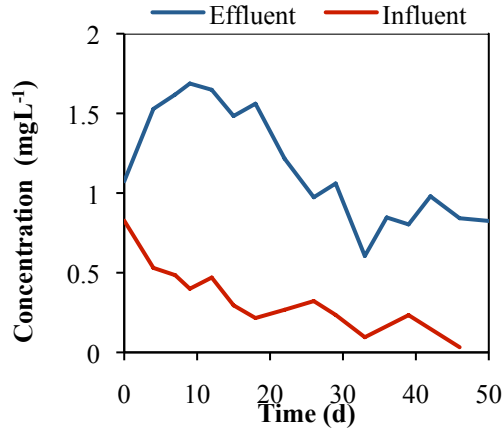


d)

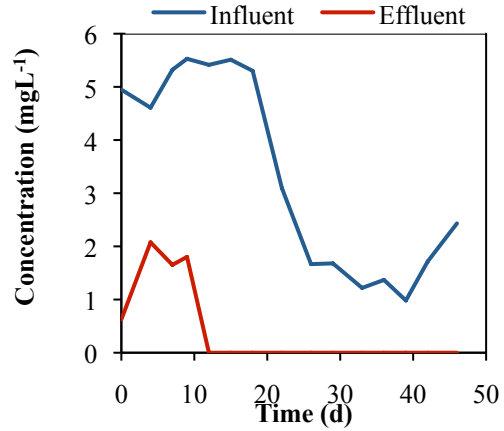


Appendix LL. Concentration of anions and cations in the influent and effluent of the second long term infiltration-outflow experiment on the Sandy Beach.

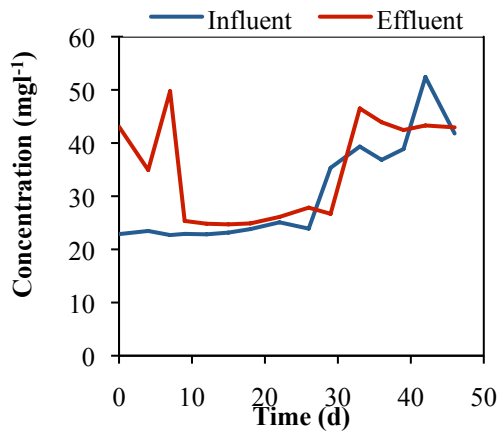
Sandy Beach, run 2 - phosphate



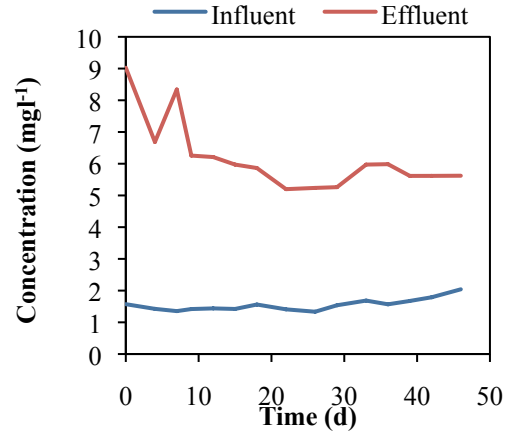
Sandy Beach, run 2 - nitrate



Sandy Beach, run 2 - chloride



Sandy Beach, run 2 - potassium



Sandy Beach, run 2 - magnesium

